**AIR GAP ELIMINATION IN PERMANENT MAGNET MACHINES**

By

Andy Judge

A Dissertation

Submitted to the Faculty

of the

WORCESTER POLYTECHNIC INSTITUTE

In partial fulfillment of the requirements for the

Degree of Doctor of Philosophy

In

Mechanical Engineering

by

_____

March 2012

APPROVED:

_____
Dr. James D. Van de Ven, Advisor

_____
Dr. Cosme Furlong-Vazquez, Committee Member

_____
Dr. Alexander E. Emanuel, Committee Member

_____
Dr. Eben C. Cobb, Committee Member

_____
Dr. David J. Olinger, Graduate Committee Representative

## ABSTRACT

In traditional Permanent Magnet Machines, such as electric motors and generators, power is transmitted by magnetic flux passing through an air gap, which has a very low magnetic permeability, limiting performance. However, reducing the air gap through traditional means carries risks in manufacturing, with tight tolerances and associated costs, and reliability, with thermal and dynamic effects requiring adequate clearance. Using a magnetically permeable, high dielectric strength material has the potential to improve magnetic performance, while at the same time offering performance advantages in heat transfer.

Ferrofluids were studied as a method for improved permeability in the rotor / stator gap with a combined experimental and computational approach. Results show promise for the ferrofluid technique. An off-the-shelf motor system showed improved performance with ferrofluids vs. fluids of equivalent viscosity, and improved performance vs. an air gap at low RPM. New generator designs showed design dependent performance gains, although some potential for negative performance effects. A proof of concept generator was built and tested, with increased voltage vs. RPM predicted through virtual prototyping, and validated through experimentation, showing ~10% improvement on voltage vs. RPM at the <600 RPM range. More repeatable engineering tests demonstrated a ~30% increase in the voltage / RPM relationship for designs with an isolated stator chamber and a large stator – rotor gap. However, the effects were negative for a similar system with a small stator-rotor gap due to leakage flux effects.

New contributions to the body of knowledge in this area include:

- Application of the ferrofluid technique to axial flux designs.
- Development of a virtual prototype, including variations in the fluid viscosity due to ferrohydrodynamic effects.
- Consideration of negative effects of ferrofluid immersion, such as shear losses and increases in leakage flux.
- Optimization of the design to eliminate increased viscous losses. The improved design has been designed, built, and tested, featuring isolation of the ferrofluid from the rotating region. This offers all of the performance gain of improved magnetic permeability, while minimizing the offsetting losses from increased shear effects.

## ACKNOWLEDGEMENTS

To start, I would like to thank the faculty of Worcester Polytechnic Institute, including the members of my dissertation committee, and throughout the University. It had been a few years since I had last taken a class, and the overall graduate experience at WPI reminded me of why I became an engineer in the first place – my love of learning and technology. I am especially grateful to my advisor, Dr. James Van de Ven, who reminded me of what engineering research was all about, helping me get started, offering support whenever needed and giving me the freedom to make my own path throughout the process.

None of this would have been possible without the financial support of my employers, ITT for the first three years of my PhD coursework and research, and DRS for the past few months. Also, I am appreciative of John Schneider and Mark St. Pierre, two former supervisors of mine, who wrote my recommendations to WPI, and were a pleasure to work for. I am also grateful to my co-workers, including those who helped me learn the basics of Permanent Magnet Machines when I started in the field, and those who taught me the fine points as my understanding of the topic grew.

Of course, my most heartfelt thanks go to my family, including my father, for giving me his work ethic, and my mother, for giving me her love of life. To my children, Sawyer and Delaney, I am always grateful for, and want nothing more than to have you continue living happy, healthy lives. Finally, to my wife Wendy, thank you for supporting me in this, for loving me back, and for understanding me in such a complete way.

## TABLE OF CONTENTS

## LIST OF TABLES

## LIST OF FIGURES

## NOMENCLATURE

For convenience, all symbols appearing in this dissertation are listed below. Subscripted terms, such as $A_m$ for "Magnet Area", for specific applications that do not change the main term under consideration are not listed. When both US and SI units are used, both are provided. When only SI terms are common, only the SI units are shown.

| SYMBOL | DESCRIPTION | UNITS |
|---|---|---|
| $A$ | Area | $Inch^2$ (US) or $Meter^2$(SI) |
| $B$ | Magnetic Flux Density | Gauss (US) or Tesla (SI) |
| $C_d$ | Coefficient of Drag | Dimensionless |
| $d$ | Distance | Inch (US) or Meter (SI) |
| $E$ | Electric Field | Newtons/Coulomb |
| $\varepsilon$ | Permittivity | Farads/meter |
| $F$ | Force | Newtons |
| $f$ | Frequency | Hertz |
| $f_{LKG}$ | Leakage Factor | Dimensionless (ratio) |
| $\Phi$ | Magnetic Flux | Weber |
| $H$ | Magnetic Field Strength | Oersteds (US) or Amp/meter (SI) |
| $I$ | Current | Ampere |
| $J$ | Current Density | $Ampere/meter^2$ |
| $K$ | System Efficiency | Dimensionless |
| $Ke$ | Voltage Constant | RPM/Volt |

| SYMBOL | DESCRIPTION | UNITS |
|---|---|---|
| $Kt$ | Torque Constant | Torque/Amp |
| $k_{w1}$ | Winding Factor | Dimensionless |
| $k_{w1}$ | Bearing Friction Coefficient | Dimensionless |
| $L$ | Length | Inch (US) or Meter (SI) |
| $M$ | Magnetization | Oersted |
| $m$ | Mass | Kilograms |
| $m_1$ | # of phases | Dimensionless |
| $N$ | # of Turns | Dimensionless |
| $\eta$ | Viscosity | Centipoise |
| $p$ | # of poles | Dimensionless |
| $P$ | Permeance | Gauss*Newton*meter/Oersted |
| $\mu$ | Magnetic Permeability | Gauss/Oersteds |
| $\mu_r$ | Relative Permeability | Dimensionless (ratio) |
| $\rho$ | Density | Kilogram/meter$^3$ |
| $R$ | Reluctance | Oersteds/Gauss*Newton*meter |
| $r$ | Radius | Meter |
| $Re$ | Reynolds Number | Dimensionless |
| $\Omega$ | Resistance | Ohms |
| $RPM$ | Revolutions Per Minute | 1/Minute |
| $s$ | Conductivity | Siemens |
| $t$ | Time | Seconds |

| SYMBOL | DESCRIPTION | UNITS |
|---|---|---|
| $\tau$ | Shear Stress | Newtons/meter$^2$ |
| $T$ | Torque | Newton*meter |
| $v$ | Velocity | Meter/second |
| $\vartheta$ | Vortex Viscosity Coefficient | Dimensionless |
| $\dot{\gamma}$, | Shear Rate | Newton/Meter$^2$*second |
| $W$ | Power | Watts |
| $\omega$ | Rotational Velocity | Radians/Second |

# Chapter 1

## Introduction

This chapter provides an introduction to permanent magnet machines (PMM's), and provides a description of their applications. A detailed description then follows on existing research on the main area of PMM performance that is the focus of this dissertation – the air gap. A detailed literature review is presented consisting of both primary and secondary sources. The chapter is concluded with an overview of the remaining chapters of this thesis.

## 1.1 Background

With increased focus on efficiency of electromechanical systems, such as alternative energy power generation and electric vehicles, as well as advances in material science over the last few decades, permanent magnet machines (PMM's) are enjoying more usage in the field of electromechanical power conversion. The basic physics of PMM's consists of alternating poles of permanent magnets rotating past either a ferromagnetic material wrapped in conductive windings, or other magnets (with or without an intermediate ferrous material between them). For electromagnetic power conversion, either an input torque / RPM (alternator / generator applications) or an input electrical voltage / current (motor applications) is supplied and the other provided as an output, providing electromechanical power conversion. For pure magnetic mechanical power conversion, torque and rotational velocity is transmitted through magnetic force from one

shaft to another, either in a 1:1 ratio or with a gear ratio through means of passing through an intermediate set of ferrous poles.

PMM's transmit magnetic flux for power conversion through a gap between the rotor and stator, which is traditionally air in electromagnetic systems. With all other factors, such as size, speed, magnet material, et al., being equal, efficiency would be improved if the gap material had better capability to transmit magnetic flux. Ferrofluids, which are magnetic fluids described in more detail in Chapter 3, have this property, and is the main focus of this research. Ferrofluids are liquids containing nanoscale sized iron particles, making them magnetically permeable. A system with a ferrofluid gap, as opposed to an air gap, would maintain the required spacing between the rotor and the stator, but would offer efficiency improvements.

## 1.2 LITERATURE REVIEW

This research focuses specifically on permanent magnet machines, and improving their performance with ferrofluids, a specialty engineered material for magnetic applications. Existing research is studied, so as to leverage past work in the field. An extensive search was made for existing studies of ferrofluids in permanent magnet machines, with only one major source of research identified. This publication featuring ferrofluid immersion of permanent magnet machines is presented in detail, as well as its areas needing

improvement, which compromises much of the new contributions to the field for this research.

Primary sources highlight the resources used for PMM design and analysis, as well as the unique considerations for ferrofluids. Secondary sources include methods of improving magnetic flux across the air gap that do not relate to the gap material. Flux guides, non-conventional manufacturing techniques, and Halbach arrays are reviewed as competing methods of system improvements. Various types of non-traditional permanent magnet ferrofluid electromagnetic power conversion devices are also presented.

### 1.2.1 PRIMARY SOURCES

Magnetism and electromagnetism are broad, general topics with numerous publications available to present the basics physics involved. K.E. Lonngren, S.V. Savov, R.J. Jost, "Fundamentals of Electromagnetics with MATLAB ®" [1], was used as a basic text on the general terms.

With the success of PMM motors and generators in the marketplace, numerous research and source material is available for PMM performance characterization. The most often referenced textbook in the field commercially is J.R. Hendershot and T.J.E. Miller, "Design of Brushless Permanent-Magnet Motors" [2]. This book provides an overview of PMM's in general, and delves into the specific theory of electric motor and generator

performance and characterization. Equations from Hendershot and Miller's text were used in chapter 3 to develop the "virtual prototype" model of the generator on a macro-scale.

Besides their industry standard text, Hendershot and Miller have done extensive research on permanent magnet machines through the SPEED [Scottish Power Electronics and Electric Drives] Consortium, part of the Department of Electronic and Electrical Engineering at the University of Glasgow. SPEED is also the name of the software program for electric motor design and analysis, developed by Hendershot and Miller and the SPEED Consortium as a motor design tool. The SPEED software program collects the motor / generator performance equations presented in the text in a "design wizard" / spreadsheet type of format. The training manual for SPEED[14] has also proved to be a critical component of this research. One limitation for the SPEED software program is that it assumes air as the barrier between the rotor and stator, which is the focus of this dissertation to change.

Another common industry-referenced textbook is by D. C. Hanselman, "Brushless Permanent Magnet Motor Design"[6]. This work from Professor Hanselman, from the University of Maine, is less of a general reference material than the book from Hendershot and Miller, and focuses more on windings and the effects of electrical inductance and motor controls. This text was used as a practical guideline to develop the experimental hardware, especially the basic configuration and winding.

The main reference used for the development of the axial flux generator used in experiments two through four was Jacek Gieras, Rong-Jie Wang, Maarten Kamper, "Axial Flux Permanent Magnet Brushless Machines" [3]. This textbook was specific to "pancake" style PMM's, which lend themselves very well to ferrofluid immersion in the single rotor style. Gieras, et al. modified the general motor equations presented by Hendershot and Miller for axial flux geometry. These equations were the basis of the "virtual prototype" presented in chapter 3.

While all three textbooks, along with the SPEED training manual, present basics of electric motor design, none of these references work with any material in the stator / rotor gap other than air. The main focus of this research is ferrofluid gaps, which is not discussed in any of the textbooks.

R.E. Rosenweig, "Ferrohydrodynamics", [11] provided the basis for ferrofluid specific effects on fluid flow, and was the primary reference cited for all other white papers found on the subject. Chapter 2.4 of this paper references this Primary Source extensively.

Calculations for Windage Losses for the radial system were derived in a technical publications from NASA, "Prediction of Windage Power Loss in Alternators", James Vrancik [27]. This data is presented in Chapter 3, along with the windage losses for the axial system, derived in Gieras, et al. [3]

The Journal of Physics: Condensed Matter, Volume 18, Number 38, featured a "special issue" on ferrofluids. This reference contained numerous helpful articles, including a closely related paper on ferrofluid immersion, "Improving the Efficiency of Electric Machines Using Ferrofluids" by A Nethe, T Scholz, and H Stahlmann [9]. The authors present a magnetic circuit, shown in Figure 1.2.1-1, highlighting in red the flux / magnetic resistance of the air gap. Note that the network is then simplified to neglect leakage flux in the air gap. One of the new contributions to the field of this dissertation project is the consideration the effect of ferrofluid immersion on leakage flux.

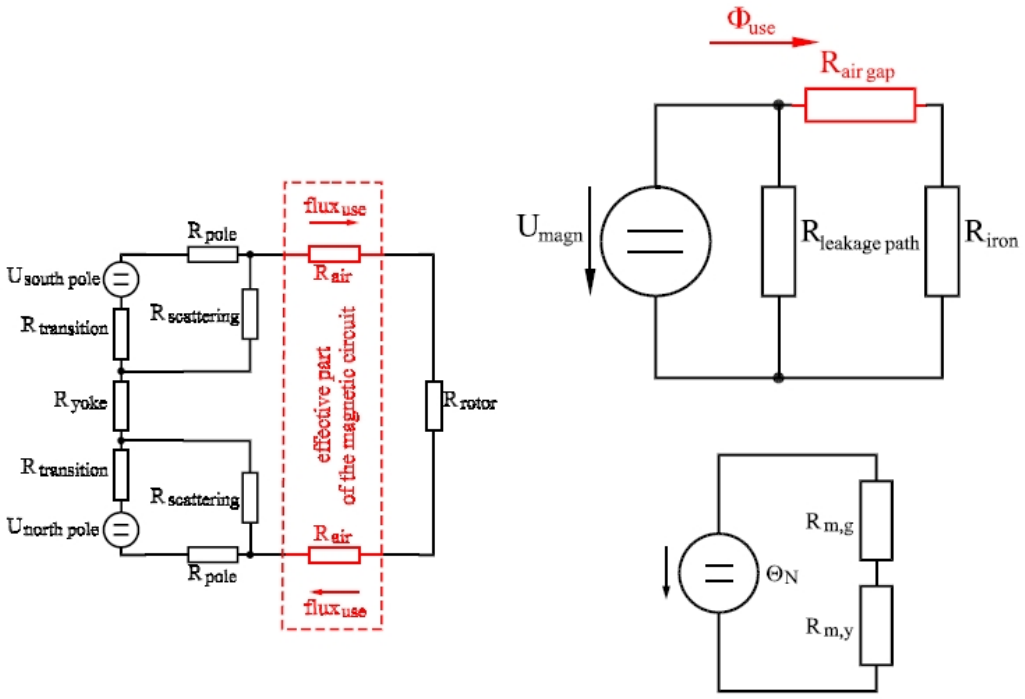


Figure 1.2.1-1 – Nethe, et al. Magnetic Circuit [9]. This figure shows the magnetic circuit used by Nethe, et al. Note the network neglects leakage flux in the gap.

Using magnetic circuit calculations, similar to those presented in chapter 3 of this thesis, the authors presented the potential increase in system performance by increasing

permeability across the gap through ferrofluid immersion and / or decreasing gap distance. Figure 1.2.1-2 shows their plot of magnetic force vs. gap permeability for various air gap distances of a magnetic system shown in Figure 1.2.1-3, consisting of two magnets separated by a layer of ferrofluid. Note that the magnetic force increases with increased permeability up to an optimal level, then decreases with further increases in permeability. One note on the graph not discussed by the authors is that the leakage flux is geometry dependent, as discussed in chapter 3 of this thesis, and varies from system to system.

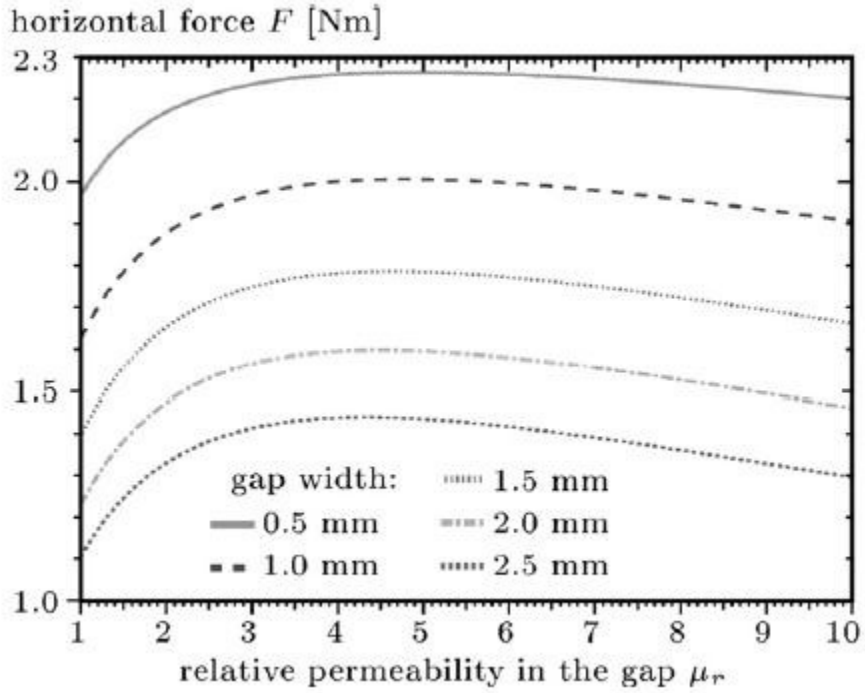


Figure 1.2.1-2 – Nethe, et al. Force vs. Relative Permeability for Various Air gap Distances [9]. This figure shows the graphs obtained Nethe, et al., showing the effects of air gap size on the force of a magnetic design, as well as the effects of gap relative permeability. Note that the improvements from permeability reach a maximum point, then increased permeability has a negative effect on overall performance.

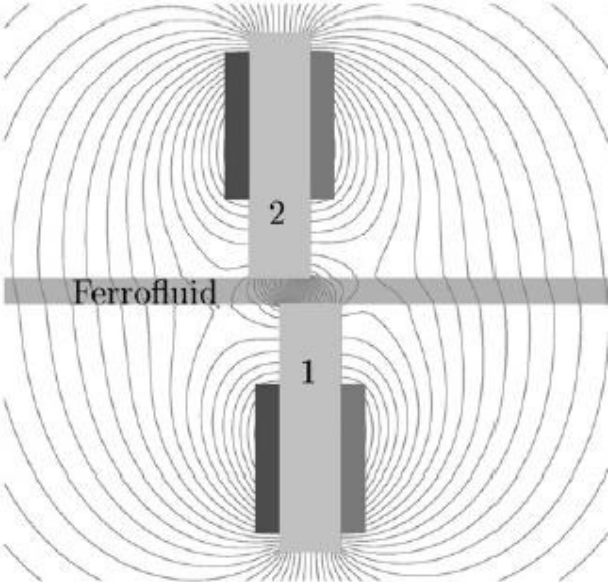


Figure 1.2.1-3 – Nethe, et al. Analytical Model for Force vs. Relative Permeability for Various Air gap Distances [9]. This figure shows the system analyzed by Nethe et al. for various air gap distances and ferrofluid material permeabilities, the results of which are shown in Figure 1.2.1-2.

Some limits to the approach are discussed by Nethe, et al. Saturation effects, the limited ability of a magnetic material to offer increase magnetic performance with increased flux, discussed in further detail in chapter 2, is presented for various systems. Figure 1.2.1-4 shows plots of torque vs. gap width (shown in terms of size and diameter ratio) for various levels of saturation of ferrofluid. Note that as the saturation level increases for the ferrofluid, the torque increase grows. This effect is amplified for larger air gaps.

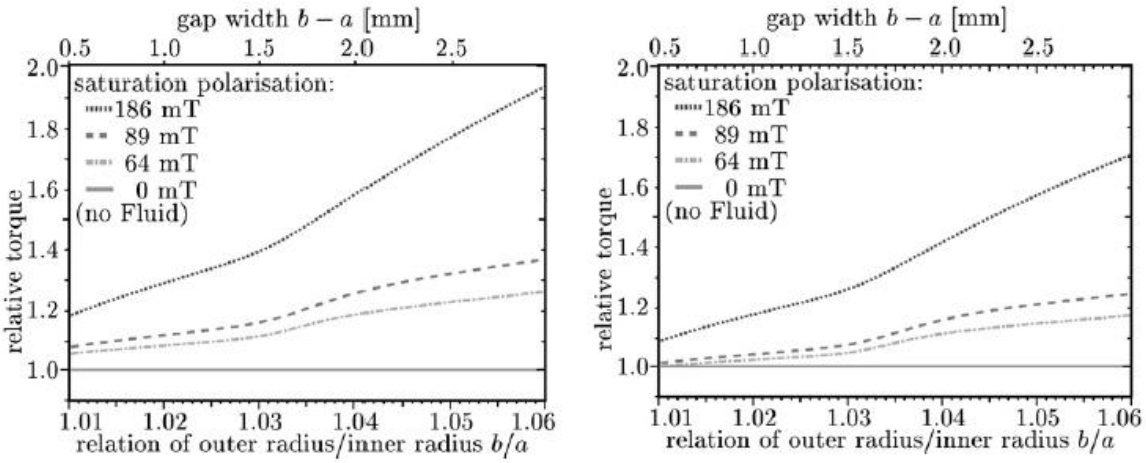


Figure 1.2.1-4 – Nethe, et al. Torque vs. Various Air gap Distances for Various Maximum Levels of Magnetic Saturation. [9]. This figure shows the effect of air gap distance, expressed both in terms of outer radius minus inner radius and in terms of outer radius to inner radius ratio on torque for a given permanent magnet machine. Summarizing, the larger the gap distance and the greater the ability of the fluid to transmit magnetic flux, the larger the increase in performance for a given design.

Thermal benefits for the ferrofluid technique are presented, as the liquid filled system offers improved thermal conductivity compared to an air system. However, the effects of windage losses, frictional air losses in a traditional system or viscous liquid friction in a ferrofluid based system, adds to the overall heat that is generated and must be dissipated. As discussed in chapter 3, this effect becomes more significant at higher RPM and smaller air gaps. Figure 1.2.1-5 [9] shows the effects of thermal performance for various thermal conductivity values of ferrofluid at various RPM levels. Note that the solid lines represent the gain of heat dissipation for typical values of thermal conductivity for several ferrofluids in the gap area, the dotted lines the additional heat created by the fluid friction; the arrow indicates the growth of the parameter. Also, note that the overall effect

could be positive or negative depending on system configuration (speed, geometry, and material).

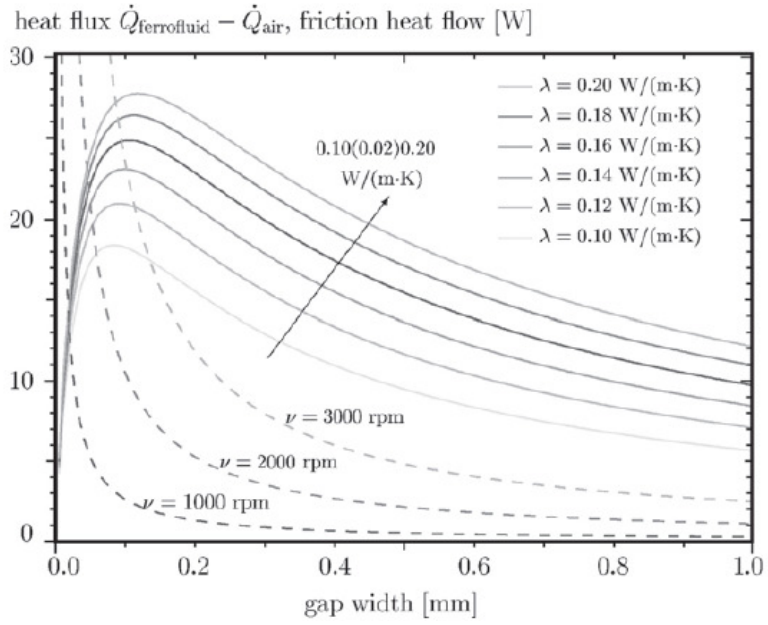


Figure 1.2.1-5 - Nethe, et al. Heat Flux Versus Gap Width for Various Thermal Coefficients and Speed Ranges [9]. This figure shows the effect of heat flow as a function of gap width for various heat transfer coefficients for various speed ranges. Summarizing, ferrofluid immersion adds additional heat to the system compared to standard air systems, and this effect becomes greater for higher speeds, smaller gaps, and higher thermal coefficients.

Two experiments were presented by Nethe, et al. In their first experiment, a linear system was designed and constructed, as shown in Figure 1.2.1-6. This device featured a lower electromagnet in a ferrofluid bath, energized with an upper permanent magnet translating on a fixture moving on low friction bearings. The electromagnet was energized with various levels of current, and the resulting force was measured. The system was baselined for its performance with a standard air gap, then filled with ferrofluids of various

maximum saturation points and re-measured. Results for the first Nethe, et al. experiment are shown in Figure 1.2.1-7, where "amplification [%]" is the gain in system performance, as measured by resultant force between the electromagnet and the permanent magnet, and "current [A]" is the input current to the electromagnet. Note that a large percentage gain was seen for a low power system, with smaller gains seen as power increased.

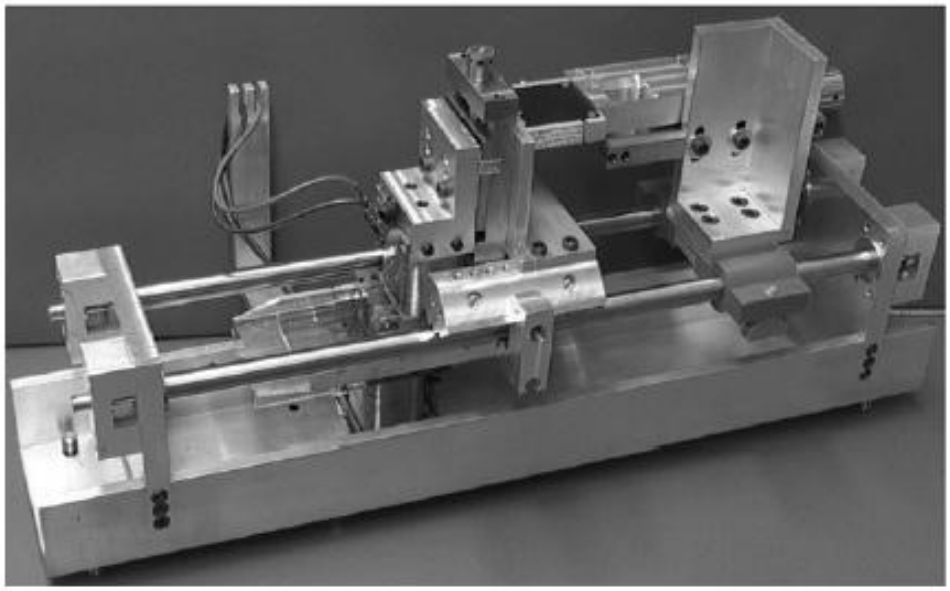

Figure 1.2.1-6 – Nethe, Et al. Linear Permanent Magnet Machine Experimental Fixture [9]. This figure shows the experimental set up for the first experiment performed by Nethe, et al. A linear permanent magnet machine was constructed, baselined with a standard air gap, then immersed in various ferrofluids to measure the effects of the fluid change

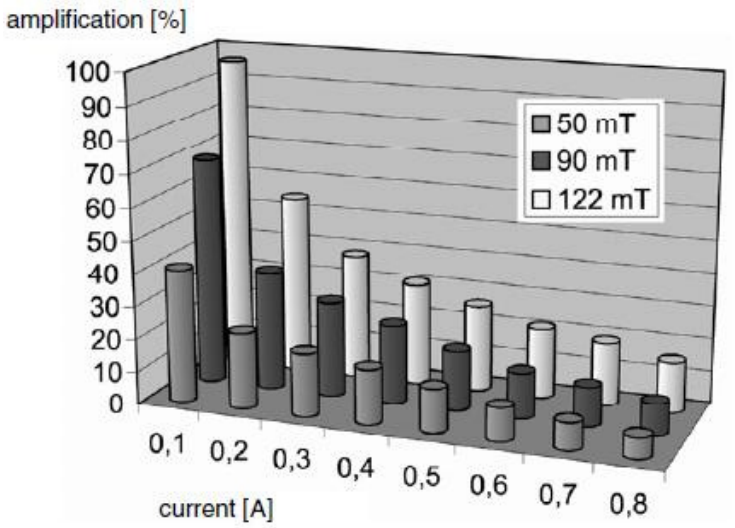


Figure 1.2.1-7 – Nethe, Et al. Linear Permanent Magnet Machine Experimental Results [9]. This figure shows the experimental results of the linear permanent magnet machine from Nethe, et al. All effects are shown as positive, with greater force amplification shown for greater saturation values of ferrofluid and lower currents.

The second experiment performed by Nethe, et al. involved a radial / rotating system, and a similar experiment was performed. Figure 1.2.1-8 shows the CAD model of the system (no experimental setup photos were provided). The system is an interior rotor permanent magnet machine, designed to be sealed for ferrofluid immersion.

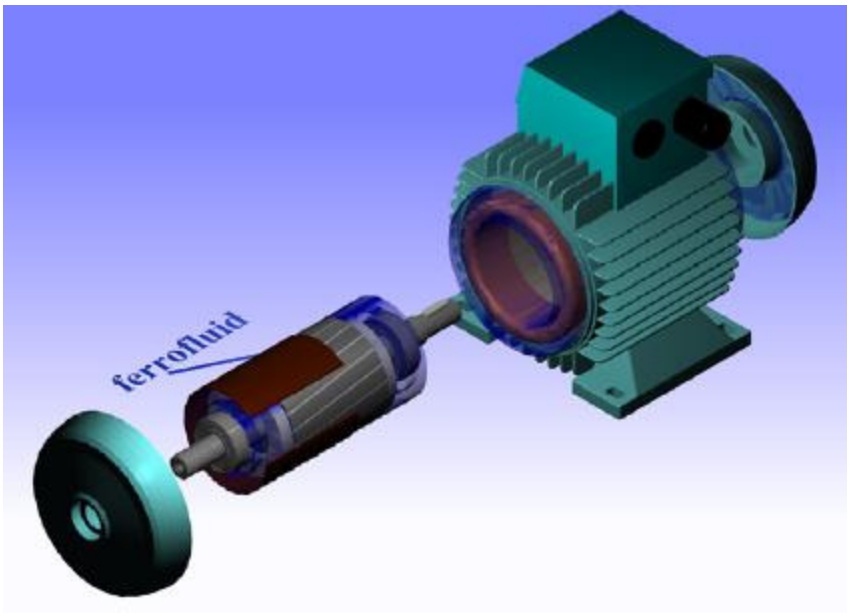


Figure 1.2.1-8 – Nethe, Et al. Rotating Permanent Magnet Machine CAD model [9]. This figure shows the CAD model for the second experiment from Nethe, et al., which featured a rotating permanent magnet machine.

Results for the second Nethe, et al. experiment are shown in Figure 1.2.1-9, expressed in terms of "efficiency % vs. torque load" and "increase of efficiency % vs. torque load". Note that a large percentage gain was seen for a low torque load system, with smaller gains seen as torque load increased. Also, note that the percentage increase of efficiency decreases with increasing RPM, becoming negative at torque loads higher than 1.2 N*m at 500 RPM.

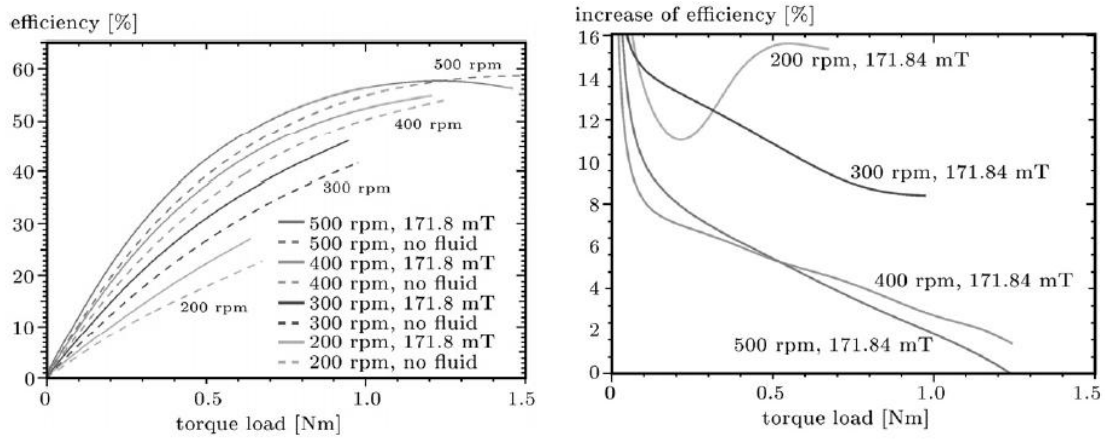


Figure 1.2.1-9 - Radial Permanent Magnet Machine Experimental Results, Nethe, Et al. [9]. This figure shows the results for the second experiment from Nethe, et al., which featured a rotating permanent magnet machine. All effects are shown as positive, with greater efficiency gains at lower RPMs, with a maximum rotational velocity of 500 RPM shown for the experiment.

One main drawback to the Nethe, et al. paper is that it deals only with linear and radial flux motor generator applications. The main focus of the research work for this project will be on axial flux devices. Also, the paper from Nethe, et al. focuses only on ferrofluid effects that are positive, and de-emphasizes trade-offs for increased shear losses and leakage flux, which are discussed later in this paper. The authors briefly discuss Ferrohydrodynamic effects, but use a constant value for viscosity in their calculations. Finally, for motor / generator applications, Nethe, et al. offer only a complete fluid immersion of an existing system, while this paper presents an optimized design with an isolated ferrofluid stator chamber.

Similarly titled works presenting the same experimental results, pictures, and graphs appear from the same authors in numerous other technical journals [27, 28, et al.].

### 1.2.2 SECONDARY SOURCES

Numerous studies have been done to characterize the effect of reducing the air gap. For example, a 2002 study on Magnetic Gears by Yang Zhiyi and Zhao Han [19] investigated improved torque from decreasing the air gap. Varying only the air gap size on a permanent magnet machine, from 1 mm to 2mm to 3 mm, Zhiyi and Han found drastic improvements in torque production, as shown in Figure 1.2.2-1.

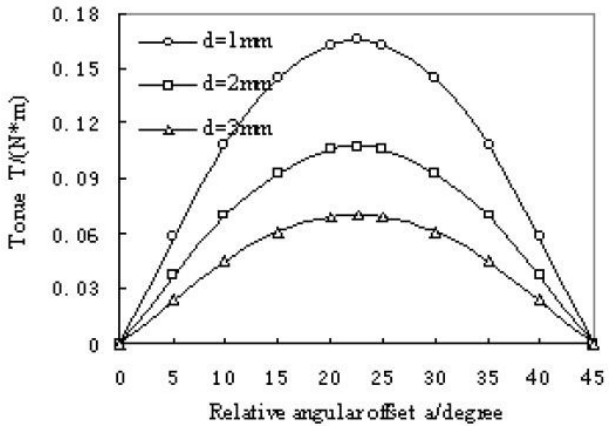


Figure 1.2.2-1 - Torque versus Relative Angular Offset and Air gap Distance (d) [19]. This figure shows the effect of air gap distance, keeping all other factors constant, across an angular section of a radial permanent magnet machine. Summarizing, shorter air gaps provide increased torque capability.

Tight air gaps can be achieved through means of tightly controlled manufacturing processes. For example, Thingap, Inc. of Ventura, CA, specializes in minimal air gap machines [25], developed through proprietary manufacturing techniques, as shown in Figure 1.2.2-2. Although this provides high power / torque dense machines, it carries with it associated penalties in cost from tightly toleranced, highly controlled processes. It also does not account for spacing required in dynamic applications, with potential

displacement due to shock or vibration, or expansion and contraction due to large temperature variations due to the coefficients of thermal expansion of the various materials.

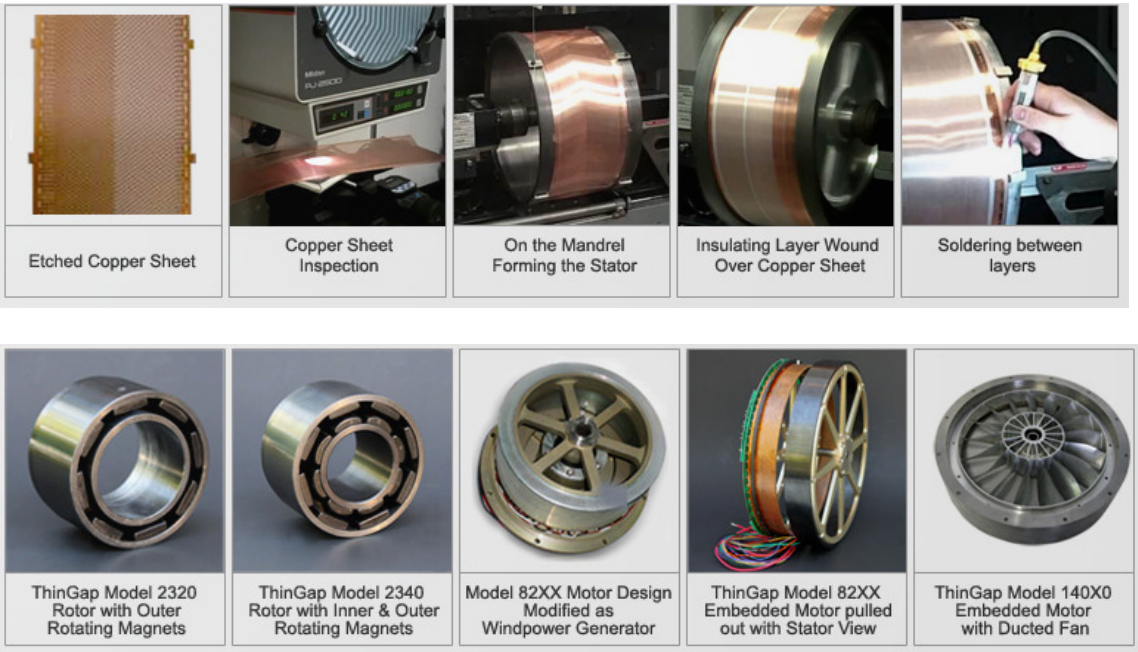


Figure 1.2.2-2 - Thingap Manufacturing Process [25]. This figure shows the specialized manufacturing process of Thingap LLC, a company that specializes in providing tightly toleranced, small air gap permanent magnet machines. Through their unique process, Thingap claims higher torque and power density devices than standard motor / generators.

Other methods of improving permanent magnet machine efficiencies typically focus on areas outside of air gap elimination, such as improved windings in motor / generator applications or design changes to flux path geometry. For example, a 2001 study by John Hsu at the Oak Ridge National Laboratory investigated the use of “flux guides”, shown in Figure 1.2.2-3, for magnetic performance improvement [18].

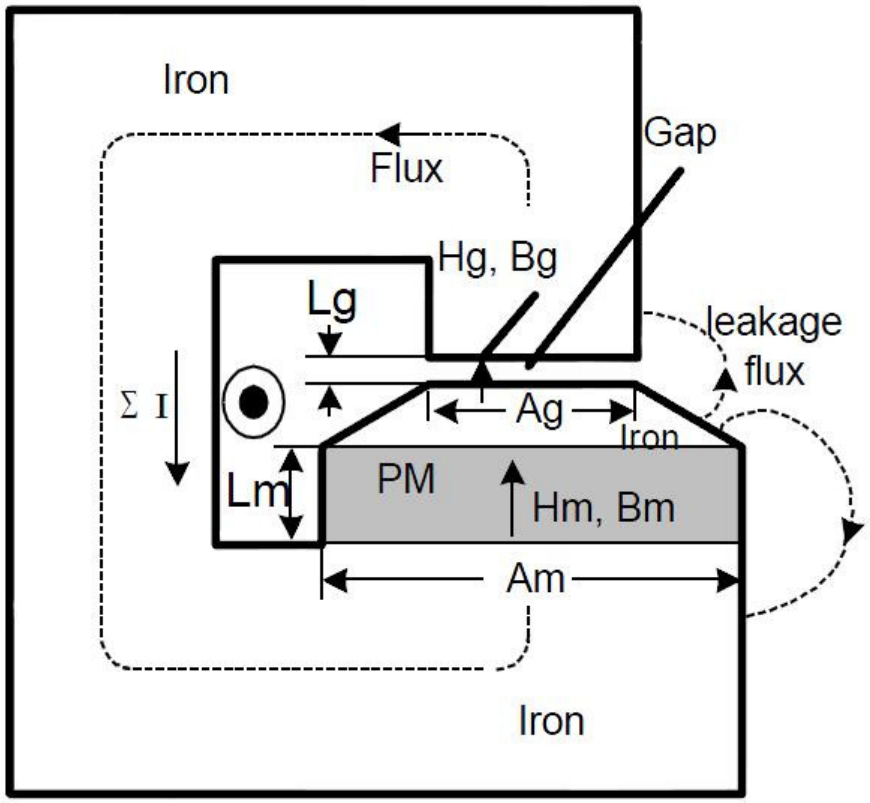


Figure 1.2.2-3 - Flux Guide for Permanent Magnet Machines [18]. This figure shows a Flux Guide, which increases flux density across the air gap through means of a pole cap with geometry designed to concentrate the transmitted magnetic flux.

The concept for the improving permanent magnet machine performance by immersing it in ferrofluid presented in this dissertation was derived from considering the PMM, then improving on the air gap permeability. Other designs from other researchers have been conceived by starting with the properties of ferrofluid in mind, and developing energy conversion devices based on their unique properties. In these systems, the magnet and windings are both stationary, providing two stators, and ferrofluid is pumped by various methods through the air gap. With the change in the gap permeability, a corresponding electromagnetic reaction is generated. An early patent for this application is US Patent

#4,064,409, “Ferrofluidic Electrical Generator”, by Charles Redman [30]. Shown in Figure 1.2.2-4, Redman’s device heats a ferrofluid to move it through a coil, converting heat energy to electrical energy, as opposed to passing a magnet past a coil to convert kinetic energy to electrical energy as is traditionally done in PMM’s.

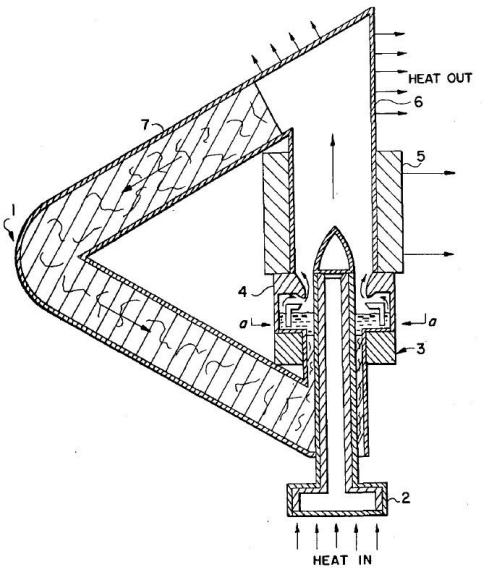


Figure 1.2.2-4 - Ferrofluidic Generator, Heat Powered [30]. This figure shows a US Patent for an electromagnetic device to convert thermal energy to electrical energy with no moving mechanical parts. A ferrofluid is put through a closed thermal loop, cycling past an electromagnetic element to periodically change the magnetic field strength and drive an electrical response.

Patents have been issued for Ferrofluidic Generator designs similar to Redman’s concept. US Patents # 6,489,694, “Ferrofluidic, Electrical Power Generator”, #6,504,271, “Ferrofluidic, Electromagnetic Power Generator”, #6,628,017, “Ferrofluidic, Electromagnetic Power Supply”, all by Jacob Chass, feature a cylindrical model proposed for installation in a vehicle tire. Figure 1.2.2-5 shows a concept sketch of the system [31].

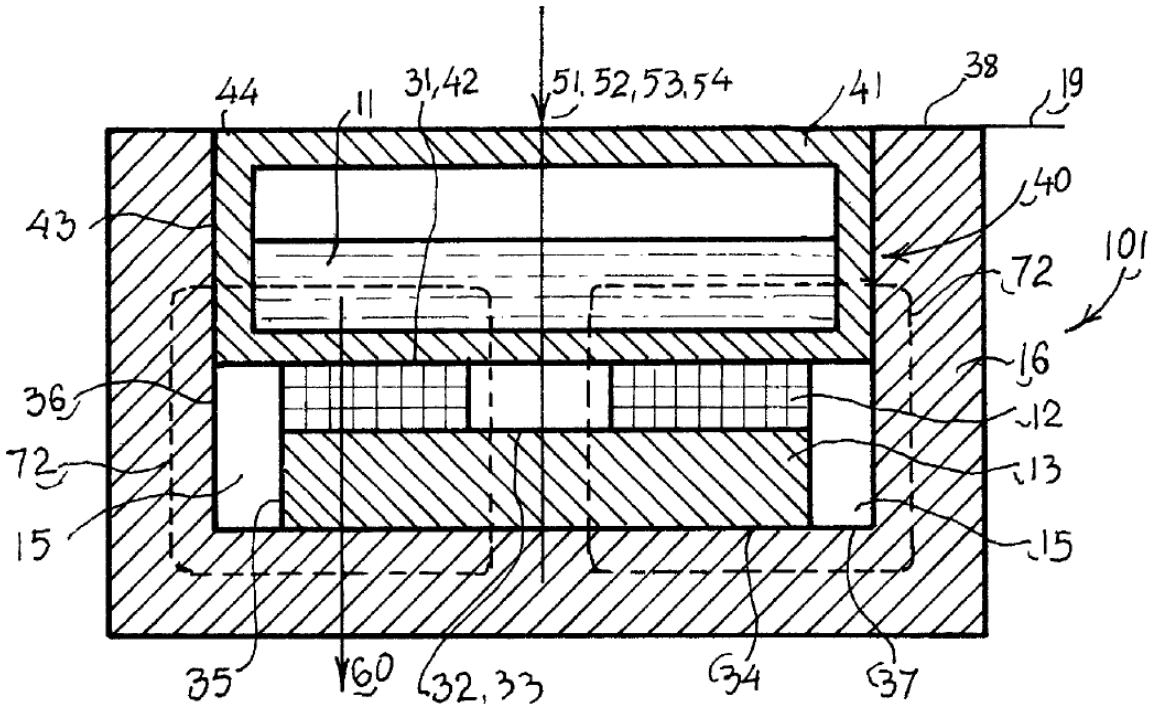


Figure 1.2.2-5 - Ferrofluidic Generator, Rotary Motion Powered [31]. This figure shows a US Patent for an electromagnetic device to convert mechanical energy to electrical energy. A ferrofluid rotates through an electromagnetic element to periodically change the magnetic field strength and drive an electrical response.

Another method of overcoming the magnetic reluctance of the air gap is to increase the magnetic strength of the magnets themselves. Materials research into the chemical composition of the magnets would certainly fall into this category. Currently, the highest strength magnets are formulations of Neodymium Iron Boron, with its highest end formulations current produced possessing a maximum energy product of 60 MegaGauss*Oersteds, with a Residual Flux Density of 1.6 Tesla. Compared to the magnetic saturation of standard silicon steels, typically greater than 2 Tesla, greater remnant magnetic flux density, the characteristic of permanent fields inherent in "permanent" magnets, would lead to positive results. However, the maximum theoretical

limit of Neodymium Iron Boron is 65 MegaGauss*Oersteds, showing less than a 10% potential for improvement [23].

Another way of gaining additional magnetic performance out of existing magnets is through magnetic system designs that maximize the magnetic flux sent through the air gap. A Halbach array uses this concept, with an alternative arrangement of magnets, as shown in Figure 1.2.2-6. In a traditional system, magnets are oriented with alternating polarity in a "-North-South-North-" manner. Halbach arrays use an arrangement of "-North-East-South-West-North" to direct flux that would otherwise be sent through the back iron, or that would be lost through leakage flux, across the air gap and into the stator. This configuration typically yields as much as a 15% improvement in maximum flux density [24].

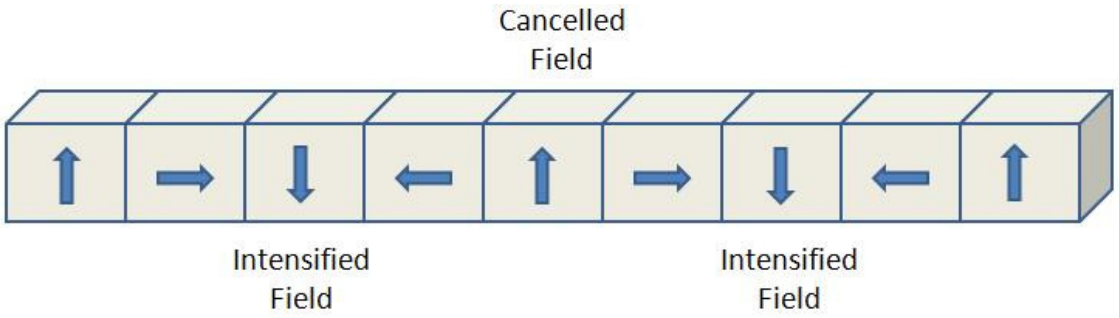


Figure 1.2.2-6 - Standard Halbach Arrays. This figure shows a standard Halbach array, which uses a set of alternatively oriented magnets between active poles to redirect flux otherwise lost through the back-iron across the air gap.

Extending this concept even further, as shown in Figure 1.2.2-7, an Extended Halbach Array makes used of a "-North–Northeast-East-Southeast-South-Southwest-West-Northwest-North-" configuration to attain as much as a 40% improvement in maximum

flux density [24]. Other arrangements are also possible, such as the supporting magnets oriented at 60°, or using varying thickness of magnets between the active poles and supporting magnets. However, more exotic approaches come with drawbacks such as of ease of magnetization of the magnets in non-orthogonal directions, handling and insertion of the magnets, additional part count for design for assembly and manufacturing concerns, additional magnet cost in the supporting magnets, et al.

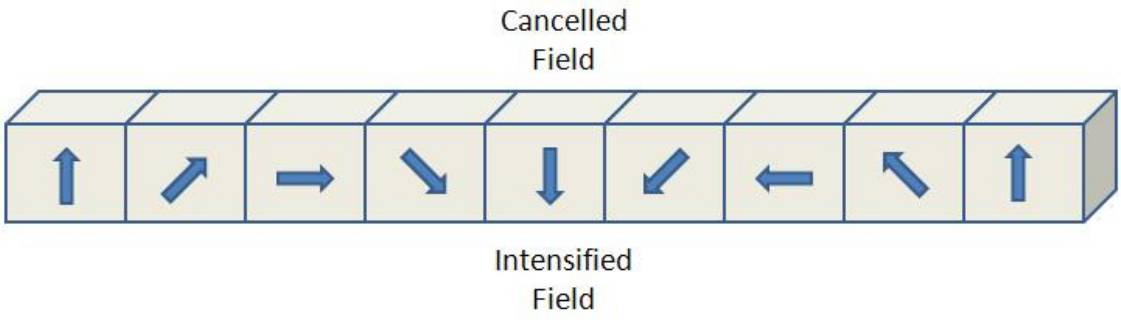


Figure 1.2.2-7 - Extended Halbach Arrays. This figure shows an extended Halbach array, which uses multiple sets of alternatively oriented magnets between active poles to redirect flux otherwise lost through the back-iron across the air gap.

However, even standard Halbach arrays have their draw-backs. As shown in Figures 1.2.2-6 and 1.2.2-7, Halbach arrays tend to consist of square blocks as opposed to longer arcs. This leads to a higher rotor pole count, driving the magnetic frequency up and increasing eddy current losses (described in Chapter 2.1), as well as presenting difficulties in controls and power regulation.

### 1.2.3 – CITATION SUMMARY

Traditional references for Permanent Magnet Machines assume the rotor / stator gap is air, with none of the major texts cited or studied addressing the concept of a liquid in the

gaps of PMM's. A major research paper by Nethe, et al., published in numerous journals, demonstrated a performance improvement for Permanent Magnet Machines using ferrofluid, and presented the effect as completely positive. However, several negative effects were omitted by the authors, such as the increased shear losses at high RPM, as their experiments were only performed to 500 RPM, and the potential for negative magnetic performance, as they neglected leakage flux considerations. Also, their experiments and analysis considered only radial flux and linear flux machines. Major texts on Ferrofluids, such as Ferrohydrodynamics by Rosenweig, list several applications for the material, but do not discuss immersion of a permanent magnet machine. This dissertation adds axial flux device optimization for ferrofluid immersion, as well as negative effects from ferrofluid immersion to the body of knowledge.

Secondary sources show industrial interest for improved gap performance and for ferrofluid applications of electromagnetic power conversion. At least one organization focuses their efforts on reduced gap reluctance, and numerous patents exist for non-traditional electromagnetic power conversion using ferrofluid. However, these ferrofluid devices have yet to gain a strong foothold in the market place, showing room for research and growth in this area.

## 1.3 OVERVIEW

This research focuses on the optimization of air gap elimination in permanent magnet machines. Mathematical models of the basics of fluid and magnetic effects are developed. Basic equations for motor / generator performance are presented, along with magnetic

circuit finite element analysis. These analytical tools are utilized as a macro-scale "virtual prototype" model, which is used to predict performance of ferrofluid immersed systems, and validated through a series of experiments. Finally, a new generator design was built and tested, demonstrating the potential performance improvement from air gap elimination in permanent magnet machines through ferrofluid immersion, as well as potential drawbacks from the approach.

Chapter 2 presents the basics of magnetics, providing the foundation to then focus on the specific applications of electromagnetism. These sections discuss the physics and mathematics of the system, showing why improved air gap permeability would be a benefit. The chapter then focuses on ferrofluids. It describes their physical composition and static properties, as well as the dynamic fluid flow effects specific to ferrofluids, known as ferrohydrodynamics. Also, drawbacks to ferrofluid immersion are discussed, including increased system losses from shear loss from the ferrofluid as opposed to windage from a standard air gap.

Chapter 3 details the "virtual prototype" developed for motor / generator development. A macroscopic model is presented, which is influenced by finite element calculations for component level effects, specifically saturation and leakage factors.

In Chapters 4-7, experimental results are presented, which validate the ferrofluid method, as well as the mathematical models. Chapter 4 presents an experiment featuring ferrofluid immersion of an off the shelf motor. The motor is baselined with its designed operation with a standard air gap. From there, the motor is immersed in a non-ferrofluid oil to study

the effects. An identical motor is then immersed in a ferrofluid of equivalent viscosity to study its operation relative to the air gap and to the non-magnetic fluid. Chapter 5 presents an experiment featuring a "proof of concept" new design. This design features an axial flux generator with a stator capable of ferrofluid immersion. Chapter 6 presents an experiment featuring a more repeatable design with a large stator –rotor gap. This design features an axial flux generator with a stator capable of ferrofluid immersion, with a containment tank to prevent ferrofluid leakage. The stator to cover gap is 0.282", offering a large benefit from the ferrofluid immersion. Chapter 7 presents an experiment featuring an identical system to the previous experiment, except for a smaller rotor to stator gap. The stator to cover gap is 0.032", and leakage flux is examined analytically as a performance factor.

Chapter 8 summarizes the thesis, and offers conclusions and areas of potential future research.

# CHAPTER 2 - FUNDAMENTALS OF MAGNETICS

This chapter provides a description of the physics and mathematics foundation of magnetics, providing the motivation for using increased permeability materials in the air gap.

Also presented is a description of electromagnetic power conversion, including typical motor and generator configurations that are standard in the industry. The physics and mathematics foundation of electromagnetics are provided, offering increased motivation for using increased permeability materials in the air gap. Also, drawbacks to the high permeability material approach, specific to the application, are presented, highlighting the limits of the technique and highlighting the need for a system engineered specifically for a non-air rotor / stator gap.

Finally, this chapter provides a description of ferrofluids, including fluid flow effects specific to ferrofluids, known as “ferrohydrodynamics”. The physics and mathematics foundation of ferrofluid behavior are provided, included both dynamic and magnetic considerations. Specific application considerations for ferrofluid immersion of electric motors and generators are discussed, including both positive and negative effects.

## 2.1 MAGNETICS

Understanding the basic physics of a system is critical to improving it. Before delving into the specifics of motor / generator design, it is important to first study the basics of magnetism. In its simplest terms, “Magnetism” is a property of a material describing its

response to an induced magnetic field. Highly magnetic materials contain domains that, in the absence of a magnetic field, are randomly oriented. When an external magnetic field is applied, these domains align, adding together to create a magnetic field of their own. For a given material exposed to a magnetic force, shown in figure 2.1-1, the magnetic flux density, $B$, is given by [1]:

$$B=\mu H \qquad 2.1\text{-}1$$

Where $H$ is the magnetic field strength and $\mu$ is the material's permeability.

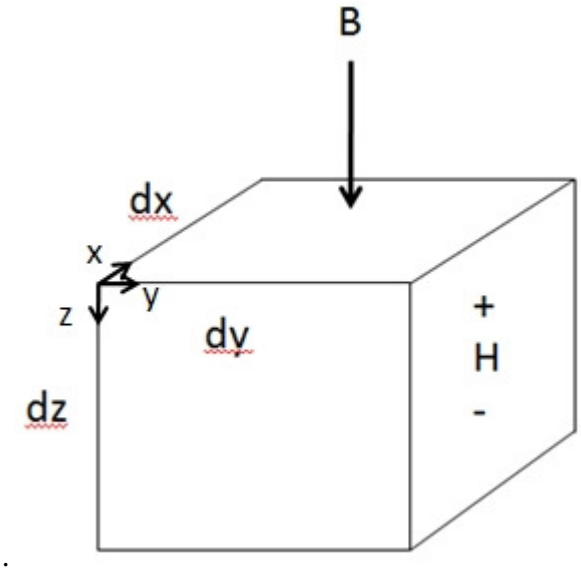


**Figure 2.1-1 – Magnetic Element.** This figure shows a magnetic element in its most simplistic form.

The total flux, $\phi$, is given by [1]:

$$\int \phi = B_z(x,y)dxdy \qquad 2.1\text{-}2$$

Which, for a constant cross-sectional area, $A$, reduces to:

$$\phi = B\,A \tag{2.1-3}$$

The magnetomotive force (MMF) for the material is given by [1]:

$$F = \int H dz \tag{2.1-4}$$

Which, for a constant cross-section across a length, $l$, reduces to:

$$F = H\,l \tag{2.1-5}$$

Substituting Eq. 2.1-5 and Eq. 2.1-3 into Eq. 2.1-1, we have:

$$\phi = u\,A\,F/l \tag{2.1-6}$$

Defining permeance, $P$, as $u*A/l$, generally, the ability of the material to transmit magnetic potential across its area per unit of length, and its inverse, reluctance, $R$, we have [1]:

$$R \equiv \frac{1}{P} = \frac{l}{uA} \tag{2.1-7}$$

Expressing Eq. 2.1-6. in terms of reluctance, we have:

$$F = \phi\,R \tag{2.1-8}$$

This presents the magnetic force in an "Ohm's Law" style form, which can be used for magnetic circuit analysis [6]. Figure 2.1-2 shows a simplified permanent magnet machine, with an overlay of a magnetic circuit, where $\phi$ is the flux from the magnets, $\phi_l$ is the "leakage flux", $\phi_g$ is the flux transmitted through the air gap, $R_m$ is the reluctance in the magnets themselves, $R_r$ is the rotor reluctance, $R_s$ is the stator reluctance, $R_l$ is the leakage reluctance, and $R_g$ is the airgap reluctance. Resistors represent magnetic

reluctance values of the various elements of the system. The permanent magnets in the system are represented by current sources in opposing directions, in accordance with the North-South orientation of the magnetic polarity. Current sources represent the remanent magnetic flux values, $B_r$, of the permanent magnets.

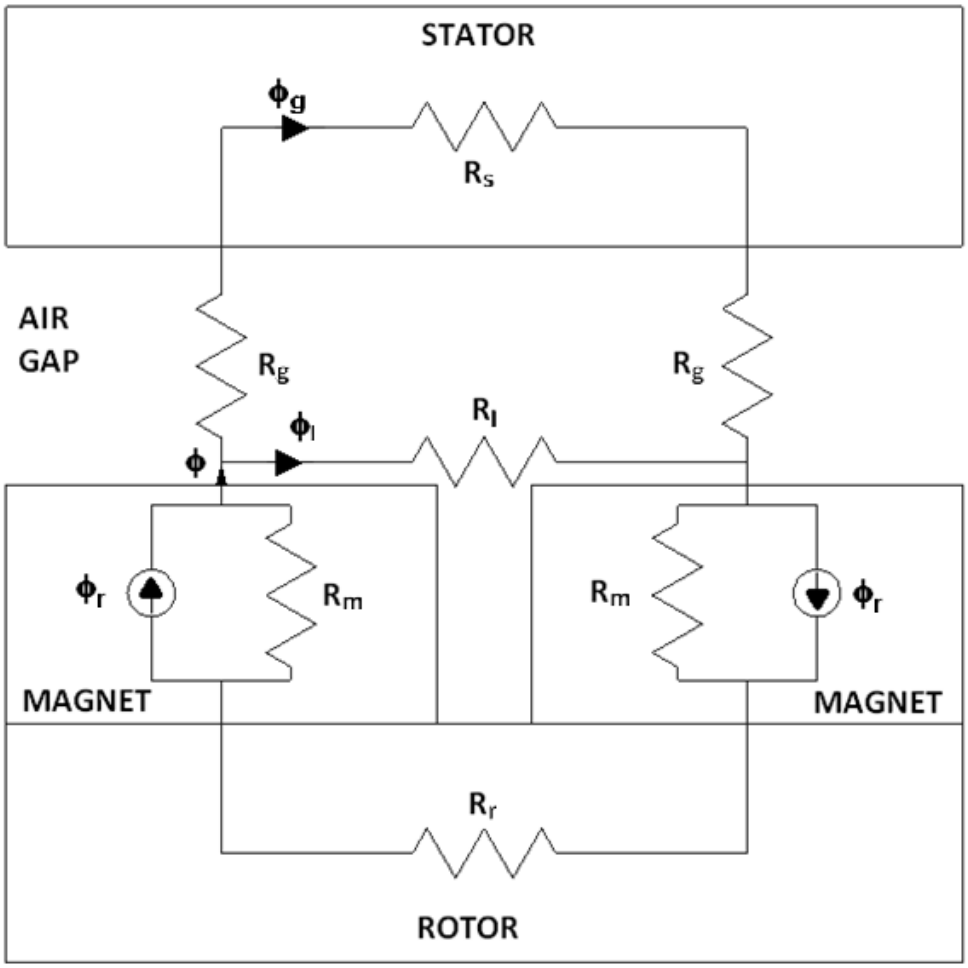


Figure 2.1-2 – PMM Resistor Network. This figure shows a basic resistor network of a Permanent Magnet Machine.

Considering the importance of the relative terms, the air gap reluctance tends to dominate the circuit. The permeability of air is $4\pi\times10^{-7}$ Henries / meter (Newtons/Ampere$^2$) [1], whereas the permeability of even low grade magnetic steel is several orders of magnitude higher in the non-saturated region (~$8.75\times10^{-4}$ Henries / meter) [1]. However, magnetic permeability is a non-linear property of ferromagnetic materials. Figure 2.1-3 shows the relationship between magnetic flux density, *B,* and magnetic field strength, *H*, for D6ac steel [32]. Materials cannot support unlimited amounts of magnetic flux. Ferromagnetic materials pass magnetic flux through an alignment of the domains inherent in their crystalline / microscopic structure [1]. Once all domains in a material are in alignment, "magnetic saturation" occurs, and additional magnetic flux density exposure leads to logarithmically declining returns. Dependent on all of the components in the magnetic circuit, the saturation factor requires FEA to determine for complex geometry.

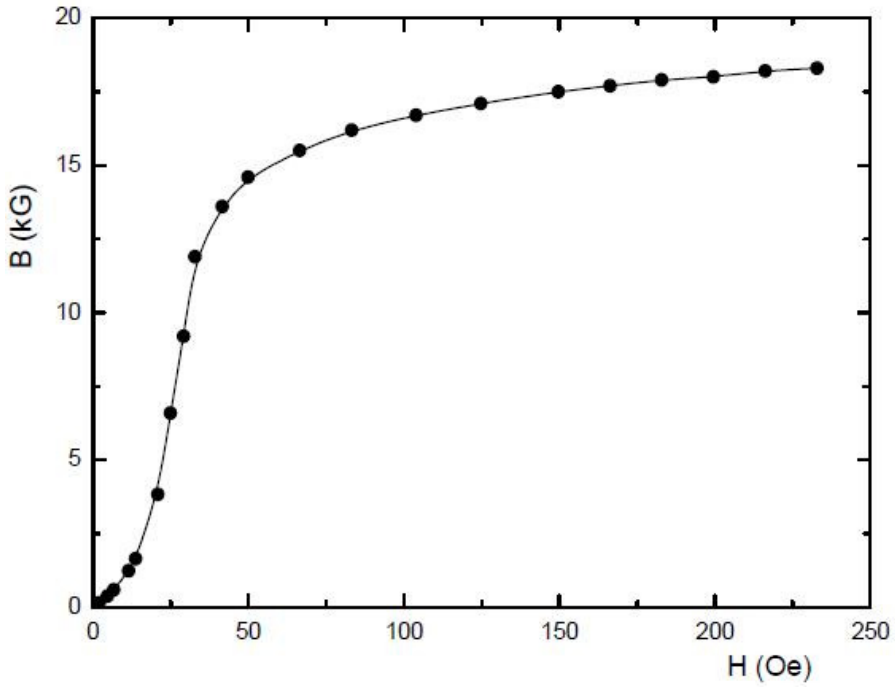


Figure 2.1-3 - Magnetic Flux Density (B) – Magnetic Field Strength (H), D6ac Steel [32]. This figure shows the Flux Density (B) vs. Field Strength (H) for a steel material. Note the non-linear nature of the relationship and limits of increasing Flux Density.

Besides saturation, another source of magnetic inefficiency is leakage flux. As shown in Figure 2.1-2, magnetic flux responds similar to other basic flow phenomenon, and follows the path of least resistance. Depending on geometry and material properties, magnetic flux may flow through the desired channels, or, if the reluctance is lower for another path, jump over to other areas of the magnetic circuit. Leakage flux is dependent on the specific design of all of the components in the magnetic circuit, and requires FEA to determine for complex circuits. The leakage factor is defined as [2]:

$$f_{LKG} \equiv \frac{\phi_g}{\phi} \qquad 2.1\text{-}9$$

Solving for the network shown in figure 2.1-2, we have:

$$\phi_g = f_{LKG}\phi = \frac{f_{LKG}}{1 + \frac{Rg}{Rm}}\phi_r \qquad 2.1\text{-}10$$

In terms of flux density across the air gap, $B_g$:

$$B_g = \frac{f_{LKG}}{1 + f_{LKG}\frac{Rg}{Rm}}\frac{Am}{Ag}B_r \qquad 2.1\text{-}11$$

Where $A_m$ is the area of the magnet, $A_g$ is the area of the air gap, and $B_r$ is the remnant flux of the permanent magnet.

Studying Eq 2.1-11, we can see ways to improve magnetic flux translated across the air gap. Remnant flux density ($B_r$), the "permanent" magnetic field in a permanent magnet, could be increased. This is a factor of the magnets themselves, and is somewhat intuitive (stronger magnet=stronger performance). Leakage factor ($f_{LKG}$) could be increased**.** This is a factor of the overall geometry of the complete magnetic circuit. Decreased performance from increased leakage will be discussed later in this paper (see chapter 3). The magnet size relative to the air gap could be increased. While "overhanging" the magnets past the stator provides some benefits, the air gap tends to be the same cross section as the magnets. Magnet reluctance could be increased. This is a factor of the magnets themselves, and is somewhat intuitive (thicker magnet=stronger performance). Airgap reluctance could be reduced. As discussed, the air gap must be larger than the tolerance stack-ups from the variation in each applicable component to avoid interference

issues. Shock, vibration, thermal expansion, rotational forces, magnetic stresses, and other dynamic loading conditions add to the air gap required for safe operation, reducing the ease of simply reducing the air gap in most configurations. This leaves increasing the permeability of the air gap as an option for improved performance, which is the focus of this research.

## 2.2 FUNDAMENTALS OF ELECTROMAGNETISM

The primarily application of magnetics that is the focus of this study is permanent magnet machines (PMM's). PMM's offer numerous advantages compared to traditional field wound electromechanical conversion systems. In traditional, "field wound" systems, an example of which is shown in figure 2.2-1 [21], a magnetic field is generated by powering a set of stator coils wrapped around a set of iron poles. This, in turn, excites a second set of coils wrapped around a second set of iron poles on the rotor, producing torque / RPM in motor applications. For generator applications, torque and RPM in addition to the supplied electrical power, produce voltage and current. In both cases, electrical power is transmitted from the rotating components through slip rings or "brushes".

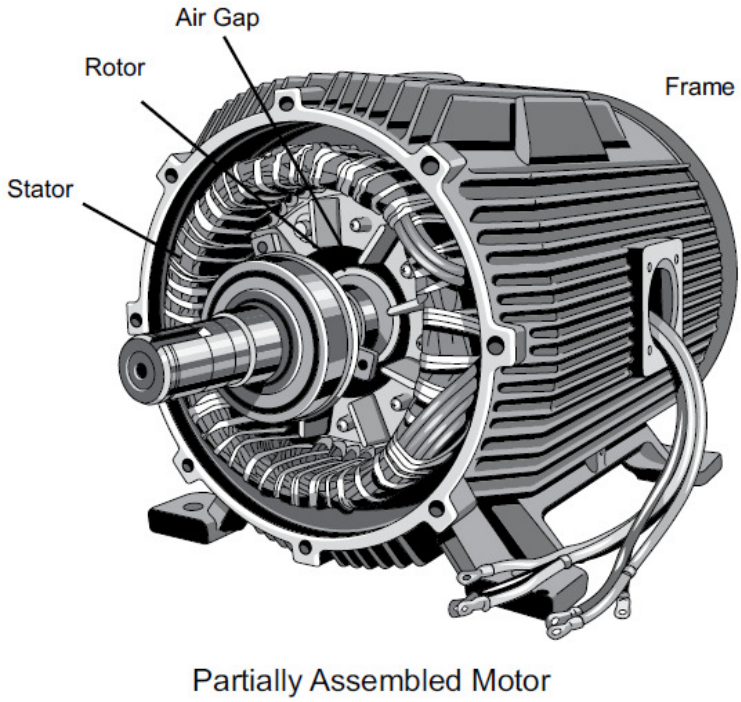


Figure 2.2-1 – Traditional Brushed Motor / Generator [21]. This figure shows a CAD model of a traditional non-permanent magnet motor / generator.

Traditional field wound systems suffer from numerous inherent inefficiencies. The copper in both the rotor and the stator have losses equal to the square of the current times the resistance of the wire. Slip rings suffer from frictional losses, and are a source of wear and breakdowns. Leakage flux, referred to as "stray load losses" occur in both rotor and stator, and is discussed in more detail in Chapter 3. The iron in both the rotor and the stator suffer from "eddy current losses" which result from changing electrical fields introducing a parasitic perpendicular reactionary electromagnetic effect in the magnetic medium. Eddy current losses can be reduced by providing resistance to the perpendicular electromagnetic flow by using laminated insulated magnetic materials as opposed to solid conductive structures, but these losses cannot be eliminated.

Compared to these systems, PMM's offer the following benefits:

- **Higher efficiency.** PMM's do not experience rotor copper losses and have fewer stray load losses, with much lower rotor iron losses, which generate 40-50% of the inefficiencies of traditional induction machines [10].
- **Higher reliability.** PMM's do not have "brushes" or slip rings to transfer power by directly linking rotating electrical wires to a stationary connection. These connections are a constant source of wear / fatigue failures in traditional electric motors and alternators.
- **Higher power density**. Permanent Magnets, especially high performance materials such as Neodymium/Iron/Boron, have exceptionally high magnetic flux densities, and can generate higher magnetic fields for a given size, improving power density [2].

However, there are numerous challenges inherent in the design of PMM's. As shown in equation 2.2-6, voltage is proportional to speed. As a PMM generator operates, raw voltage is produced which varies in both voltage and frequency. This "wild AC" voltage must be regulated to produce stable DC voltage required for most applications, then inverted back to controlled AC for standard plug-in devices. Large RPM ranges provide challenges to electrical systems, which must be flexible enough to handle the variable input. High voltage is also a safety concern, providing a potentially fatal hazard in the

high speed / high voltage rotating machines and associated power transmission lines. Efficiency losses for the electrical conversion can be a large part of overall system performance.

Higher strength Neodymium Iron Boron is sensitive to demagnetization at elevated temperatures. Samarium Cobalt is more temperature resistant than Neodymium, but higher in cost and lower in maximum energy product. Figure 2.2-2 shows a typical demagnetization curve for a rare earth magnet, N40, which is a Neodymium Iron Boron Material with a 40 MegaGauss Oersted Maximum Energy Product [39]. Various temperature curves and performance curves are shown for the material. The "Performance Coefficient", Pc, is known as the "Load Line", with its slope related to the amount of magnetic field exposure of the magnet. Low values of Pc correspond to high magnetic field strength, while high values correspond to low strength magnetic fields. Demagnetization occurs when the material is exposed to a combination of temperature and magnetic field strength which brings the magnet past the "knee point" of the curve. In general, the higher the maximum energy product of the magnet, the lower the maximum operating temperature will become.

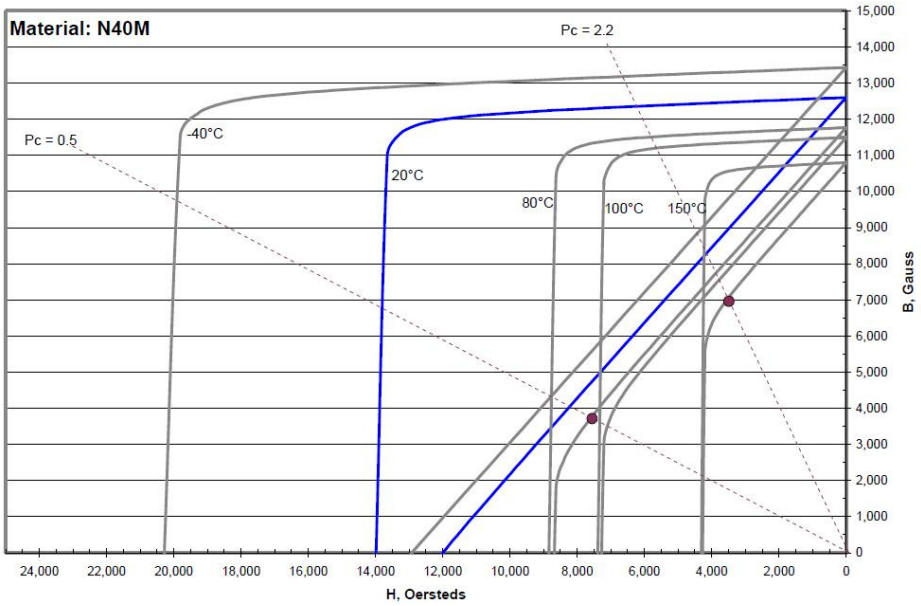


Figure 2.2-2 – Demagnetization Curve for N40M Rare Earth Magnet [39]. This figure shows a graph of the magnetic performance of a Neodymium Iron Boron grade of material. Summarizing, the magnetic performance of the material decreases with increasing temperature or increased magnetic field exposure. “Permanent” magnets lose their residual magnetism when exposed to temperatures beyond their rated temperate, when exposed to strong magnetic fields, or a combination of both factors.

Rare earth magnetic materials, such as neodymium and dysprosium, a key element in most Neodymium Iron Boron Formulations, can be a procurement challenge with China nearly cornering the market on the rare earth supply chain [22]. Reducing the need for high strength rare earth magnets by gaining more efficiency from abundant, but weaker strength / lower cost materials such as ferrite could be presented as a benefit for reducing dependence on constrained resources.

Cooling is also an issue with permanent magnet machines. Airflow is difficult to pass through high power density systems. Liquid cooling options require piping systems,

reducing volume available for power creation, and require pumps, heat pipes, and other cost adding components and system integration challenges.

Despite these challenges, for applications sensitive to efficiency, reliability, and / or power density, the benefits outweigh the cost, as evidenced by the growth in the market for PMM's.

The three most common types of motor / generator PMM's are axial flux, interior radial flux, and exterior radial flux[1]. In an axial flux PMM, disc-shaped permanent magnet layers rotate past stationary poles and windings. Axial flux PMM's are often referred to informally as "pancake motors" due to their distinctive shape. These designs tend to allow a very small air gap, as the centripetal acceleration acts in the perpendicular direction of the air gap, resulting in no additional clearance required for dynamic effects. The small air gap results in potentially high efficiencies, reaching up to 98% in specialized applications [4]. Figure 2.2-3 shows an example of an axial flux PMM [7].

[1] Transverse-flux and other less common / more exotic designs of course exist, but, in order to limit the scope of this report, will not be discussed in detail here.

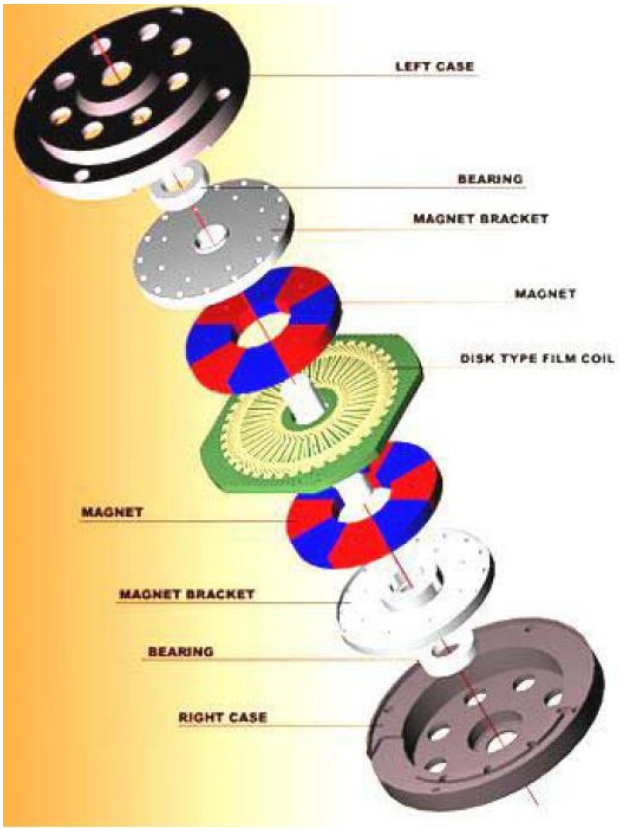


Figure 2.2-3 - Axial Flux PMM [7]. This figure shows an example of a Permanent Magnet Machine design with an axial flux configuration.

In interior radial flux motors, the magnets are attached directly to the drive shaft or embedded in a rotor steel lamination stack attached to the shaft, as shown in figure 2.2-4, and are on the inside of the windings. The embedded lamination stack style, known as "IPM style" is a popular commercial choice, the most well known application being the Toyota Prius hybrid electric drive motor [5]. The IPM style offers a low cost system to retain the magnets in high speed applications and enables block shape magnets, which are low in cost and "off the shelf" compared to the custom arc shapes required for a constant air gap in rotor surface mounted magnetic designs. Interior magnets can also provide a smaller air gap compared to an exterior rotor systems, described in the next section, as

the magnet “cup” of exterior styles adds to the tolerance stack up and has greater displacement in dynamic effects.

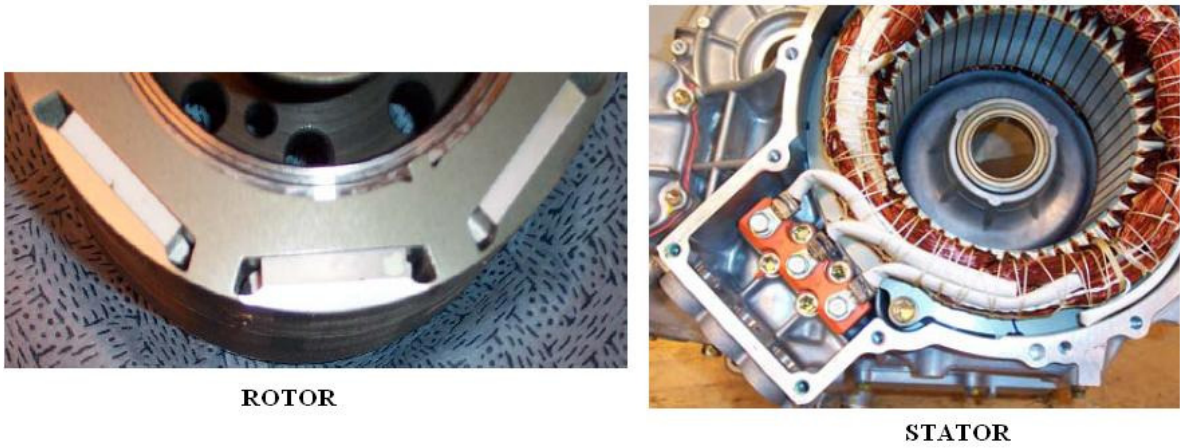


Figure 2.2-4 - Interior Magnet PMM [5]. This figure shows an example of a Permanent Magnet Machine design with a radial flux configuration and the magnets located on the interior of the stator windings.

In exterior radial flux motors, an example of which is shown in Figure 2.2-5, the magnets are located outside of the windings. As shown in Equation 2.1-11, magnetic flux is proportional to the area of the magnets, and, as described in Equation 2.2-9, efficiency is proportional to a squared factor of the magnetic flux. By placing the magnets on the exterior of the windings, these style motors offer a larger surface area for the magnets compared to interior rotors. Designing the magnets on the exterior of the stator allows the radius of the magnets to be larger than the stator by the air gap distance. This provides advantages in power density in the diametric form factor. Also, as shown in Figure 2.2-4, for interior styles of PMM, the windings are encased by the stator back-iron. This leads to challenges in winding, as automated tools, or even hand insertion techniques, must navigate through the limited space in the interior of the stator. With outward facing stator

poles, as shown in Figure 2.2-5 [26], exterior rotors suffer from no such limitations in space for windings and related tooling, which provides advantages in ease of manufacturing.

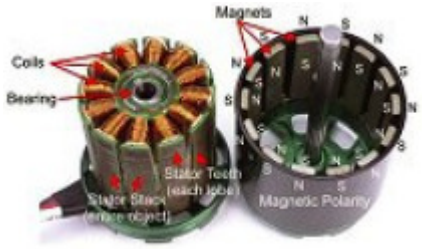


Figure 2.2-5 - Exterior Magnet PMM [26]. This figure shows an example of a Permanent Magnet Machine design with a radial flux configuration and the magnets located on the exterior of the stator windings.

The primary physics behind PMM electromechanical power conversion begins with the Maxwell equations [1]. Looking at the Maxwell-Faraday Equation (Faraday's Law of Induction) shown in equation 2.2-1 and Ampere's circuital law, equation 2.2-2:

$$\nabla \mathrm{X} E = -\frac{\delta B}{\delta t} \qquad 2.2\text{-}1$$

$$\nabla X B = \mu J + \mu\epsilon \frac{\delta E}{\delta t} \qquad 2.2\text{-}2$$

Where $\nabla$ is the del operator, $E$ is the electric field, $B$ is the magnetic field, $t$ is time, $J$ is current density, $\mu$ is magnetic permeability, and $\epsilon$ is permittivity, the ability of a material to transmit an electrical field. We can see that a changing electric field results in a changing magnetic field, and vice versa. By attaching magnets in alternating polarity to a rotating shaft, and rotating that shaft past a series of electrical coils, torque and rotational velocity can be converted to voltage and current (generator applications), or current and

voltage can be applied to the electrical coils, producing torque and rotational velocity (motor applications).

The basic equation for power balance in electromagnetic conversion [2] can be given by:

$$T\omega = V\ I\ K \tag{2.2-3}$$

Where $T$ is torque, $\omega$ is the rotational velocity, $V$ is voltage, $I$ is current, and $K$ is the system efficiency. This can be broken down into Torque and RPM components as follows [2]:

$$K = Ke\ kT \tag{2.2-4}$$

$$\mathrm{T} \approx \mathrm{I}\ B\ Kt \tag{2.2-5}$$

$$\mathrm{RPM} \approx \mathrm{V}\frac{Ke}{B} \tag{2.2-6}$$

Where $Ke$ is the speed constant, and $Kt$ is the torque constant. The equations for the speed constant are torque constant [3] are given by:

$$Kt = \frac{m_1}{\sqrt{2}} p N_1 k_{w1} \Phi_f \tag{2.2-7}$$

$$Ke = \pi\sqrt{2} p N_1 k_{w1} \Phi_f \tag{2.2-8}$$

Where $m_1$ is the number of phases, $p$ is the number of poles, $N_1$ is the number of turns in series per phase, $k_{w1}$ is the winding factor, and $\Phi_f$ is the magnetic flux, given by:

$$\Phi_f = B_{mg} A_{eff} \tag{2.2-9}$$

Where $A_{eff}$ is the effective area and $B_{mg}$ is the flux density across the airgap. Substituting 2.2-9 into 2.2-7 and 2.2-8 and substituting those results into 2.2-4, the system efficiency is given by:

$$K = \pi m_1 p^2 N_1^2 k_{w1}^2 B_{mg}^2 A_{eff}^2 \quad \text{2.2-9}$$

Thus, we can see that increasing the flux density across the air gap is a squared factor in increasing the efficiency of the machine, and is the focus of this research.

Equation 2.2-9 shows the various methods of getting additional performance from a PMM. Some of these methods, such as increasing area, come with penalties in increased weight, and are sometimes not feasible for the given space for the application. Others, such as increasing speed, come with reliability drawbacks, as greater rotational velocity increases bearing wear and dynamic stress on rotor components, as well as increasing windage losses. However, increasing the magnetic flux across the airgap by decreasing the airgap or increasing the permeability can increase the performance of the PMM without increasing the size or weight. Lower air gap distances or improved permeability would result in more efficient machines, capable of higher power density and higher torque density.

However, smaller air gaps come with a tradeoff in terms of manufacturability and greater risk factors / performance limitations due to displacement for dynamic loading conditions and thermal expansion and contraction. For vehicle applications, dynamic loads also include induced shock and vibration. At a minimum, even for stationary devices, such as

land based generators, the air gap must be larger than the tolerance stack-ups from the variation in each applicable component to avoid interference issues. Shock, vibration, thermal expansion, rotational forces, and other dynamic loading conditions add to the air gap required for safe operation.

## 2.3 Permanent Magnet Machines – Air Gaps

Efficiency losses related to the air gap have been estimated at >11% of total system losses in electric motors and generators, as shown in Table 2.3-1 [8]. Core losses, estimated at ~ 20% of total system losses, include eddy current losses, described in chapter 2.2, magnetic saturation, described in section 2.1 (see Figure 2.1-3), and losses across the air gap, the main topic of this paper. Friction and windage losses, which are size and speed dependent, making them vary greatly from system to system, are described in more detail in section 2.4.1. Stray load losses occur from leakage flux, described in more detail in section 3, and are dependent on design geometry and manufacturing tolerances. Stator losses are given by equation 2.3-1 [2]:

$$W_s = I^2 \, \Omega \qquad 2.3\text{-}1$$

Where $I$ is current, $\Omega$ is resistance, and $W_s$ is power lost through stator coil resistance.

In traditional field wound systems, eddy current losses also occur in the rotor, and the rotor also suffers from resistive "$I^2R$" losses. Permanent Magnets Machines provide efficiency improvements by eliminating these sources of loss.

**COMPARISON OF LOSS DISTRIBUTION BY PERCENT FOR MOTORS TESTED IN THE EASA/AEMT STUDY [12].**

| Losses | Two-Pole Average | Four-Pole Average | Design Factors Affecting Losses |
|---|---|---|---|
| Core losses ($W_c$) | 19% | 21% | Electrical steel, air gap, saturation, supply frequency, condition of interlaminar insulation |
| Friction and windage losses ($W_{fw}$) | 25% | 10% | Fan efficiency, lubrication, bearings, seals |
| Stator I2R losses ($W_s$) | 26% | 34% | Conductor area, mean length of turn, heat dissipation |
| Rotor I2R losses ($W_r$) | 19% | 21% | Bar and end ring area and material |
| Stray load losses ($W_l$) | 11% | 14% | Manufacturing processes, slot design, air gap, condition of air gap surfaces and end laminations |

Table 2.3-1 - Losses in Permanent Magnet Machines [8]. This figure summarizes the losses in Permanent Magnet Machines. Losses partially related to air gap design are core losses and stray load losses, which sum to 30-35% of the losses of the machine.

However, in order to avoid electrical shorts between various phases and windings in motor / generator applications, the material in the gap must be electrically insulative. Also, any material change would ideally improve the heat transfer mechanisms in the system. All power lost in electromagnetic power conversion ultimately ends up in the system as heat, which must be dissipated from the system to prevent thermal rises that would take the winding insulation beyond its rated temperature, increase the magnet temperatures beyond their demagnetization point, or cause system failure in other thermal related modes.

The air between the rotor and stator is used in convective cooling in the complex thermal systems of motor / generators as seen in Figure 2.3-1 [14]. The thermal network shown below relies on air cooling. Heat sources, shown as two circles, transfer heat through various materials containing a thermal resistance, shown as a rectangle, or have some thermal capacitance, shown as two parallel lines. A permeable liquid material would

provide not only magnetic benefits, but improved thermal performance as well. Every thermal resistor in the network that is air-based would improve, specifically the stator core / frame interface, heat transfer across air gap, and direct convection from rotor to frame. Also the thermal capacity of the fluid would increase, specifically air absorption. This effect is not unique to ferrofluids; any liquid immersion would have a positive cooling effect.

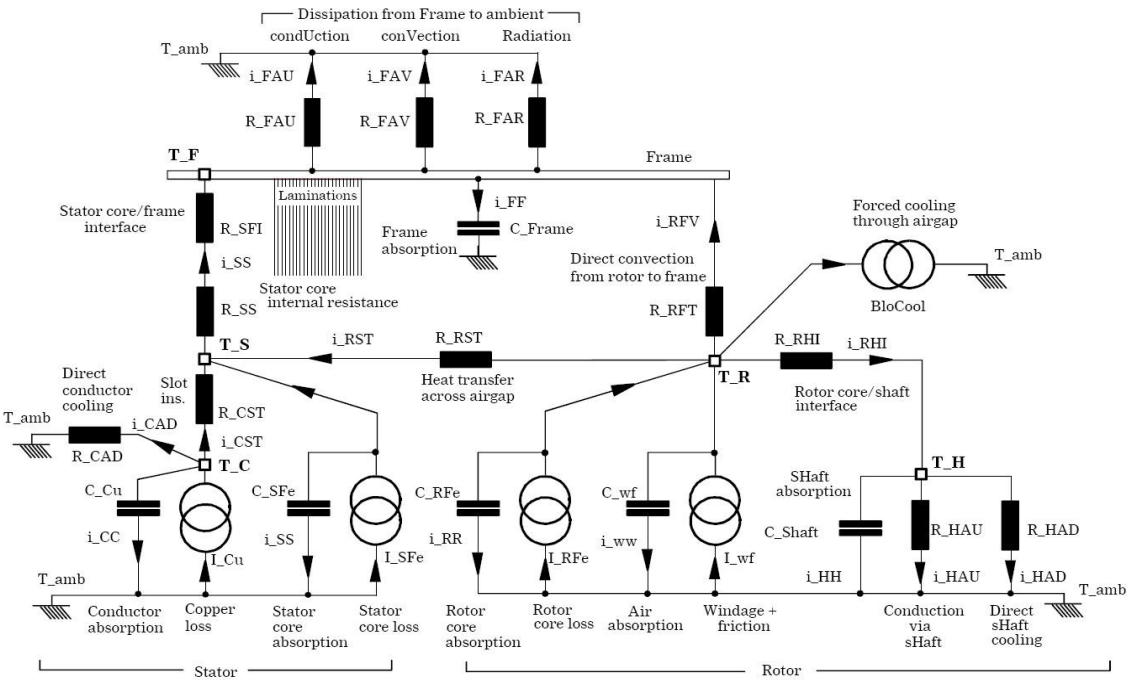


Figure 2.3-1 - Thermal System Diagram, Electric Motor [14]. This figure shows a thermal network for an electric motor. For a liquid gap, as opposed to air, improvements would be seen in Air Absorption, Direct Convection from rotor to frame, and Heat Transfer across air gap. Negative effects would occur in Windage – friction.

As an additional benefit for magnetically permeable liquid immersion, cogging torque can be reduced. Cogging torque is the unsteady torque output dominated by the magnets attempting to align to a set of stator poles. While this may be a desirable effect in

servomotors or stepper motors, where a rotor must be continually indexed to a set position, for generator applications and continual duty motors, cogging torque is a negative effect. Cogging torque results in efficiency losses, noise / vibration in the system, higher required starting torque, unwanted harmonics, and other issues. Higher permeability gap materials would reduce the large variation between the permeability of the stator poles and the air, which the magnets see as "bumps" in the rotational path. Figure 2.3-2 [14] shows a typical motor design in terms of magnetic flux density variation. Increasing gap permeability would reduce this variation, thus decreasing the magnitude of the variations in B(θ) and reducing cogging torque.

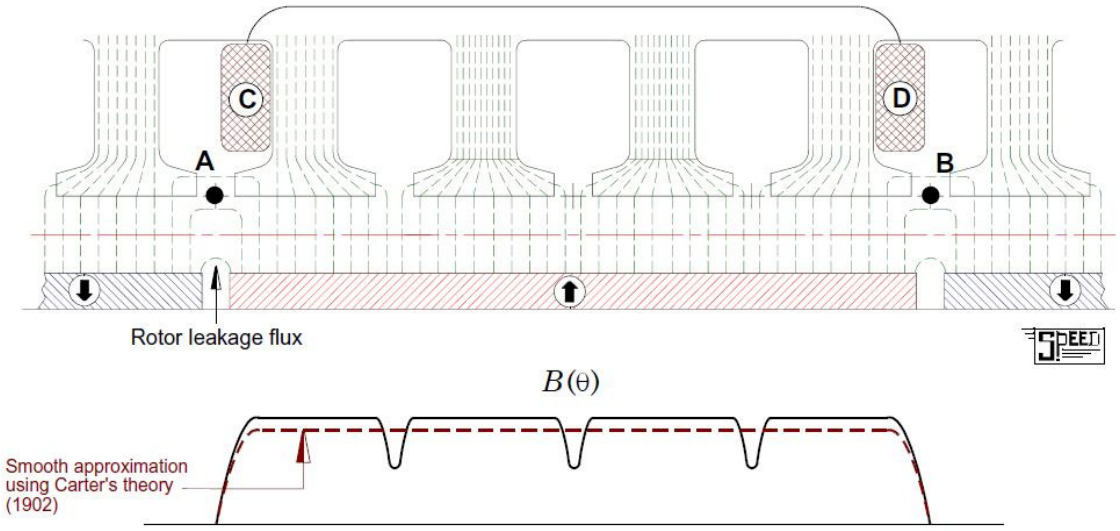


Figure 2.3-2– Graphical Representation of Cogging Torque [14]. This figure shows a graphic of variation in magnetic flux density across stator poles due to the large difference in permeability between the gap and the iron poles. With a permeable fluid, this variation would decrease.

## 2.4 FUNDAMENTALS OF FERROFLUIDS

A ferrofluid is a stable colloidal suspension of nanoscale magnetic particles in a liquid carrier [11]. Colloids, such as milk (butterfat and proteins suspended in a water-based fluid), consist of microscopic particles evenly dispersed throughout a carrier fluid. As opposed to magnetoheological fluids, which contain larger (micrometer scale) particles, which can settle over time and completely solidify in the presence of a strong magnetic field, ferrofluids are stable and provide a homogenous composition throughout their lifespan [11]. Ferrofluids maintain their liquid state regardless of magnetic field strength (although magnetism does affect its viscosity, as will be discussed). Ferrofluid particles are coated with a stabilizing dispersing agent, called a surfactant, with a chemical polarity. This prevents particle agglomeration even when a strong magnetic field is applied to the ferrofluid. Figure 2.4-1 [11] shows a crude molecular sketch of a ferrofluid. The central molecule, based on iron, has a magnetic susceptibility, aligning in the presence of a magnetic field. The surfactant coating has an atomic polarity, repelling the molecules from each other, which keeps them from conglomerating.

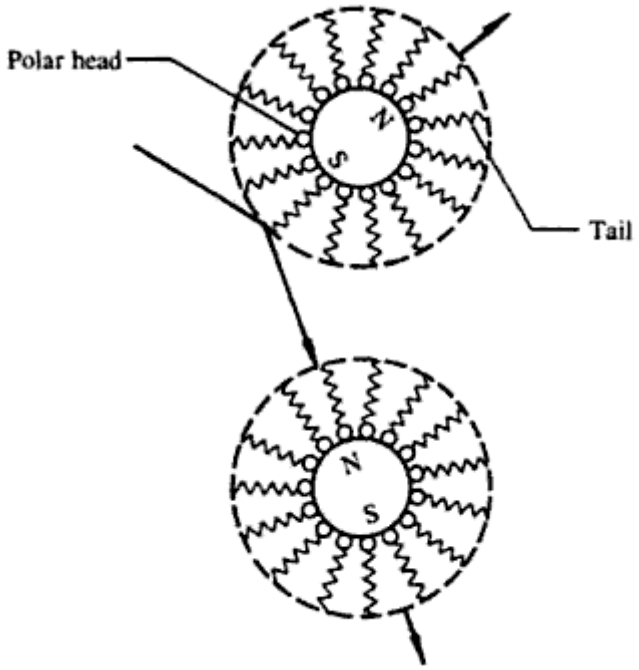


Figure 2.4-1 - Ferrofluid Microscopic Sketch [11]. This figure shows an atomic level sketch of a ferrofluid. The polarized tails contain a chemical polarity greater than the potential magnetic forces, keeping the material from conglomerating.

In the absence of a magnetic field, the magnetic moments of the particles are randomly distributed and the fluid has no net magnetization. When a magnetic field is applied to a ferrofluid, the magnetic moments of the particles orient along the field lines almost instantly. The magnetization of the ferrofluid responds immediately to the changes in the applied magnetic field and when the applied field is removed, the moments randomize quickly.

As a colloidal substance, ferrofluids are comprised of individual particles, whose size and distribution can vary. Ferrofluids can be engineered for various applications with total particle count ranging from small amounts (<1%) to a relatively large amount of the overall fluid composition by volume, but typically maxing out under 20% due to current

process and practical limitations. A typical ferrofluid may contain by volume 5% magnetic solid, 10% surfactant and 85% carrier. Within the given percentage of particles, the size of the individual particle will vary.

Generally, the effects of larger particles are negative, as with larger particle sizes, particles tend to agglomerate [11]. These agglomerates form effectively larger magnetic bodies, which would have a larger dipole moment collectively. Moreover, the newly formed clusters could act as nucleation sites for further agglomeration, by capturing large particles and having the magnetic strength to capture smaller particles over time. However, larger particles offer increased permeability, so a greater number of smaller particles must be present to make up for any decrease in particle size.

A measure of permeability often used to describe materials is relative permeability, $\mu_r$,defined as [1]:

$$\mu_r \equiv \frac{\mu}{\mu_o} \qquad 2.4-6$$

Where $\mu$ is the material's permeability and $\mu_o$ is the permeability of air ($4\pi\times10^{-7}$ Henries/meter) [1]. The relative permeability of a ferrofluid, to some extent, can be engineered to specification, but is limited by the amount of carrier fluid and surfactant required. Typical values range from 2 to 10 in low magnetic fields, but the permeability is dependent on the applied magnetic field, as shown in figure 2.4-2 [13], with stronger magnetic fields decreasing the relative permeability of the ferrofluid. Various plots are

shown for various formulations of ferrofluid, showing increased permeability with increased concentrations of iron particles.

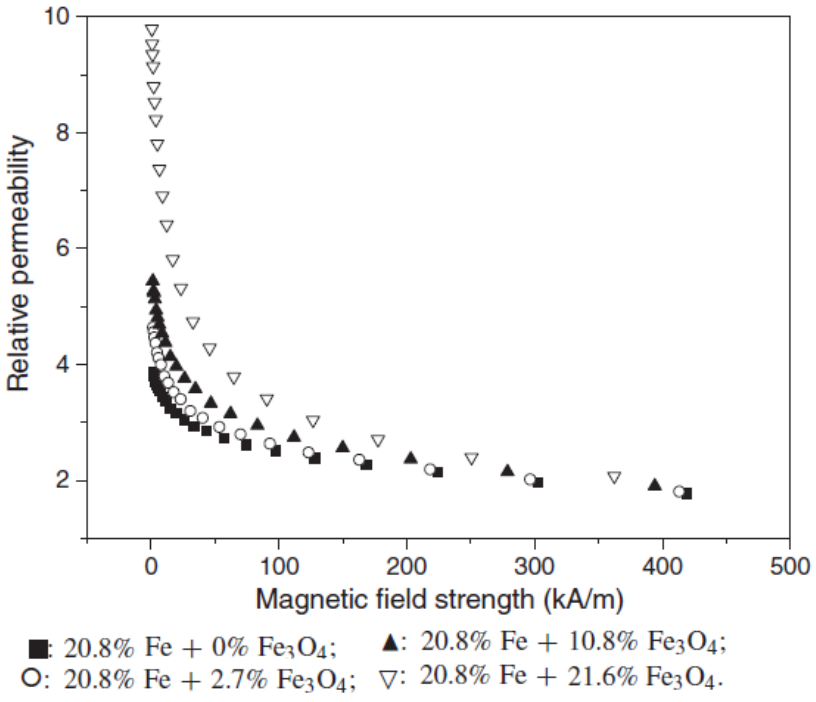


Figure 2.4-2 - Ferrofluid Permeability [13]. This figure shows the magnetic permeability of various formulations of ferrofluids in a graph of Relative Permeability vs. Magnetic Field Strength. Note that for significant magnetic fields, regardless of formulation, the relative permeability reduces to a value ~ 2.

### 2.4.1 Tradeoffs to Ferrofluid Immersion

While the improved magnetic permeability of ferrofluid offers performance benefits for the magnetic circuit, it comes with a tradeoff in terms of windage / shear force losses, which are the frictional losses inherent in any solid body moving through a fluid. Looking at the basic equation for shear losses we have [11]:

$$\tau = \eta \frac{dv}{dy} \qquad 2.4.1\text{-}1$$

Where $\tau$ is the shear stress, $\eta$ is the fluid viscosity, $v$ is the velocity, and $y$ is the gap distance. From equation 2.4.1-1, we can see that the shear losses are proportional to the fluid viscosity, system speed, and inversely proportional to length. Looking at terms that do not charge by changing the gap material, speed and air gap size, we can see that higher speeds and small air gaps lead to increased losses. For a ferrofluid, this rather straightforward equation can have some subtle terms that complicate the shear calculation, as the viscosity of a ferrofluid is dependent on magnetic factors as well as its chemical composition.

Ferrofluids can be engineered from a wide variety of carrier fluids. The carrier fluid properties dominate the viscous properties of the material. Table 2.4.1-1 shows a sample of common carrier fluids and their viscosity values. Note that the viscosity of the fluids starts around three orders of magnitude higher than air. Given the relative permeability limits of ferrofluids, the overall effects of complete ferrofluid immersion would be negative in high velocity or small air gap systems.

| Carrier Fluid | Viscosity (cP) | Density (kg/m^3) | Typical Application |
|---|---|---|---|
| Synthetic Light Hydrocarbon Oil | 2-8 | 500 | Audio Speakers |
| Synthetic Heavy Hydrocarbon Oil | 60 | 1000+ | Non-evaporative applications |
| Ester Oil | 2-5 | 870 | Audio Speakers |
| Water | 1-2 | 1000 | Biomedical |
| Air | 0.02 | 1.28 | Provided for Reference |

Table 2.4.1-1 – Ferrofluid Viscosity and Density. This table shows the viscosity and density of several variations of ferrofluids. Values for air are provided as a reference.

Prior research [11] has shown that ferrofluid shear stress can increase with flux density as well, as internal magnetic spin of the ferrofluid particles contributes to opposing the flow velocity. The change in viscosity in terms of the magnetic force is given by [11]:

$$\Delta\eta = \vartheta\left(1 + \frac{2\omega_y d}{v}\right) \qquad 2.4.1\text{-}2$$

Where $\eta$ is the fluid viscosity, $\vartheta$ is the vortex viscosity coefficient, which is proportional to the magnetic energy / thermal energy, and thus dependent on particle size, $\omega_y$ is the vortex velocity, $d$ is the airgap distance, and $v$ is the linear velocity.

The vortex viscosity is directly proportional to the applied magnetic field, as shown in equation 2.4.1-4 [11]:

$$\omega_y = \frac{1}{2}\nabla X v + \frac{\mu}{4\vartheta} MXH \qquad 2.4.1\text{-}4$$

Where $M$ is the magnetization of the domain.

From these equations, we can see the increase in viscosity becomes less prevalent in systems with low magnetic energy, high velocities, small air gaps, and small particle size. Figure 2.4.1-1 [16] shows the results of increased shear rate, $\dot{\gamma}$, and magnetic field strength, $H$, on several samples of various particle sizes (increasing in diameter from F1=8 nm to F5=11 nm). Studying Figure 2.4.1-1, we can see that the smallest particle size, 8 nm, had no Ferrohydrodynamic effects on viscosity. This highlights the

importance of maintaining small particle size in precision applications. Also, we can see that in areas of weak magnetic fields, viscosity increases are small to non-existent, showing that a key area for the application is in low magnetic strength circuits. Finally, we can see the effects decrease with increasing shear rate, which shows that high velocity systems suffer from minimal viscous increases.

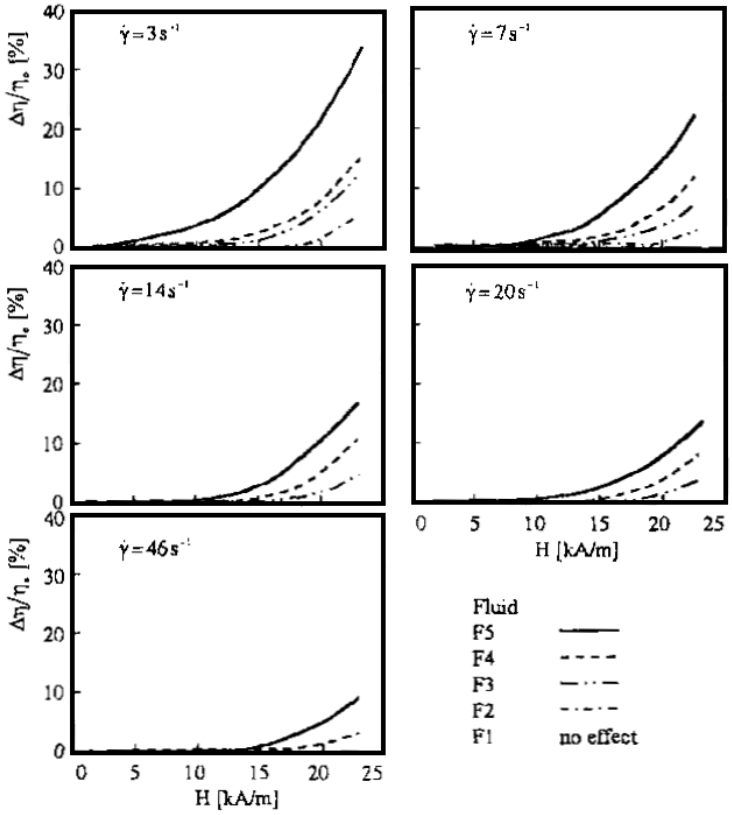


Figure 2.4.1-1 – Effect of Shear Rate and Particle Size on Ferrohydrodynamic Viscosity Increase [16]. This figure shows the effect of increased shear rate, $\dot{\gamma}$, and particle size, given by various plots, F1-F5, on ferrohydrodynamics, plotting the change in fluid viscosity, $\Delta\eta/\eta$ [%], vs. magnetic field strength, H, for various particle size formulations of ferrofluids. Summarizing, high shear rates, such as tight rotor to stator gaps and / or high rates of speed greater reduce or even eliminate ferrohydrodynamic effects on viscosity. Also, lower strength magnetic fields cause no change in fluid viscosity. Finally, for smaller (8 nm or smaller) particle sized ferrofluids, there is also no change in fluid viscosity.

It is currently theorized [11, 16] that the viscosity increase comes from the iron particles forming a magnetic chain in the presence of a strong magnetic field. These chains become weaker as magnetic field strength decreases. Also, they are broken in the presence of high velocity fluid flow.

Surface roughness also plays a role in shear stress in the turbulent regimes associated with flow in the typically small air gaps of a PMM[2]. Generally, for fluid flow, increased surface roughness leads to increased shear losses. This becomes more relevant in ferrofluid immersed systems, where the shear stresses represent a larger overall percentage of system loss. Unique to ferrofluids, systems with larger surface roughness values than particle size can lead to trapped particles in surfaces, leading to uneven colloidal particle distribution and additional losses and inconsistencies in system performance.

Looking at the total effect on the system from ferrofluid immersion, we must study only at the magnetic effects, but also the effects of submerging rotating systems in a liquid, as opposed to air. To quantify the full 3-D effect of the losses from increased rotational friction, looking at the basic equation for fluid shear loss in a rotating cylinder, such as a radial flux PMM, as developed in NASA TN D-4849 [17], we have:

$$W = \pi C_d \rho R^4 \omega^3 L \qquad 2.4.1\text{-}5$$

[2] As an example, the Reynolds number of the generator tested in experiments 3 and 4 reached 13,500 at top RPM.

Where $W$ is the power loss through fluid friction, $C_d$ is the coefficient of drag, $\rho$ is the density, $R$ is the rotor radius, $\omega$ is the rotational speed, and $L$ is the length.

For a rotating disc, such as an axial flux PMM, as presented by Gieras [3], we have:

$$W = \frac{1}{2} C_d \rho (2\pi w)^3 ({R_{disc}}^5 - {R_{shaft}}^5) \quad \text{2.4.1-6}$$

Where and $R_{disc}$ is the disc radius, $R_{shaft}$ is the shaft radius, and the coefficient of drag for turbulent flow, as presented by Gieras [3], is:

$$C_d = \frac{3.87}{\sqrt{Re}} \quad \text{2.4.1-7}$$

The coefficient of drag is inversely proportional to the square root of the Reynolds number, $Re$, which is given by [3]:

$$Re = \frac{\rho w L}{\eta} \quad \text{2.4.1-8}$$

Where $\eta$ is the fluid dynamic viscosity.

From these equations, we can see the viscous losses are lowest with the largest air gaps, lowest speeds, or smallest viscosity fluids, leading to the drive for low viscosity ferrofluids in the applications, or, ideally, a system designed to remove all rotating components from the fluid immersion. Typical values of viscosity for ferrofluid are in the 0.005 to 0.01 Ns/m$^2$ range vs. $1.78 \times 10^{-5}$ for air, 8.94e-4 for water, 0.0041 for SAE grade 10 motor oil. However, as discussed, ferrofluid viscosity is dependent on magnetic

field strength, particle size, and rotational velocity. On a positive side note from this effect, for some applications, greater losses at high RPM's can be a benefit. For example, in wind power applications, high rotational velocity from excessive wind speed can lead to complications in controls and energy storage. A ferrofluid immersed generator has the potential for greater power at lower speed, where it is most needed, and lower power at higher speeds, where this is a concern. These windage losses are frictional, and translate directly into heat that is added to the system. As discussed, in systems where the windage losses exceed the magnetic gains, such as high speed systems, shear losses can become greater than magnetic gains, offering an overall efficiency loss.

Another potential tradeoff to improved permeability in the air gap is more complex controls for systems that use "field weakening", also referred to as "flux weakening". In these applications, speed is increased by electrically or mechanically reducing the flux field. Top speeds in electric motors can be limited by supply voltage, supply frequency, and system design. In order to overcome these constraints, weakening the flux across the air gap can trade efficiency, power, and torque for increased speeds.

Recalling equations 2.3-5 and 2.3-6, we can see that lower Flux Density increases speed, but decreases torque. Figure 2.4.1-2 [20] shows a variable air gap system, with the effect on the torque / speed curve. Note that larger air gaps provide higher speeds, but have lower efficiencies.

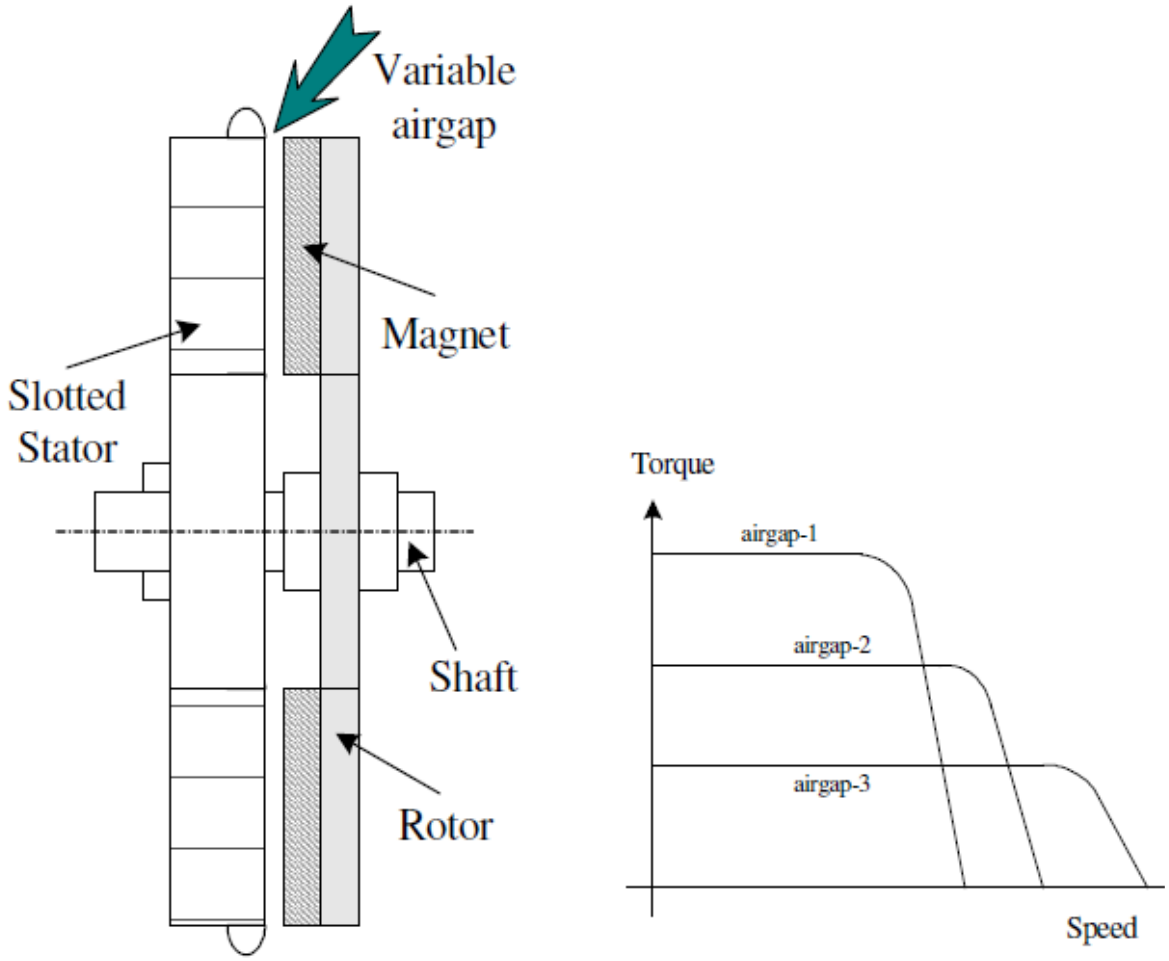


Figure 2.4.1-2 – Torque / Speed vs. Air gap (Higher Speed / Lower Torque = Larger Air gaps) [20]. This figure shows the effect of air gap size on the torque / speed curve for a given power level. Larger air gap systems are capable of greater speed, with a trade-off of lower maximum torque.

Figure 2.4.1-3 [14] shows a typical motor performance curve. Note that one would expect a linear torque / speed relationship. However, motor controllers are limited by current carrying capability for low speed / high torque, and the flux weakening has a non-linear effect on speed, as weaker flux enables higher speed, but reduces total power in the system. In the first region of the curve, shown in slanted cross-hatching, the motor is

operating in the constant torque region, limited by current in either the controller or the motor. In the second region, shown in horizontal criss-crossed crosshatching, the motor is operating in the constant power region, where the motor is in its maximum efficiency. In the third region, shown in straight criss-crossed crosshatching, the motor is operating in a flux weakened condition, which drives the motor past the levels of speed that would be available without flux weakening, but at the expense of efficiency and complexity of controls. As shown in Eq. 2.3-6, for a system of given efficiency, flux density is inversely proportional to speed, which is a negative effect from a controls perspective, as it requires additional flux weakening and related efficiency losses to attain higher speeds.

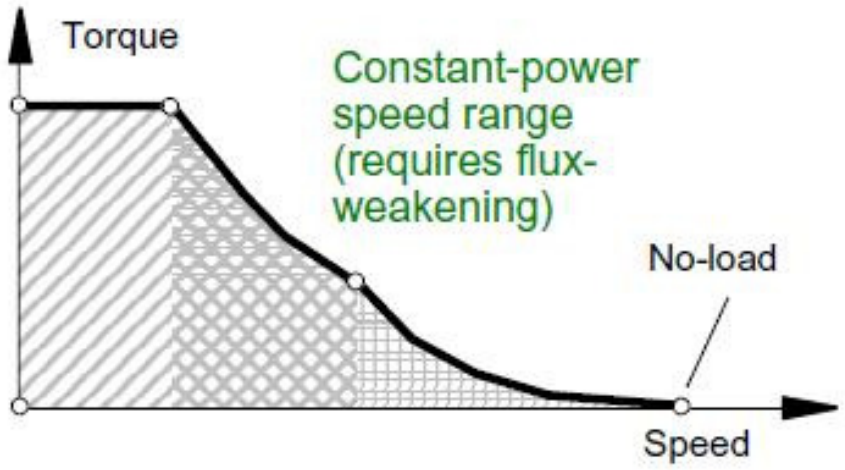


Figure 2.4.1-3 – Motor Power Curve [14]. This figure shows a typical motor power curve. Higher speeds can be obtained than would be possible with a linear torque / power relationship by providing flux weakening in the windings.

Magnetic force providing increased torque but lower speed is fairly intuitive, as less magnetic resistance makes the rotor easier to spin, but provides less attractive / repulsive force for torque. Overall, the net effect is of reduced magnetic flux is negative on power

and efficiency, especially considering the electrical or mechanical devices that must drive the flux weakening. Also, when magnetic flux is weakened electrically (through means of inducing opposing currents to the stator windings), excessive field weakening runs the risk of demagnetizing the permanent magnets. However, in applications where speed at low torque is important, which includes numerous motor applications, flux weakening is critical to performance.

Introducing improvements to the permeability of the air gap increases the complexity of field weakening, adding challenges to the motor controls from a systems perspective. These systems are designed with known performance of the magnetic circuit, as well as the overall motor curves. Changing the air gap permeability by ferrofluid immersion in off the shelf system would need the controls systems recalibrated in precision applications.

Also limiting the gains from ferrofluid in the gap region is the saturation level of the ferrofluid. As discussed in section 2.1, a material can only support a finite level of magnetic flux density before saturation occurs, and the material behaves similar to air for further magnetic increases. Typical values for the saturation point of a ferrofluid are in the range of 0.05 T - 0.17 T, as tested by Nethe, et al. [9], which limits the benefits from a ferrofluid gap in high flux density systems.

# CHAPTER 3 – COMPUTATIONAL MODEL

This chapter presents the computational model – a "virtual prototype" for a ferrofluid immersed permanent magnet machine. This system is comprised of a macro-scale series of equations driven from system geometry, materials, and design, and is influenced by component level analysis for geometry and design dependent factors, specifically saturation and leakage flux.

## 3.1 BACKGROUND

One of the main focuses of this research was to develop a "virtual prototype" mathematics model to predict PMM performance. A macro scale model was developed, featuring geometry and material inputs (generator size, magnet material, windings, et al.) in order to obtain overall system output (power, efficiency, et al.). For complex geometry, some information on the macro-scale model, such as saturation and leakage factors, must be developed through the use of detailed FEA on the overall magnetic circuit, including the gap material.

## 3.2 COMPUTATIONAL MODEL

The computational work objective was to construct a design tool in the form of a model of the dynamic behavior of the zero air gap PMM that simulates the fluid and solid mechanics, predicts the system response to inputs and disturbances, and identifies all major sources of energy loss. To accomplish this objective requires accounting for a wide range of phenomena due to coupled behavior between energy domains, and complex interaction of the components in the system. By creating the model as a design

tool, it can be used in this and future works to design and to optimize PMM's for a variety of specific applications.

### 3.2.1 – MACRO-SCALE MODEL

Now that the basics of magnetism and electromagnetism have been established, a macro-scale model of the generators to be constructed and tested will be developed. An axial flux permanent magnet machine will be used due to the ease of varying the air gap distance as necessary. For ease of design and construction, as well as availability of parts and materials, a one pole pair (two magnets) rotor will be used, with three stator poles wound in series. Looking at the specific configuration, we have the circuit shown in Figure 3.2.1-1.

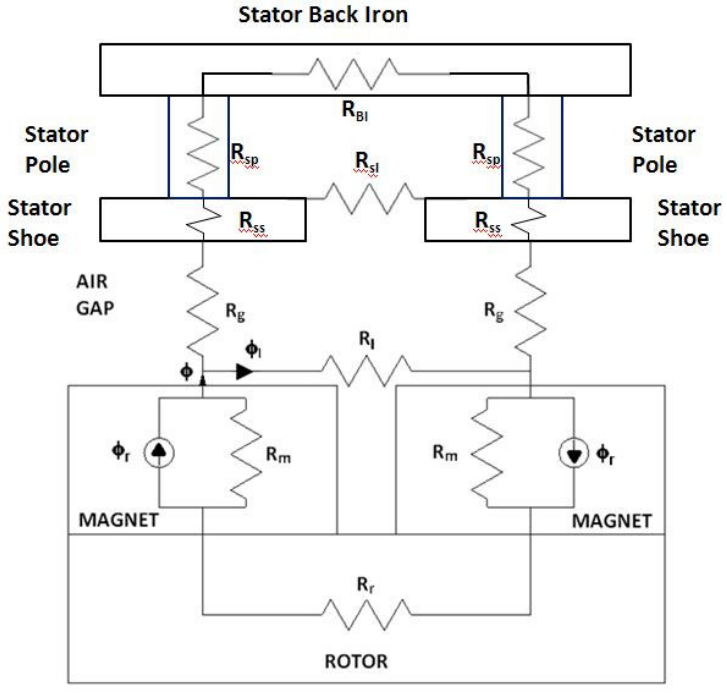


Figure 3.2.1-1 – Axial Flux Cross Section Magnetic Circuit. This figure shows a more detailed magnetic circuit, featuring the addition of stator geometry, as well as leakage flux in the stator.

Solving this circuit provides the magnetic flux throughout the system. This can be done through traditional methods, or through the usage of basic circuit solvers, as shown in Figure 3.2.1-2. Resistance values represent magnetic reluctance values of the various elements of the system. The permanent magnets in the system are represented by current sources in opposing directions, in accordance with the North-South orientation of the magnetic polarity. Current values represent the remanent magnetic flux values, $B_r$, of the permanent magnets. Although this simplified model does not predict non-linear effects, such as magnetic saturation, and becomes infeasible when geometry becomes more complex, it provides a thorough understanding of the magnetic flow, and the foundation of a macroscale model for simple geometries. For more complex geometries and systems in the non-linear range, FEA is required, as presented in section 3.2.2.

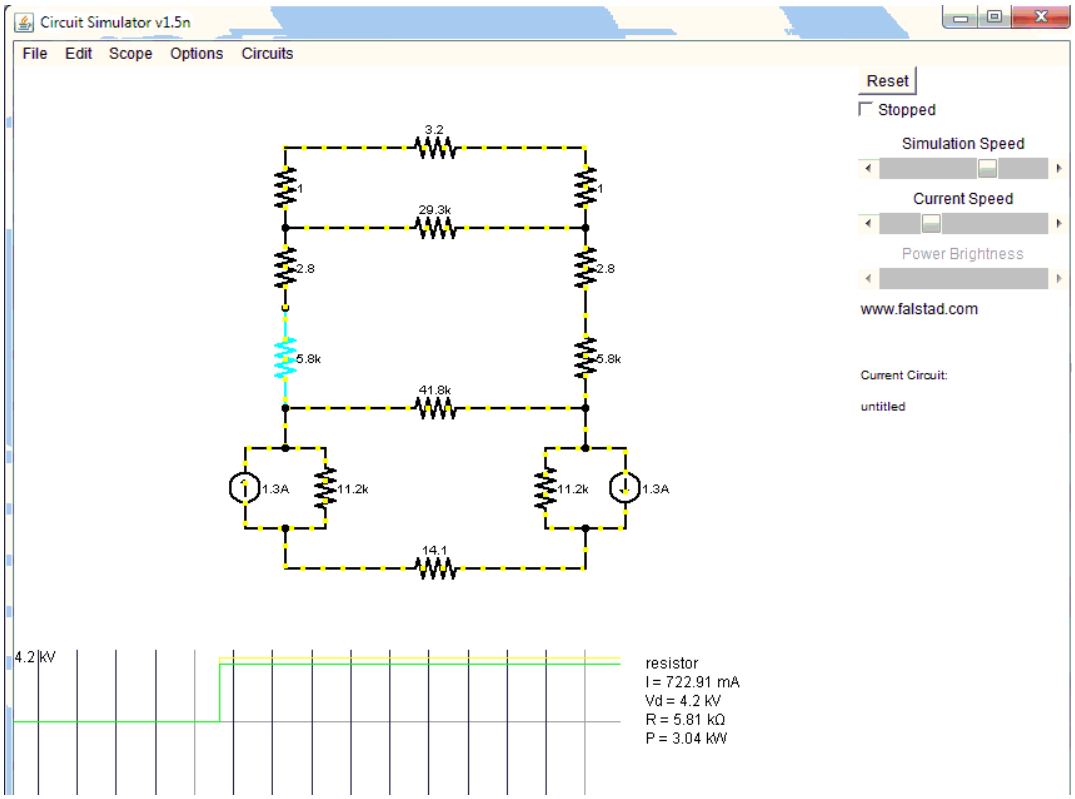


Figure 3.2.1-2 – Circuit Model. This figure shows the axial flux cross section magnetic circuit modeled in Circuit Simulator V1.5, a software program used to solve such systems. The values shown are that of the generator designed, built and tested for experiment 3.

From Gieras [3], for a one pole pair rotor and three phase stator, the voltage co-efficient is given by:

$$Ke = 3.624\, N_1\, \Phi_f \qquad 3.2.1\text{-}1$$

Where $N_1$ is the number of turns and $\Phi_f$ is the Flux across the air gap. This provides an easily measurable check in experimentation, as voltage and RPM are easy to measure, as opposed to torque, magnetic flux, efficiency, or other factors.

Completing the rest of the performance model, we have the torque constant for the given PMM style [3]:

$$Kt = 0.577 N_1 \Phi_f \quad \text{3.2.1-2}$$

With torque and RPM, or, for generator applications, voltage and current, we have the output of the motor / generator in an idealized conditions. However, several factors contribute to the efficiency of the system. This efficiency is given by equation 3.2.1-3 [2]:

$$Eff = \frac{\Delta P_{Out}}{\Delta P_{in}} \quad \text{3.2.1-3}$$

Where $\Delta P_{out}$ is the power out, Torque*RPM in motor applications or Current*Voltage in generator applications, and $\Delta P_{in}$ is the power in, Torque*RPM in generator applications or Current*Voltage in motor applications. The overall performance equation, used to fully characterize the PMM's under test, is given in equation 3.2.1-4 [3].

$$\Delta P_{Out} = P_{in} - \Delta P_e - \Delta P_{fr} - W - \Delta P_{fh} \quad \text{3.2.1-4}$$

Where $\Delta P_e$ is the electromagnetic losses, $\Delta Pfr$ is the losses due to bearing friction, $W$ is the losses due to fluid friction, and $\Delta P_e$ is the ferrohydrodynamic losses.

For electromagnetic losses, eddy current losses, described in chapter 2.1, can be calculated by Equation 3.2.1-5 [3] for round wire conductors:

$$\Delta P_e = \frac{\pi^2}{4}\frac{s_{cop}}{\rho_{cop}} f^2 d_w^2 m_{cop} B_{mg}^2 \quad 3.2.1\text{-}5$$

Where $s_{cop}$ is the conductivity of copper, $\rho_{cop}$ is the density of copper, $f$ is the frequency of the rotating machine, $d_w$ is the wire diameter, $m_{con}$ is the conductors' mass, and $B_{mg}$ is the average magnetic flux density.

For flat plates, such as the stator frame, eddy current losses are given by Equation 3.2.1-6 [3]:

$$\Delta P_e = \frac{\pi^2}{6}\frac{s_{fe}}{\rho_{fe}} f^2 d_{fe}^2 m_{fe} B_{mg}^2 \quad 3.2.1\text{-}6$$

Where $s_{fe}$ is the conductivity of steel, $\rho_{fe}$ is the density of steel, $d_{fe}$ is the effective plate thickness, and $m_{fe}$ is the stator iron mass, and $B_{mg}$ is the average magnetic flux density.

Friction Losses in the Bearings, dependent on the rotor mass and bearing itself, is given by Equation 3.2.1-7 [3]:

$$\Delta P_{fr} = 0.06 k_{fb}(m_r + m_{sh})\omega \quad 3.2.1\text{-}7$$

Where $k_{fb}$ is the bearing friction coefficient, $m_r$ is the mass of the rotor and $m_{sh}$ is the mass of the shaft.

Fluid friction loss, windage in traditional systems or fluid friction in ferrofluid immersed designs, is given by Eq. 2.4.1-6, repeated here for convenience [3]:

$$W = \frac{1}{2} C_d \rho (2\pi\omega)^3 ({r_{disc}}^5 - {r_{shaft}}^5) \quad 3.2.1\text{-}8$$

Ferrohydrodynamic losses, $\Delta P_{fh}$, discussed in Chapter 2, is given by Equation 3.2.1-9:

$$\Delta P_{fh} = (W_{fh} - W) \quad 3.2.1\text{-}9$$

Where $W_{fh}$ is the ferrohydrodynamic loss due to increased fluid viscosity from the ferrofluid due to ferrohydrodynamic effects.

### 3.2.2 FINITE ELEMENT ANALYSIS

With the above equations, a macro-scale model can be developed to predict the overall performance of the systems built and constructed to test the effects of ferrofluid immersion on permanent magnet machines. However, these series of equations fail to capture the effects of saturation on magnetic systems, and are difficult to accurately model leakage flux effects in complex geometric systems. In order to study these effects, and to graphically present the effects of changing permeability in a magnetic circuit, Finite Element Analysis was used.

MagNet, a magnetic-specific Finite Element Analysis program from Infolytica, was used for all FEA models. Specifically, the FEA computational model addressed:

- Gains in magnetic performance through the use of magnetically permeable materials as opposed to an air gap.
- Magnetic saturation of the stator poles, showing if saturation of the magnetic poles prevents improved performance through the improved magnetic path.

- Leakage flux, showing overall magnetic efficiency and if improved gap permeability increased leakage flux in the system.

In order to study the effects of improved permeability, an FEA model was created with a simple magnetic circuit to perform sensitivity analyses. Using the "C-Channel" set-up presented by Hsu [18], a finite element model (shown in figure 3.2.2-1) was created using MagNet from Infolytica. The C-Channel was selected due to its design providing a complete magnetic circuit, similar to what would be seen in a permanent magnet machine, but with very simple, basic geometry. The initial channel is 2.50" X 2.50", with 0.50" legs. An N42 Neodymium Iron Boron magnet is modeled with a short air gap, and the magnetic flux density, shown in Tesla in all tables and FEA results, is plotted to study potential magnetic saturation, along with the flux function contour plot to study flux leakage.

This model was used to investigate the effects of changing the material in the gap, shown as clear in wireframe, between the magnet, shown in green on the mesh, and the steel C-channel, shown in dark blue. In the experiment, the relative permeability was modified from 1, equal to air, to 1000, equal to high permeability steel. Intermediate values could be obtained through magnetically permeable plastics, ferrofluids, or other engineered materials.

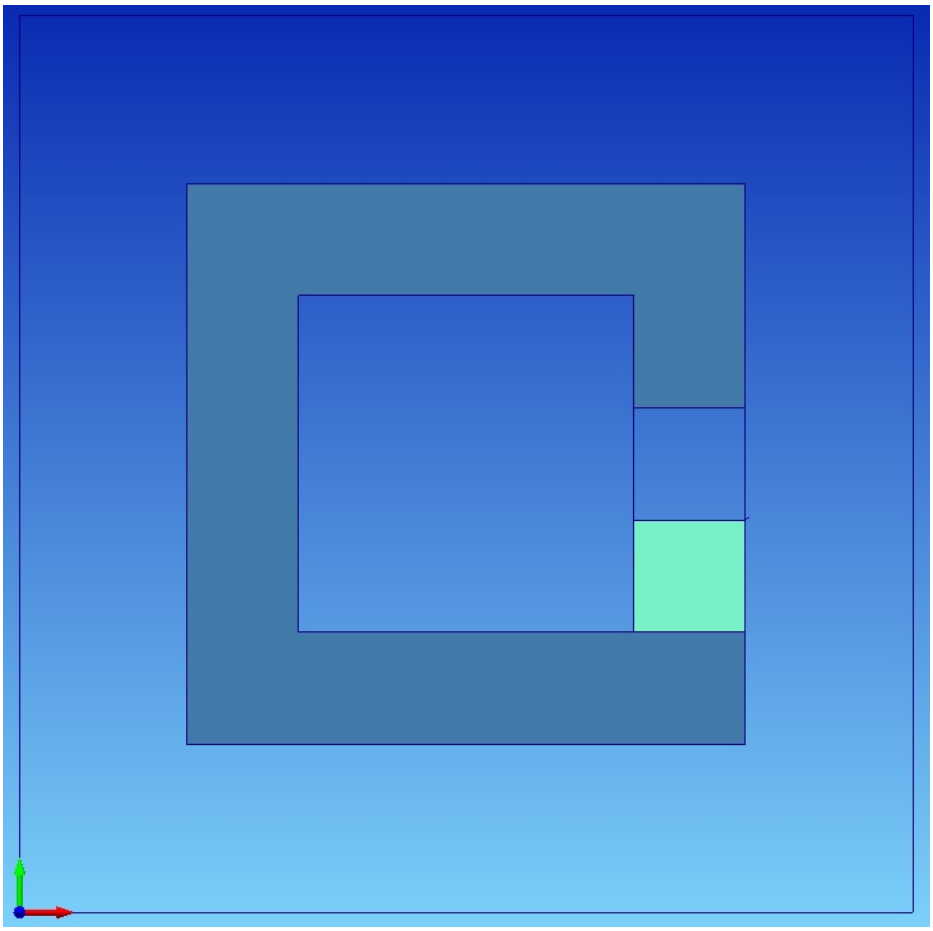

Figure 3.2.2-1 - FEA Model, C-Channel (Geometry). This figure shows the C-channel geometry used for initial FEA analysis of gap material permeability.

The default mesh of the program, which created 382 elements, was used for an initial run.

Figure 3.2.2-2 shows the initial mesh.

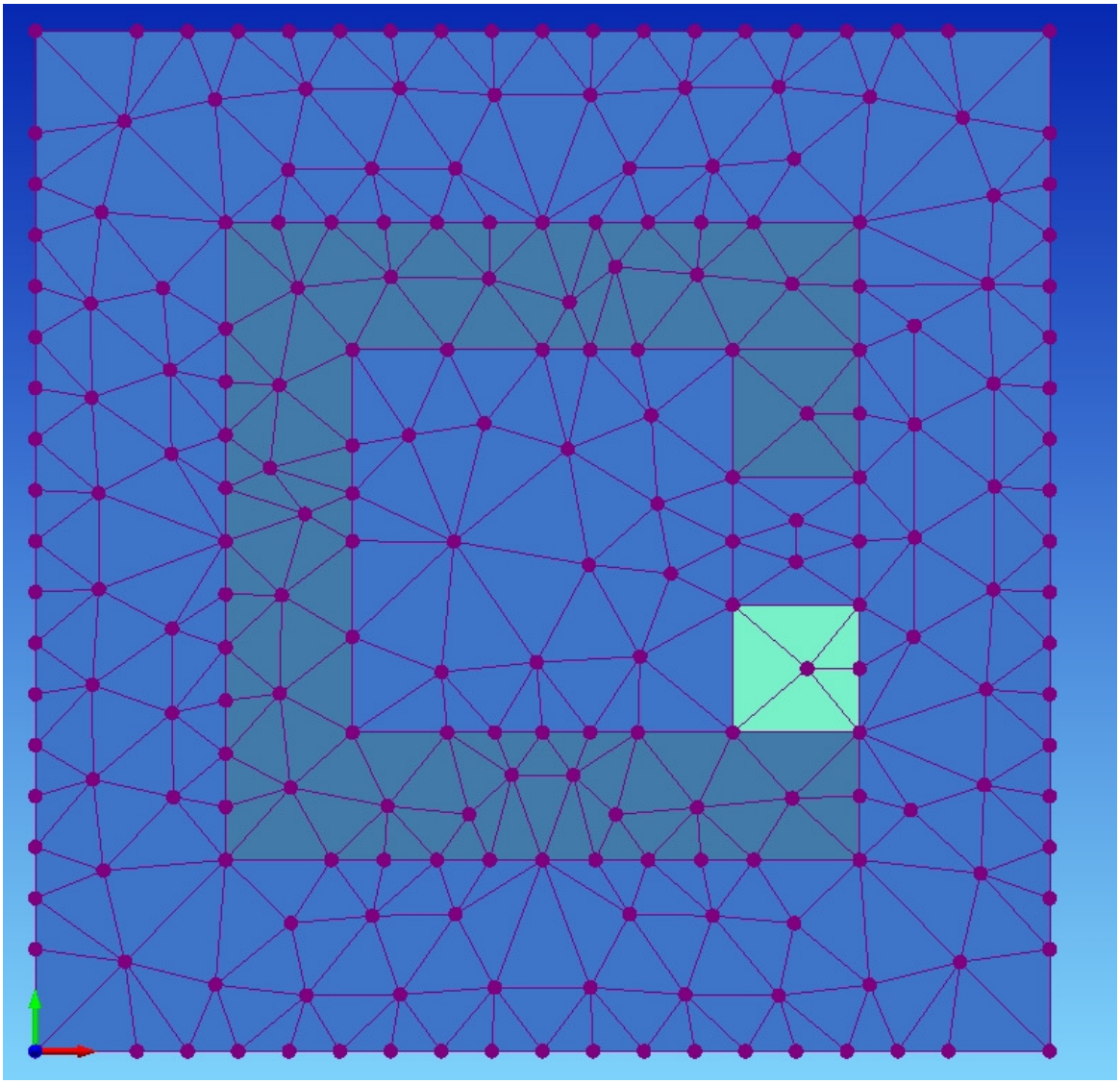

Figure 3.2.2-2 – Default Mesh (382 elements). This figure shows the default mesh created by Infolytica with 382 elements.

This coarse mesh provided the results shown in Figure 3.2.2-3, which shows the calculated flux lines and the flux density contour plot, with a maximum value of 0.8177 Tesla. High values of flux density show concentrated areas of magnetic flow. The flux

function shows the direction of the magnetic flow through overlaid contour lines. Flux lines outside of the main c-channel show leakage flux in the magnetic circuit.

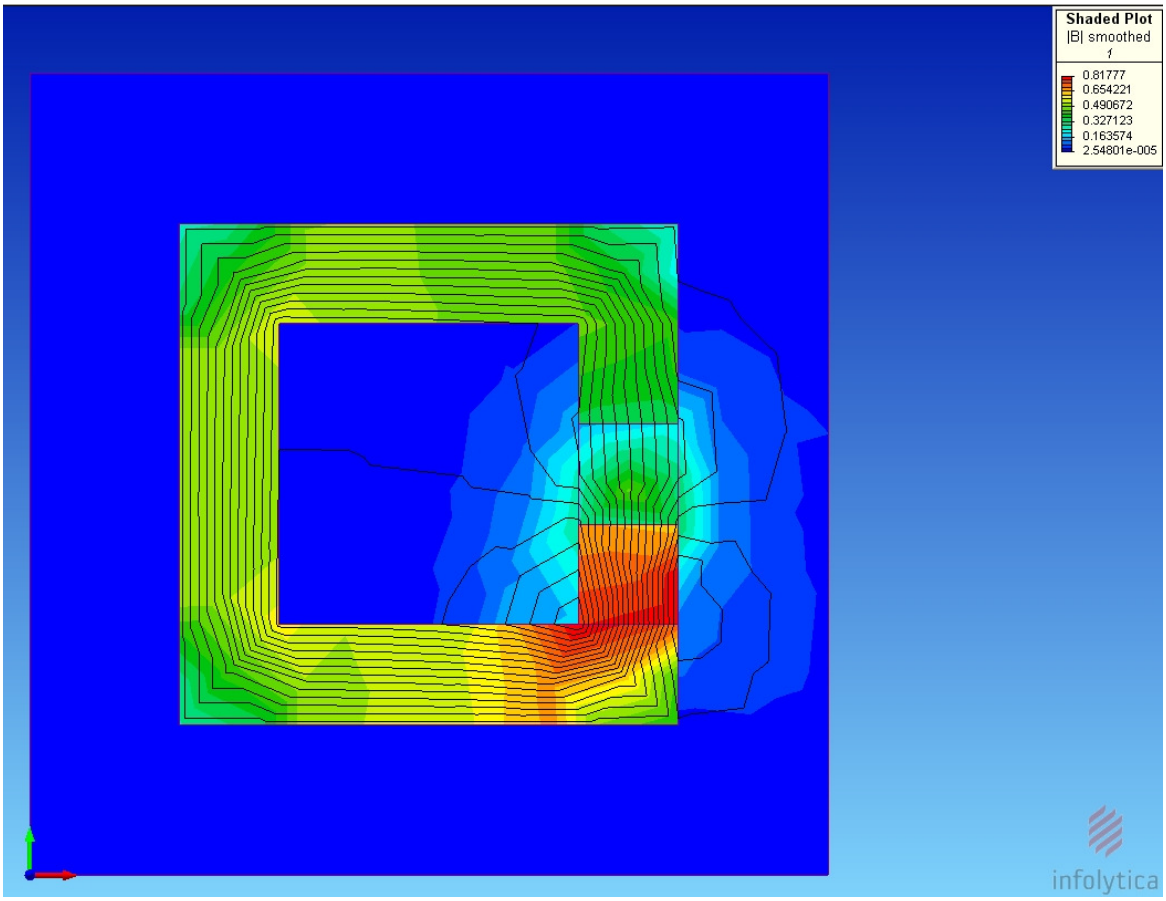


Figure 3.2.2-3 – FEA Results, Default Mesh (382 elements). This figure shows the FEA results from the default mesh created by Infolytica. Note the jagged field lines and maximum flux density value of 0.818 Tesla.

Based on the jagged results, it was decided that a mesh sensitivity study was required. Although the air gap is the primary area of interest, note that the leakage flux occurs across the entire fluid region. Also, the sharp corners of the C-channel provide an area

where values could change rapidly. Therefore, mesh refinement was performed throughout the model.

Figure 3.2.2-4 shows the final refined mesh, and Figure 3.2.2-5 shows the results.

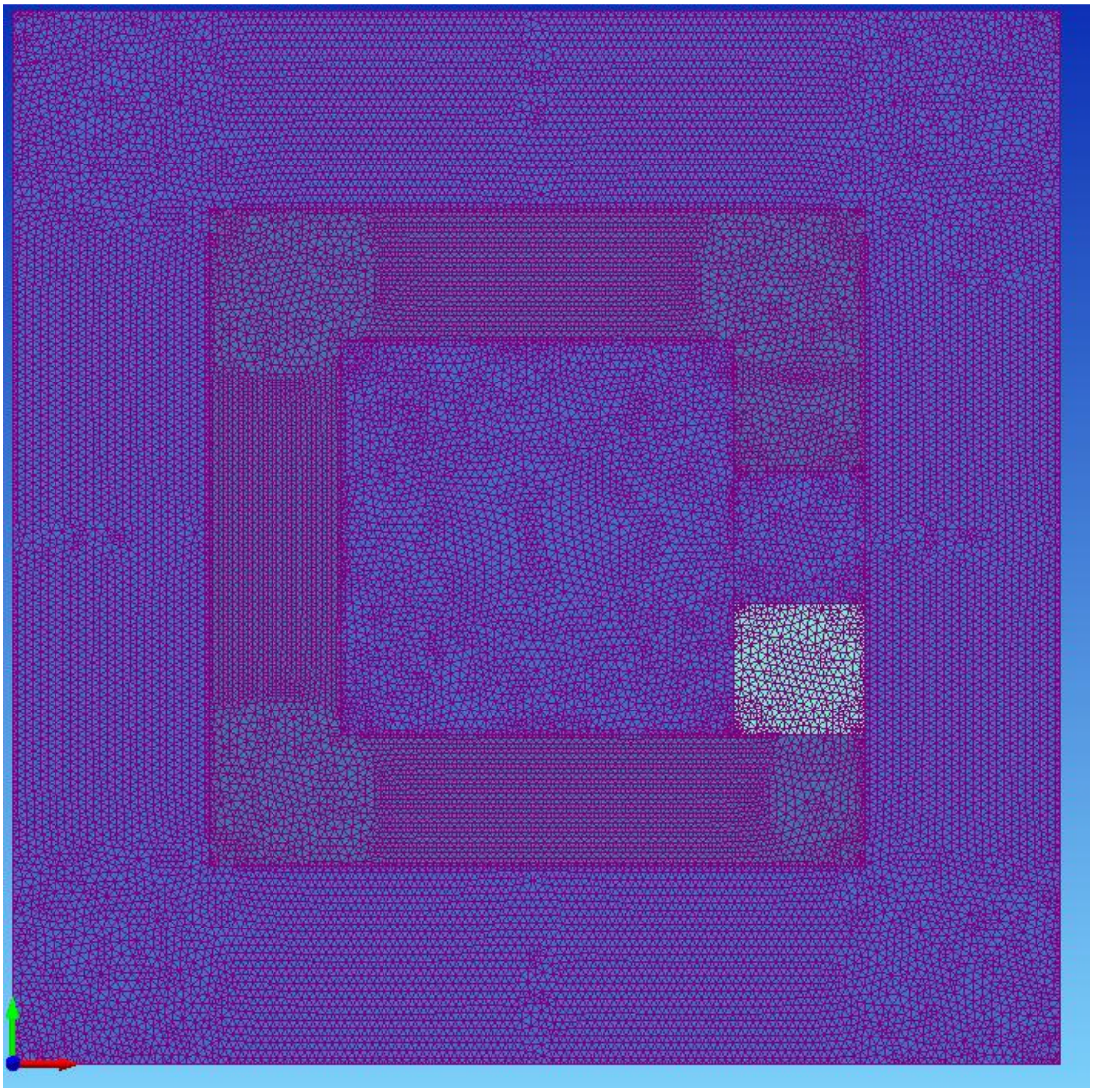

Figure 3.2.2-4 - Final Mesh Refinement (38,213 elements). This figure shows the final mesh refinement with 38,213 elements.

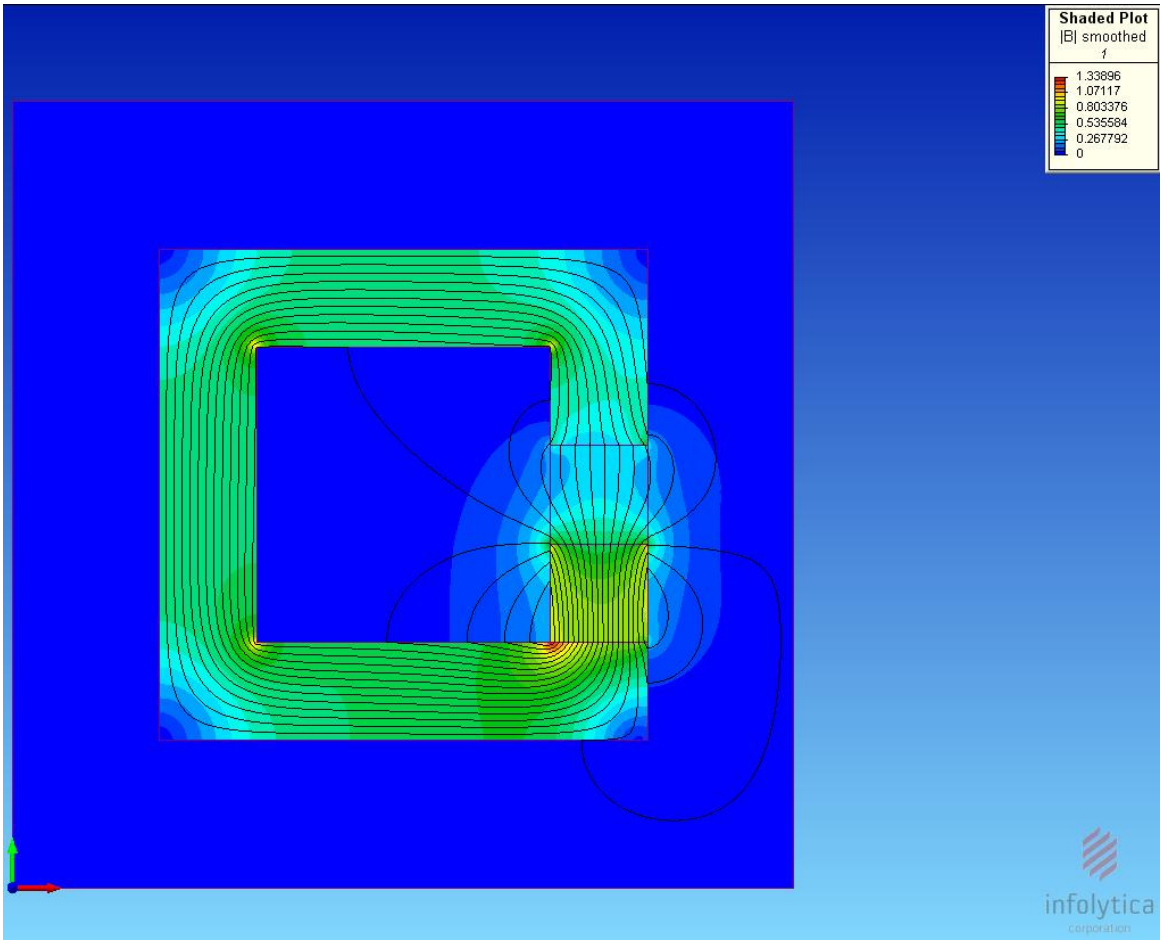


Figure 3.2.2-5 - FEA Results, Final Mesh Refinement (38,213 elements). This figure shows the FEA results from the fourth mesh refinement. Note the field lines are smooth and the maximum flux density value is 1.34 Tesla.

The final mesh refinement shows stable flux function contour lines, and the maximum flux density has increased to 1.22 Tesla. Table 3.2.2-1 summarizes the mesh sensitivity study. Looking at the results in further detail, we can see that the increased flux density is providing increased detail in a sharp corner, but the values of the rest of the system have stabilized. As a result, this mesh density will be used in the remainder of the FEA analytical example. Also, rather than maximum flux density, which could be deceiving

given the singularity at the sharp corners, measurements will be taken of the flux density across the midpoint of the C-channel, which stabilized very quickly in the mesh sensitivity study. For the baseline measurement, the flux density across the C-channel midpoint was 0.55 Tesla.

| Analysis # | Max Element Size | # of Elements | Maximum Flux Density (T) | Midpoint Flux Density (T) |
|---|---|---|---|---|
| 1 | Default | 382 | 0.8177 | 0.52 |
| 2 | | 732 | 1.031 | 0.55 |
| 3 | 0.06 | 3054 | 0.967 | 0.55 |
| 4 | 0.03 | 8068 | 1.22 | 0.55 |
| 5 | 0.01 | 38213 | 1.339 | 0.55 |

Table 3.2.2-1 – Mesh Sensitivity Study. This table summarizes the results of the FEA mesh sensitivity study. Summarizing, due to the sharp corner in the flux path, the maximum value of Flux Density of the system varies greatly (~±25%) with mesh density, and requires a high mesh count to stabilize. However, the magnetic flux density values at the midpoint of the C-Channel stabilize quickly.

Now that the basic geometry has been baselined, a study was performed to analyze the effect of increased permeability in the air gap. Figure 3.2.2-6 shows the results of the gap permeability study. Note that with increased gap permeability comes a decrease in leakage flux. Summarizing the results, presented in Table 3.2.2-2, we can see that a small increase in permeability provides a large increase in flux density, with an 18% increase for doubling the permeability of air. At high levels of permeability, the effect tailors off completely, as the limits of the magnetic strength of the permanent magnet are reached, with a 109% increase for a relative permeability of 100 vs. a 111% increase for a relative permeability of 1000.

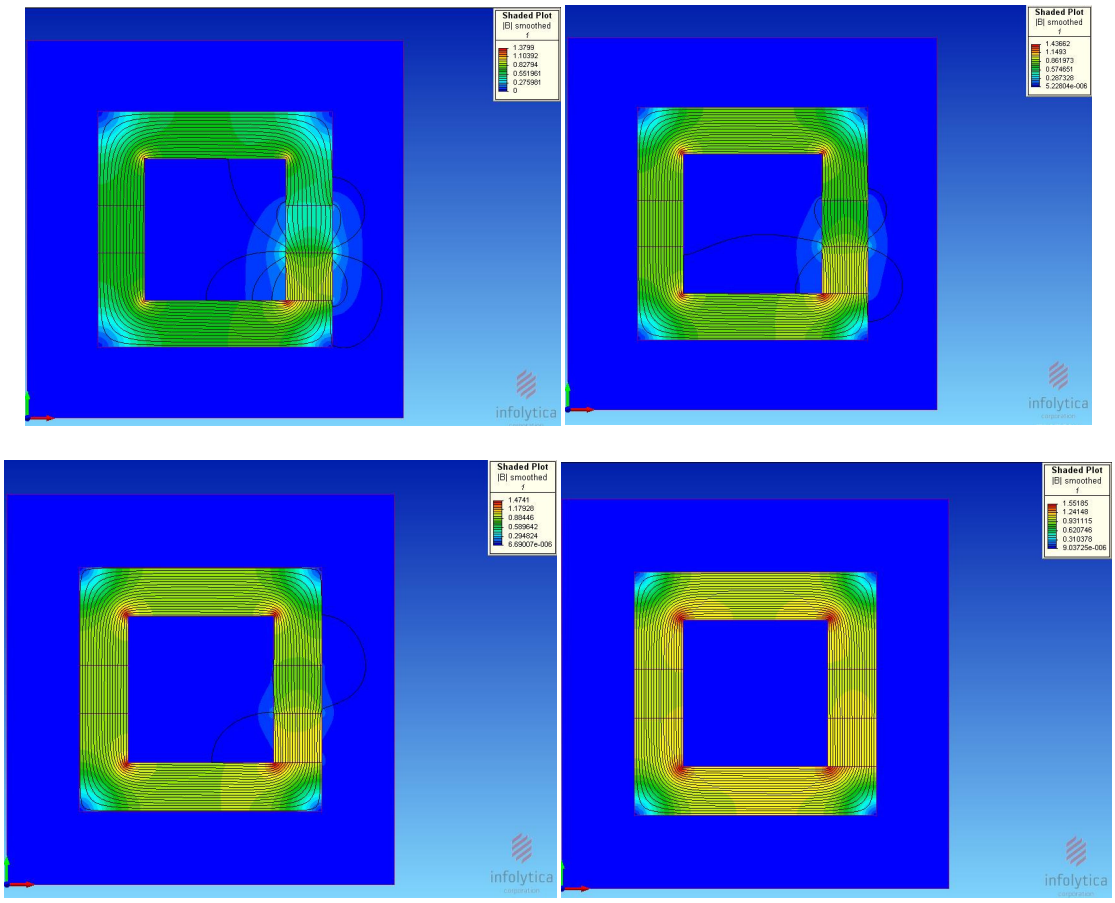


Figure 3.2.2-6 - FEA Results, Gap Relative Permeability. This figure shows the FEA results from the changing the relative permeability of the gap to values of 1, 2, 5, 10, 100, and 1000. Note that the leakage flux decreases with increased gap permeability, and is completely eliminated at the final iteration.

| Relative Permeability | Maximum Flux Density | Midpoint Flux Density | % increase, MAX | % increase, MID |
|---|---|---|---|---|
| 1 | 1.22 | 0.55 | 0 | 0 |
| 2 | 1.38 | 0.65 | 13% | 18% |
| 5 | 1.43 | 0.88 | 17% | 60% |
| 10 | 1.47 | 0.99 | 20% | 80% |
| 100 | 1.55 | 1.15 | 27% | 109% |
| 1000 | 1.56 | 1.16 | 28% | 111% |

Table 3.2.2-2 - FEA Results, Increased Gap Permeability. This table summarizes the results of the gap permeability sensitivity study. Summarizing, large increases are seen with small increases in relative permeability, but show logarithmically diminishing returns for larger values as the gap permeability approaches that of the steel C- Channel.

The above study shows the benefits of a directed improvement across an air gap, with improved flux density across the channel and an elimination of leakage flux. However, for systems with complete ferrofluid immersion, the effect is less directed. Using the same model, the analysis was repeated by increasing the permeability of the air around the entire system as opposed to just the gap. Figure 3.2.2-7 shows the FEA results of a complete immersion in a fluid, as opposed to just the gap area. Table 3.2.2-3 summarizes the results. Note as permeability increases, flux leakage increases. Ultimately, very little flux reaches the C-Channel midpoint. This shows that the complete immersion technique is effect up to a certain level of material permeability. Once the leakage factor becomes more significant than the gap permeability effect, the overall effect on the magnetic circuit is negative.

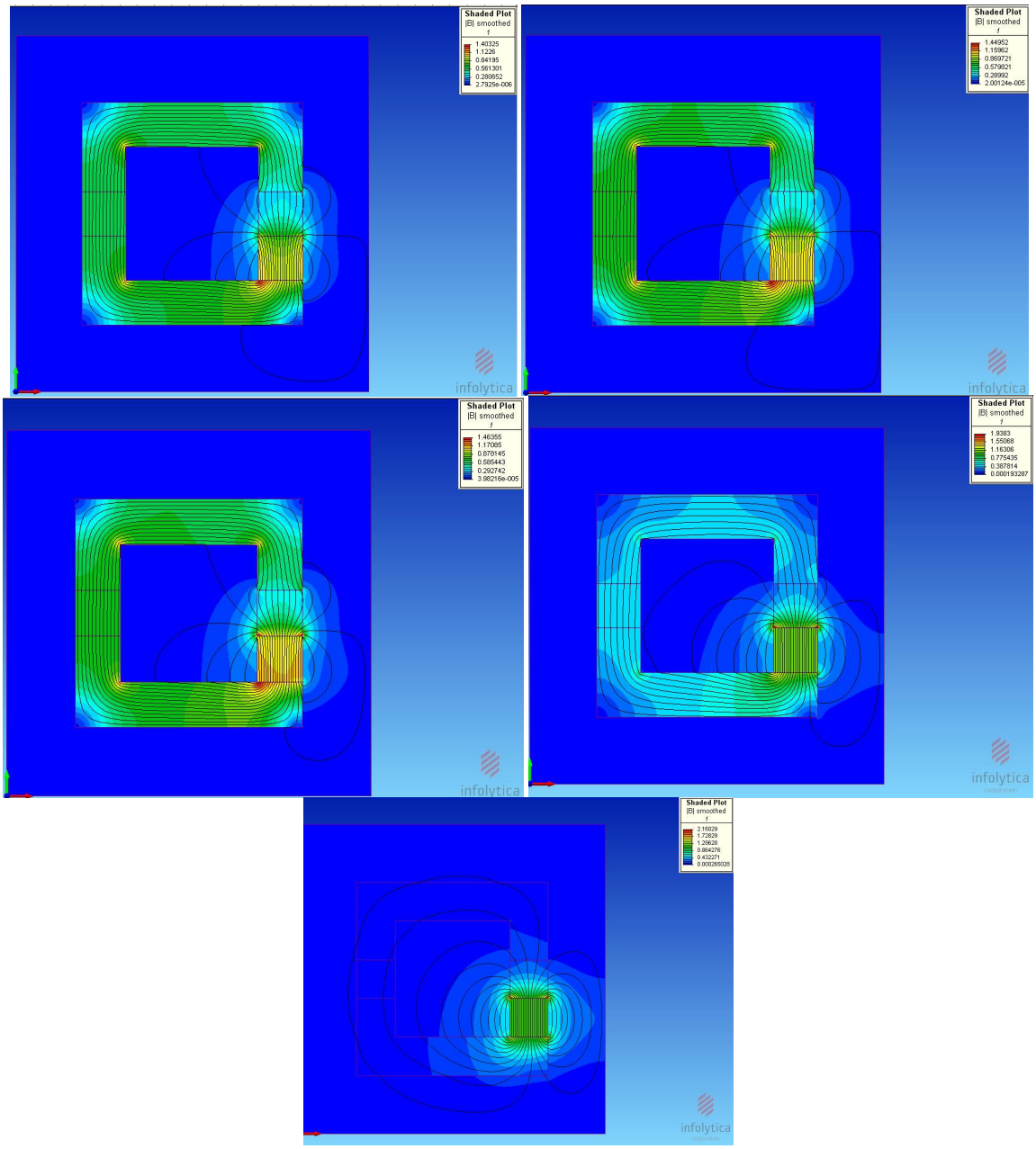


Figure 3.2.2-7 - FEA Results, Complete Immersion. This figure shows the FEA results from changing the relative permeability of the gap and all surrounding material to values of 2, 5, 10, 100, and 1000. Note that a small increase in overall permeability shows an increase in flux throughout the system and a small increase in leakage flux, larger increases lead to little flux moving through the C-channel, and a complete dominance of leakage flux.

| Relative Permeability | Maximum Flux Density | Midpoint Flux Density | % increase, MAX | % increase, MID |
|---|---|---|---|---|
| 1 | 1.22 | 0.55 | 0 | 0% |
| 2 | 1.4 | 0.73 | 15% | 33% |
| 5 | 1.45 | 0.81 | 19% | 47% |
| 10 | 1.46 | 0.99 | 20% | 80% |
| 100 | 1.94 | 0.44 | 59% | -20% |
| 1000 | 2.16 | 0.09 | 77% | -84% |

Table 3.2.2-3 - FEA Results, Increased Permeability, Complete Immersion. This table summarizes the results of the overall surrounding fluid permeability sensitivity study. Summarizing, an initial increase is seen with small increases in relative permeability, but then decline for larger values, with negative effects on system performance as the surrounding fluid permeability approaches that of the steel C- Channel.

From the above FEA study, we can see that in applications where directed magnetic flux is critical and complete high permeability material immersion is possible, increased permeability immersion would have a negative impact on overall performance. While the air gap permeability increases, besides the shear losses from the liquid immersion (as opposed to a standard air gap), the leakage flux would increase, reducing directed flux from the rotor to the stator. This negatively impacts overall system performance. However, more directed permeability improvements have the potential for increased system efficiency.

In other systems where natural design features prevent leakage flux, complete ferrofluid immersion shows greater potential for increased efficiency. For example, high power density electric motors and generators have stator poles with a high fill percentage of copper, as shown in Figure 3.2.2-8 [29]. Note the high copper fill between stator poles, limiting the possibility that ferrofluid would fill in between stator poles, providing leakage paths. Also, these stator systems are often varnished or even potted with

thermally conductive epoxy. This would prevent ferrofluid from surrounding the iron poles, keeping the material in the rotor / stator gap, and would provide increased performance.

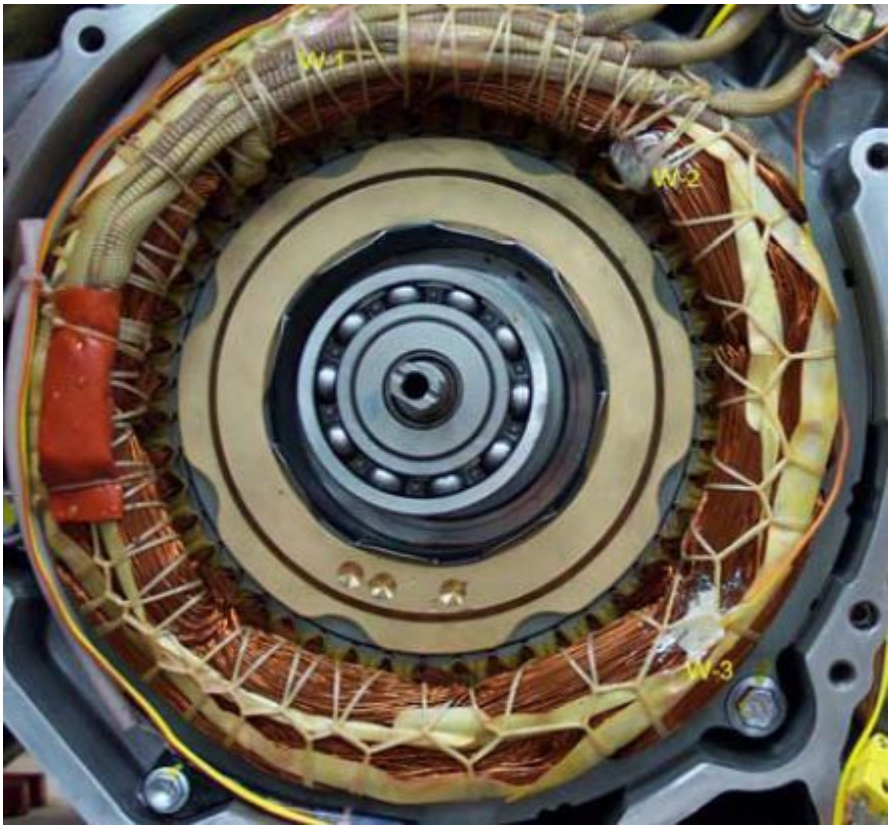


Figure 3.2.2-8 - Prius Motor [29] This figure shows a cross section of a commercial motor, the drive motor for the Toyota Prius. Note that the dense packing of copper in the steel stator slots leaves little room for ferrofluid to flow between stator poles, which would have a negative effect with increased leakage flux.

Flux leakage is dependent not just on material permeability, but on the overall geometry of the magnetic circuit, requiring FEA to determine for complex geometries. Changing the width of the C-Channel from 2.50” to 2.00” yields the result shown in figure 3.2.2-9.

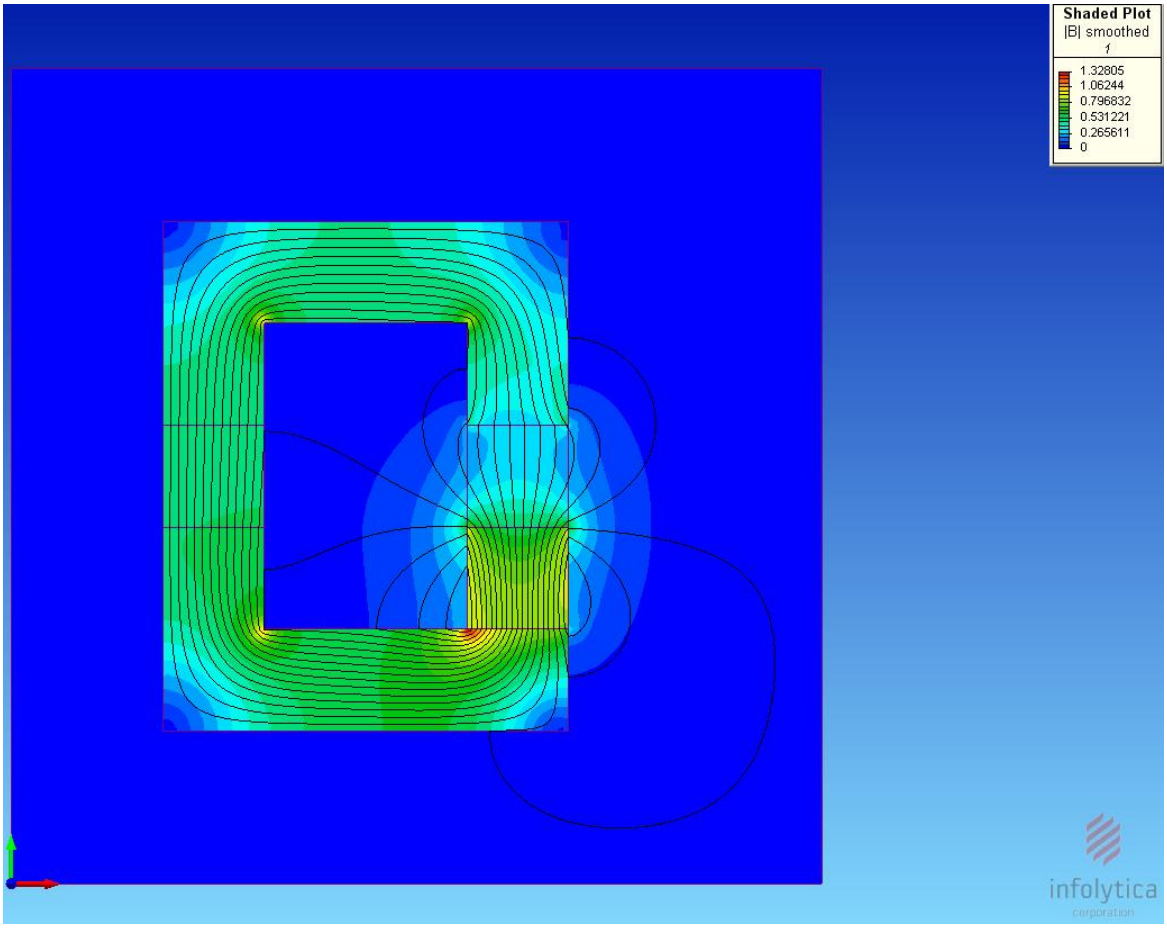


Figure 3.2.2-9 - FEA Results, Baseline Air Gap, 2" Leg Width. This figure shows the FEA results for a 2" wide C-Channel Leg with a baseline air gap. This was used as the baseline for a sensitivity study of complete immersion on a system with different geometry from the previous analysis.

Note the change in the flux function contours, showing changes in the flux leakage from the geometry modification. Repeating the study of changing the permeability in a completely immersed system, as done in the previous section, yields the results shown in Table 3.2.2-4.

| 2" LEG | | | | | |
|---|---|---|---|---|---|
| Relative Permeability | Maximum Flux Density | Midpoint Flux Density | % increase, MAX | % increase, MID | % increase, Mid Flux Density, 2.5" |
| 1 | 1.32 | 0.56 | 0 | 0 | 2% |
| 2 | 1.4 | 0.67 | 15% | 22% | -8% |
| 5 | 1.45 | 0.75 | 19% | 36% | -7% |
| 10 | 1.47 | 0.76 | 20% | 38% | -23% |
| 100 | 1.94 | 0.51 | 59% | -7% | 16% |
| 1000 | 2.15 | 0.13 | 76% | -76% | 44% |

Table 3.2.2-4 - FEA Results, Increased Gap Permeability, Complete Immersion, 2.0" Leg Width. This table summarizes the results of the permeability sensitivity study for a 2.0" C-Channel Leg. Summarizing, small increases in relative permeability leads to an initial increase in system performance compared to the air gap baseline, but negative system performance compared to the 2.5" C-Channel. However, as the surrounding fluid permeability approaches that of the steel C- Channel, larger values of relative permeability leads to negative effects on system performance compared to the baseline air gap, but positive performance compared to the 2.5" C-Channel. This highlights the geometry-dependent nature of the behavior of the magnetic circuit, and the need for FEA to study leakage flux.

This shows that the shortened magnetic path baselined against the prior section shows an increase in flux density across the midpoint of the channel. However, as the permeability of the system increases, the increased flux leakage provides a decrease in magnetic performance, even compared to the larger channel. This effect is non-linear and dependent on unique design geometry, showing the need for FEA to determine.

Another non-linear effect requiring FEA analysis is saturation. In order to demonstrate this effect, the center leg width was varied, and the air gap permeability variation analysis was run for case studies of 0.250", 0.125", and 0.062" legs. Figure 3.2.2-10 shows the results of the analysis for the 0.062" case with a standard air gap. Note that the thin leg is now the maximum flux density portion of the magnetic circuit, and the leakage flux has changed dramatically, including the addition of flux through the air surrounding the saturated leg.

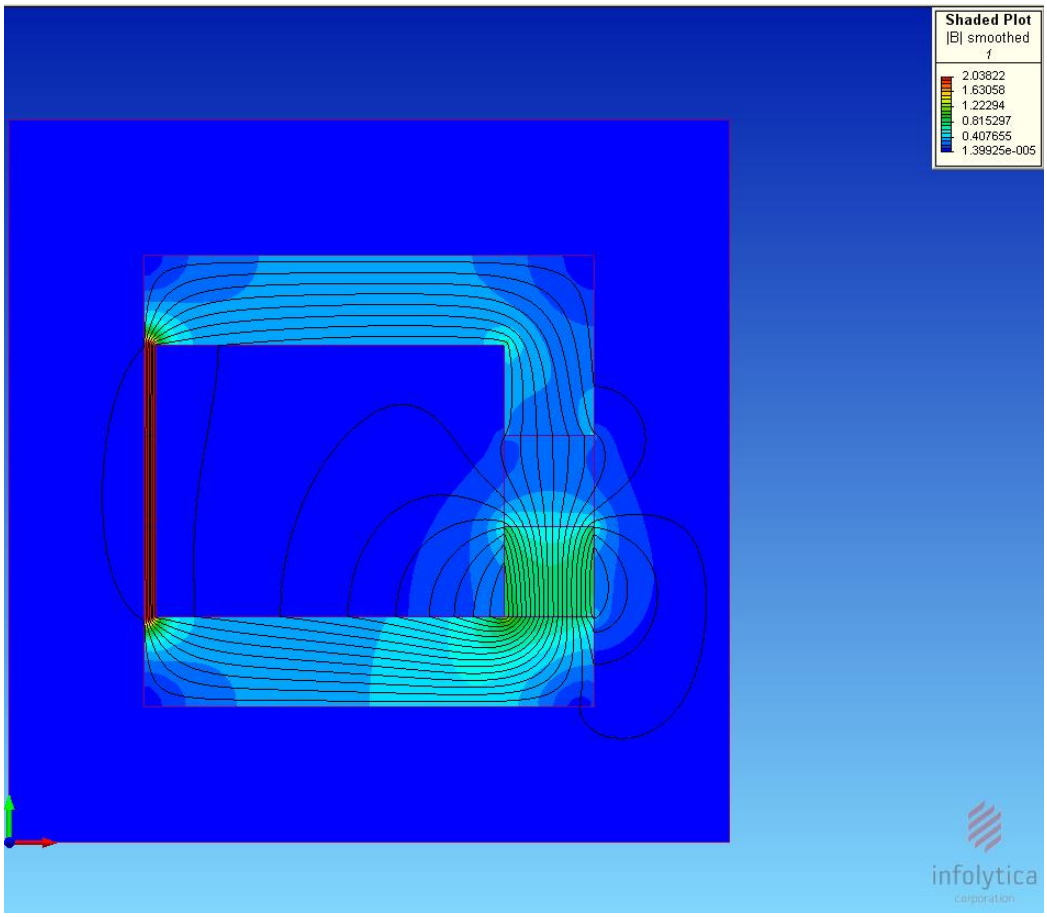


**Figure 3.2.2-10 - FEA Results, Baseline Air Gap, 0.0625" Leg Width.** This figure shows the FEA results for a 0.0625" C-Channel Leg with a baseline air gap. This was used as the baseline for a sensitivity study of gap permeability on a system with different geometry from the previous analysis.

Table 3.2.2-5 summarizes the results of the analysis. Note that as the leg width decreases, the gains from increased permeability of the air gap also decreases in a non-linear fashion.

| .25" LEG | | | | |
|---|---|---|---|---|
| Relative Permeability | Maximum Flux Density | Midpoint Flux Density | % increase, MAX | % increase, MID |
| 1 | 1.33 | 1.09 | 0 | 0 |
| 2 | 1.47 | 1.34 | 11% | 23% |
| 5 | 1.65 | 1.65 | 24% | 51% |
| 10 | 1.78 | 1.78 | 34% | 63% |
| 100 | 1.89 | 1.89 | 42% | 73% |
| 1000 | 1.9 | 1.9 | 43% | 74% |
| | | | | |
| .125" LEG | | | | |
| Relative Permeability | Maximum Flux Density | Midpoint Flux Density | % increase, MAX | % increase, MID |
| 1 | 1.8 | 1.8 | 0 | 0 |
| 2 | 1.94 | 1.94 | 8% | 8% |
| 5 | 2.03 | 2.03 | 13% | 13% |
| 10 | 2.05 | 2.05 | 14% | 14% |
| 100 | 2.07 | 2.07 | 15% | 15% |
| 1000 | 2.07 | 2.07 | 15% | 15% |
| | | | | |
| .0625" LEG | | | | |
| Relative Permeability | Maximum Flux Density | Midpoint Flux Density | % increase, MAX | % increase, MID |
| 1 | 2.03 | 2.03 | 0 | 0 |
| 2 | 2.06 | 2.06 | 1% | 1% |
| 5 | 2.09 | 2.09 | 3% | 3% |
| 10 | 2.1 | 2.1 | 3% | 3% |
| 100 | 2.11 | 2.11 | 4% | 4% |
| 1000 | 2.11 | 2.11 | 4% | 4% |

Table 3.2.2-5 - FEA Results, Increased Gap Permeability, Varying C-Channel Geometry. This table summarizes the results of the permeability sensitivity study for various C-Channel Leg Geometries. Summarizing, thinner cross sections yield less improvement from increased gap permeability. This highlights the geometry-dependent nature of the behavior of the magnetic circuit, and the need for FEA to study saturation effects.

From the above study, we can see that non-linear effects are dependent on the geometry of the specific magnetic circuit. Specifically, effects from leakage flux and saturation can drive the results when studying performance. Finite element analysis is required to quantify these factors for complex systems, which is then used to drive the macro scale model.

# CHAPTER 4 – EXPERIMENT 1 – OFF THE SHELF MOTOR

This chapter presents the results of the initial experiment. A set of off the shelf commercial motors were purchased, baselined, and immersed in both a ferrofluid and, as a basis of comparison, a fluid of equivalent viscosity. As predicted by the mathematical models, gains were seen at low RPM from ferrofluid immersion, while shear loss increases at high RPM led to a negative net efficiency. However, these losses were smaller for the ferrofluid immersion than the standard oil.

## 4.1 BACKGROUND

For the initial experimental system, a set of motors were purchased commercially. They were then fixtured and baselined for initial performance. One motor was fully immersed in ferrofluid, and the motor's performance was measured. As a control, the second motor was fully immersed in a standard oil of equivalent viscosity, and the performance was measured.

## 4.2 EXPERIMENTAL RESULTS

For the first phase of the experimental research, a set of "Commercial Off The Shelf" (COTS) permanent magnet machines were procured, along with all related test fixtures and measurement devices. Also, samples of ferrofluid and a non-magnetically permeable fluid of an identical viscosity were obtained. This PMM was placed in a test fixture and immersed in the ferrofluid. The device was then run, and measured for performance improvements in efficiency.

The motors used have a stator radius of 0.5", a rotor radius of 0.47", and are 1.0" in height with 180 turns. They are DC motors, rated for 12,000 RPM at 6V. A sample of ferrofluid was also obtained. The company considered the exact formulation of the material proprietary, although they did provide some basic material properties. The ferrofluid has a viscosity of 200 centistokes, which is equivalent to SAE Oil grade 20W, and a rated relative permeability of 5. Note that this is at zero magnetization, and would be dependent on the magnetic field. As shown in figure 2.5-2, the relative permeability in the magnetic circuit would be reduced to ~ 2.0 given the magnetic field strength of the system.

Solving for the flux across the gap, and substituting into equation 3.2.1-1, we have for the baseline system:

$$Ke = 3.624\, N_1\, \Phi_f \qquad 4.2\text{-}1$$

$$\text{Ke=(3.624) (180) (4.185e-6)} \qquad 4.2\text{-}2$$

$$\text{Ke=0.000501 Volts / Rev / Second} \qquad 4.2\text{-}3$$

Figure 4.2-1 shows the plot of RPM vs. voltage at no load.

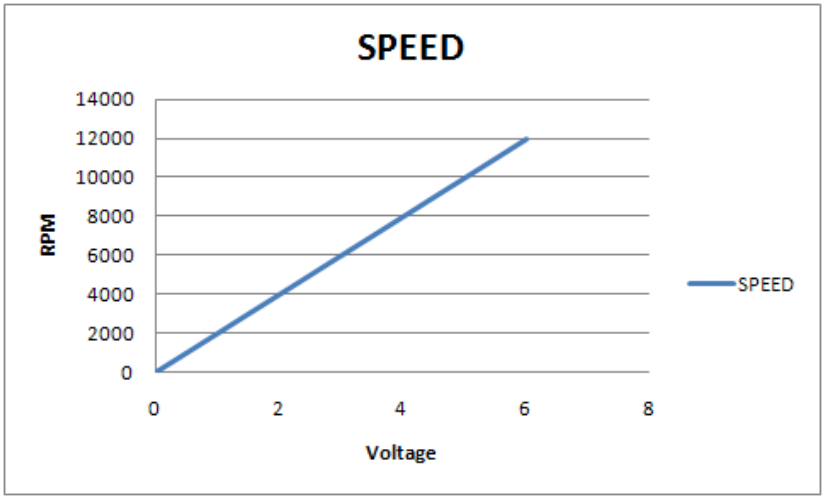


Figure 4.2-1 – Baseline Motor Performance. This figure shows the predicted values of RPM vs. Voltage for the motor used in experiment 1.

As a means of calibrating the accuracy of the macro-scale model developed for this dissertation, J-MAG Express, a "design wizard" style program for electric motors was used as a basis of comparison. Figure 4.2-2 shows the J-MAG Express model. Input data for the J-Mag model is shown in the figure, with a Ferrite Magnet, "Ferrite-br2" used, along with Copper Windings and Steel Sheets for the Rotor and Stator. 180 total turns were used in the one phase system.

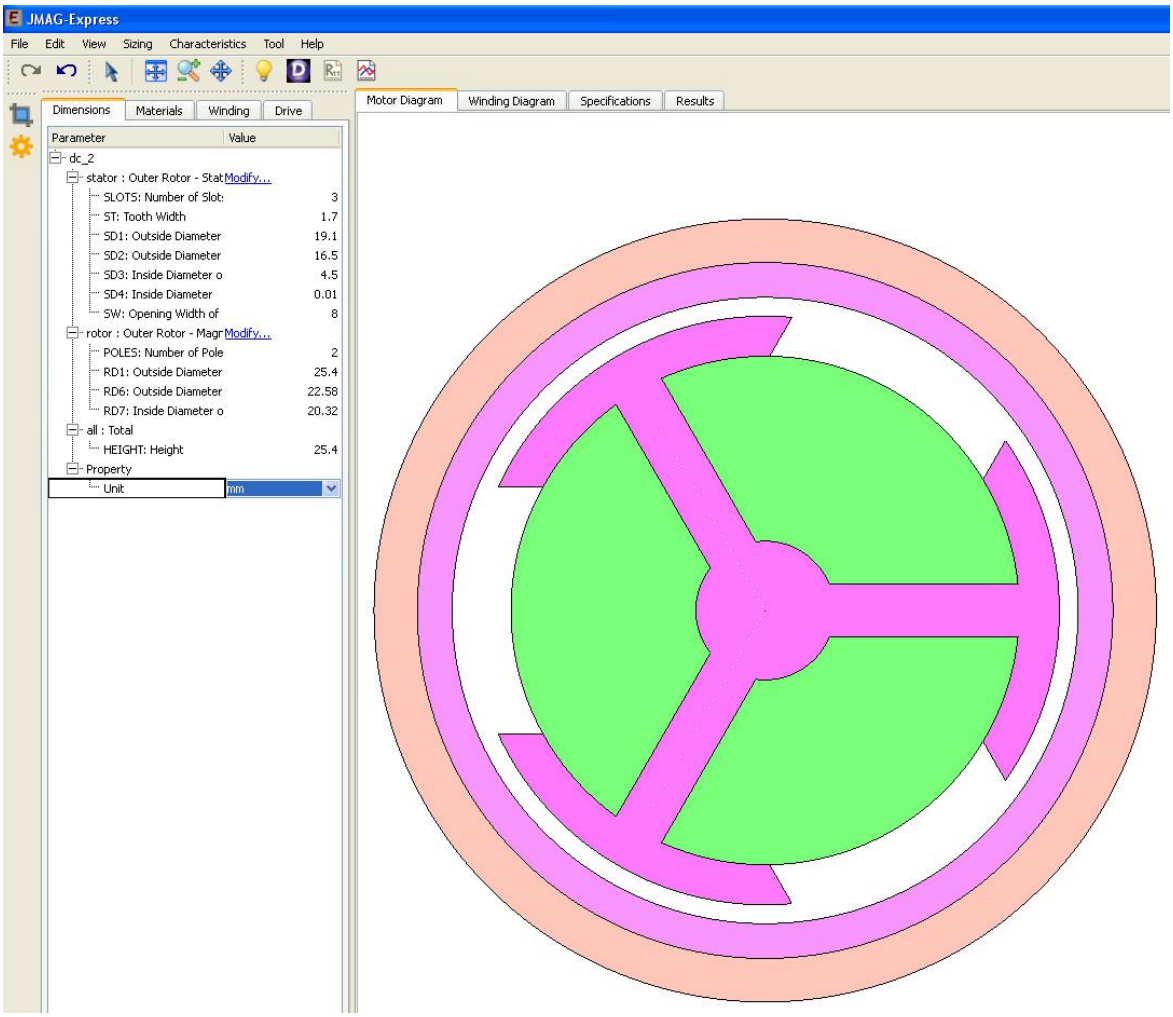


Figure 4.2-2 – JMAG Express Model. This figure shows the model set-up in a JMAG-Express, a commercial motor design software system for the motor used in experiment 1. This was done to benchmark the macro scale model.

Running the model in JMAG-Express provided the data shown in Figure 4.2-3. For the RPM vs. Voltage curve, the JMAG model shows approximately a 9% delta at maximum speed, providing a positive benchmark data point for the macro scale model.

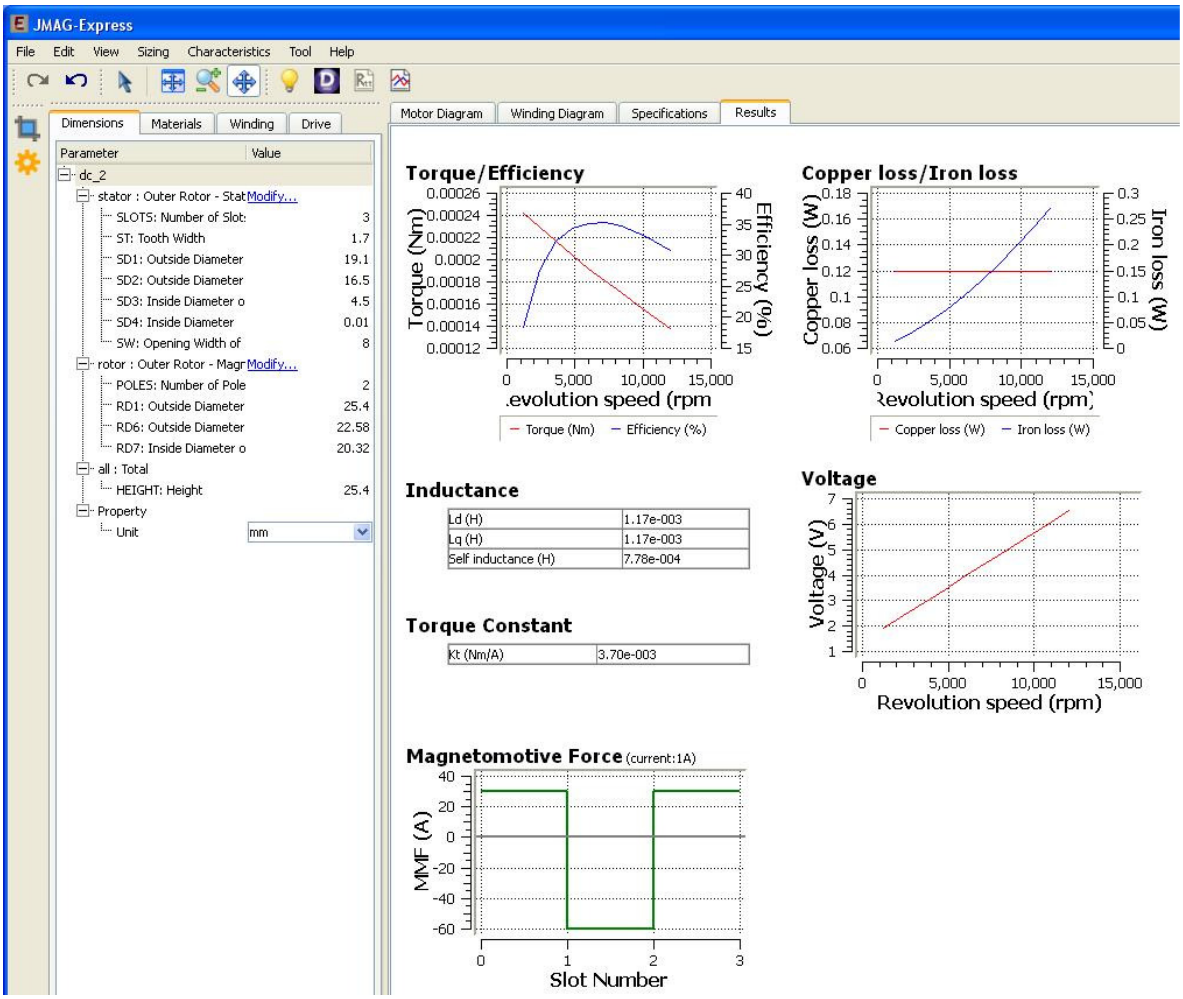


Figure 4.2-3 – JMAG Express Results. This figure shows the results from the JMAG-Express analysis. At maximum RPM, the commercial code matched the macro scale model to within 9% for Voltage vs. Speed.

Using equation 2.4.1-5, windage / fluid friction losses were calculated for air and ferrofluid / SAE Oil, shown in 4.2-4. Note that at lower RPM, there is little difference in windage losses. However, higher RPM values correspond to greater increases in losses.

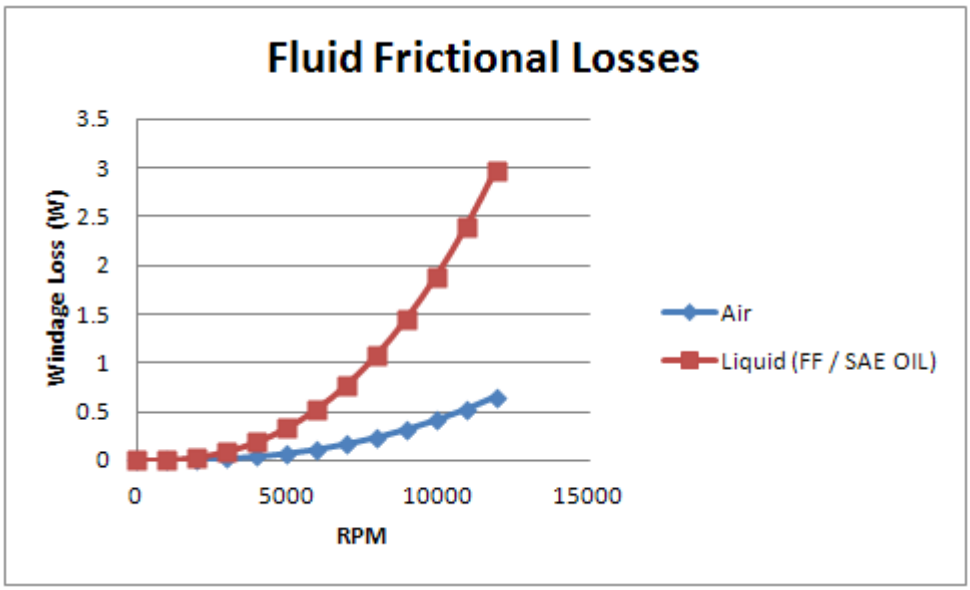


Figure 4.2-4 – Fluid Frictional Losses. This figure shows the predicted windage / fluid friction losses due to ferrofluid immersion for the motor used in experiment 1.

FEA results for the model are shown in figure 4.2-5 and figure 4.2-6. Note that the system is not saturated, which could be expected, given the low powered ferrite magnets used in the system. No significant increase is seen in the leakage flux.

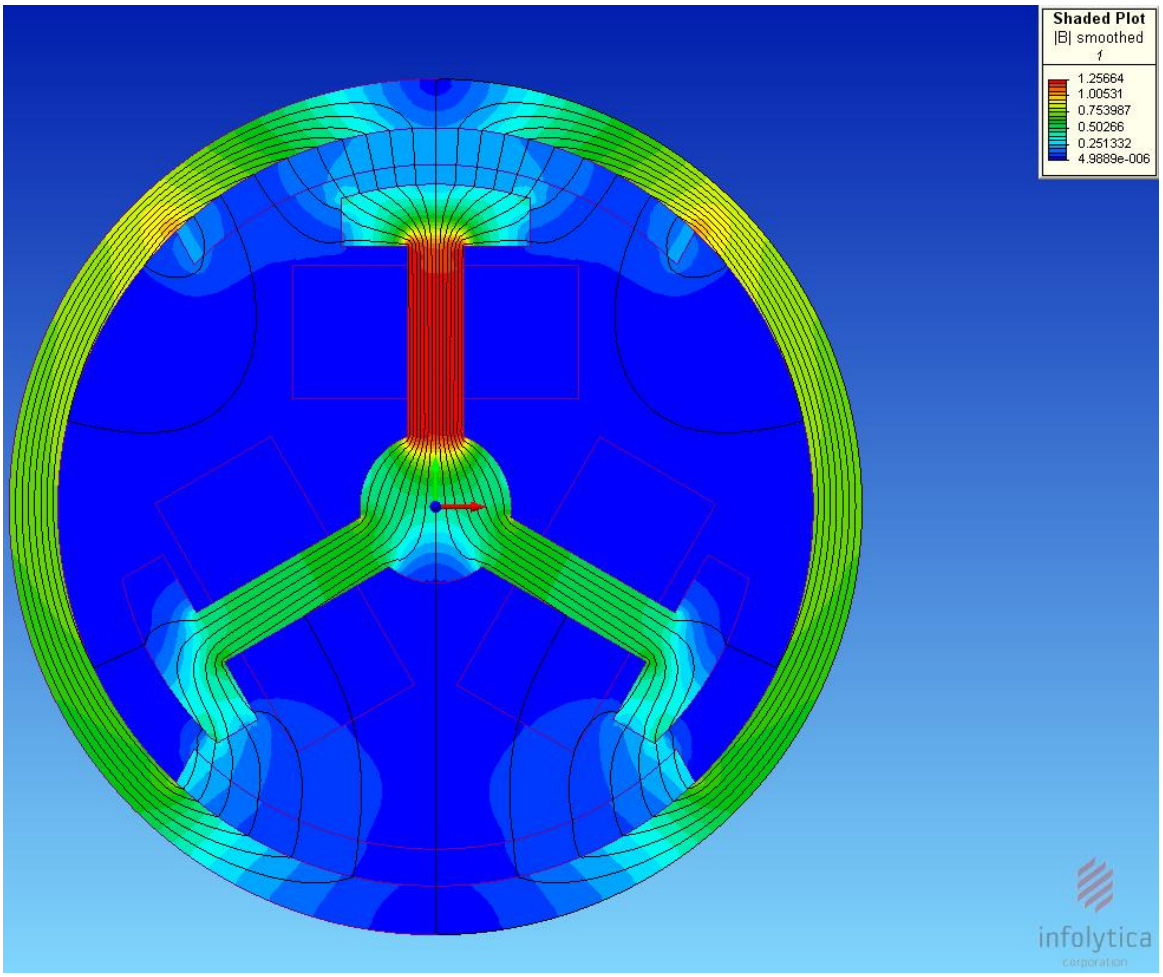


Figure 4.2-5 – FEA – COTS System, Traditional Air gap. This figure shows the baseline finite element analysis for the motor used in experiment 1. Note that there is little leakage flux in the design, and that the system is far from magnetic saturation.

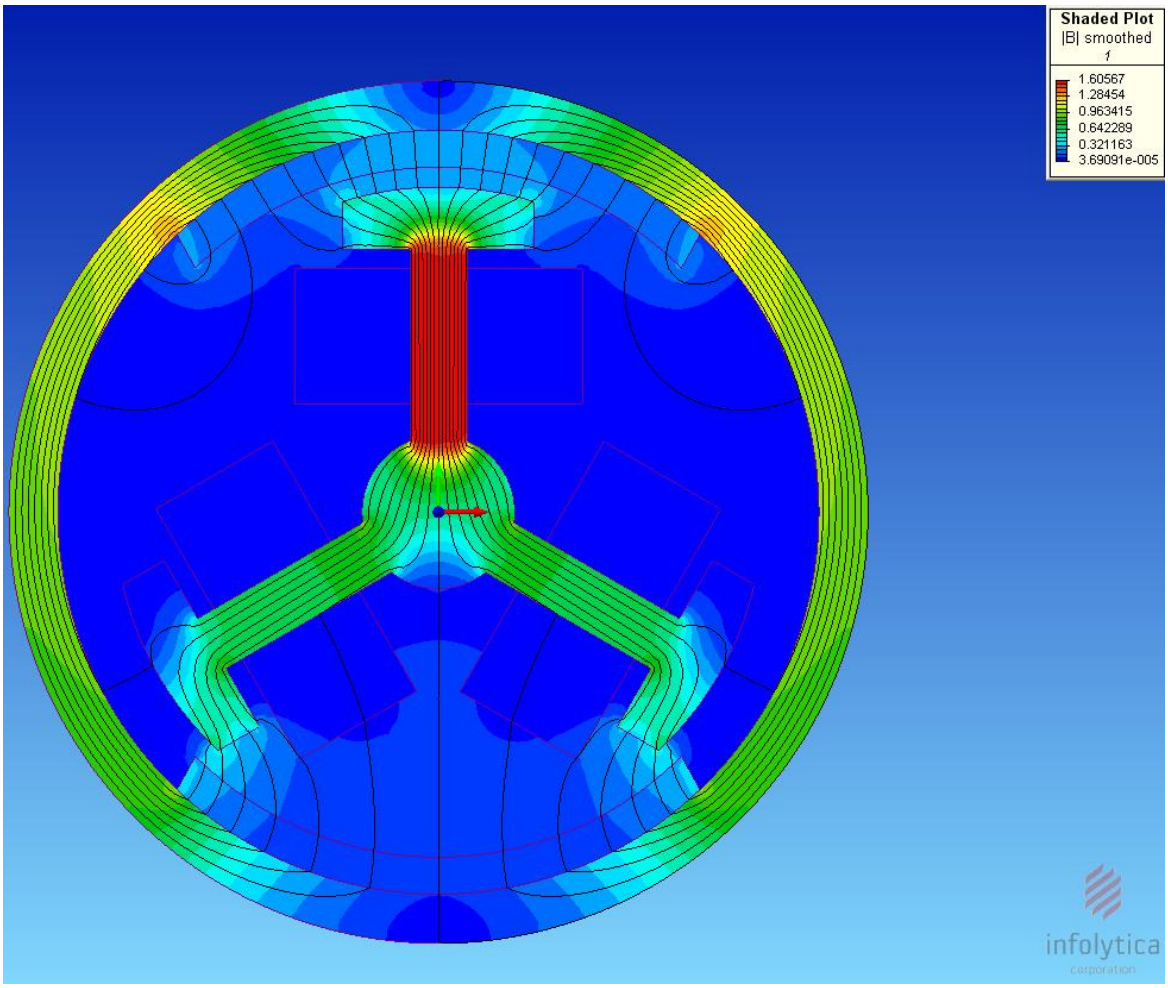


Figure 4.2-6 – FEA – COTS System, Ferrofluid Immersed. This figure shows the finite element analysis for ferrofluid immersion of the motor used in experiment 1. Note that there is little leakage flux in the design, and that the system is far from magnetic saturation.

Testing the analytical results, first the motor was characterized in its given condition. To do this, the voltage of the motor was varied in 0.5V increments using a DC power supply, and the motor's RPM was measured at various power levels with a non-contact Tachometer. In an attempt to measure torque, a digital force gauge at a set distance was used, but the force / torque applied by the micromotor were below the force gauge's

ability to detect. For one sample, the motor was immersed in ferrofluid and the effects were recorded. For a second sample, the motor was immersed in the SAE oil and the effects were recorded. Figure 4.2-7 shows a CAD model of the fluid tank / test fixture, and figure 4.2-8 shows a photo of the actual test.

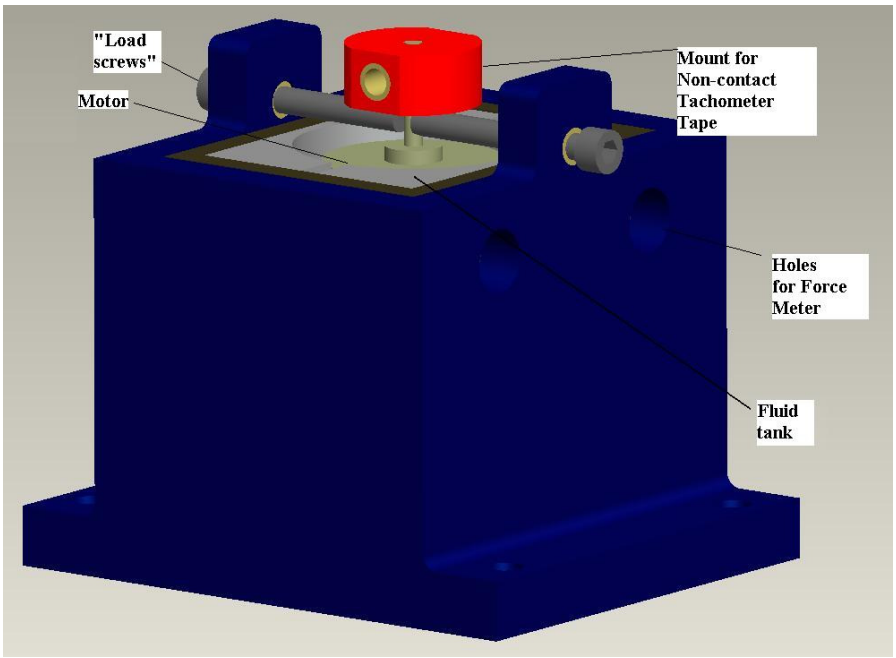


Figure 4.2-7 - COTS Motor Test Set-Up CAD Model. This figure shows the CAD Model for the test set up for experiment 1.

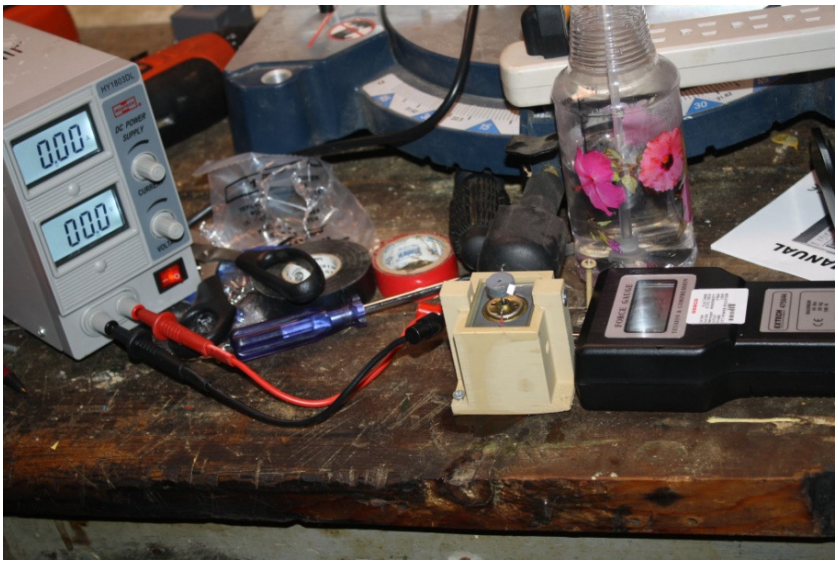

Figure 4.2-8 - COTS Motor Test Set-Up Photo. This figure shows a picture of the test set up for experiment 1.

For the SAE Oil immersed motor, losses for the motor started at 100%, failing to start until 1.0 Volts, then moved to the ~60% range before starting to decline, ending at 44% at 6.0 Volts. Current draw for the motor increased from the 0.08 to 0.15 Amps range to 0.2 to 0.85 Amps. The experimental set-up failed to record any force from the motor torque. Figure 4.2-9 shows the graph RPM vs. voltage for the oil immersed motor. Table 4.2-1 shows the raw data from the experiment.

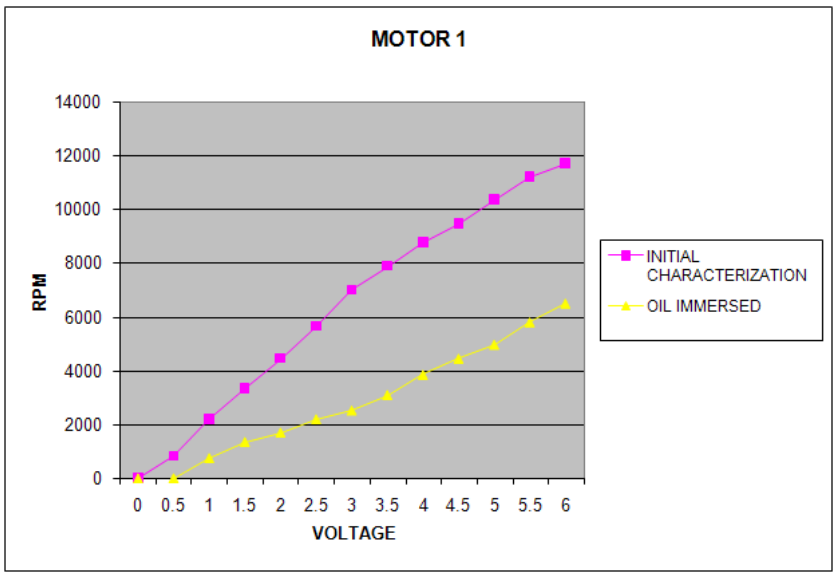


Figure 4.2-9 -Voltage vs. RPM, Oil Immersed Motor. This figure shows a plot of the measured speed vs. voltage for experiment 1 for the baseline air gap and for the oil (non-ferrofluid) immersed system.

For the ferrofluid immersed motor, low RPM performance in terms of Volts / RPM saw a modest gain, then moved to the 15% range, ramped up to a maximum of 23%, then began to decline, ending at 14% at 6.0 Volts. The Current draw for the motor increased from the 0.07 to 0.16 Amps range to 0.08 to 0.53 Amps. The experimental set-up failed to record any force from the motor torque. Figure 4.2-10 shows the graph of RPM vs. voltage for the ferrofluid immersed motor.

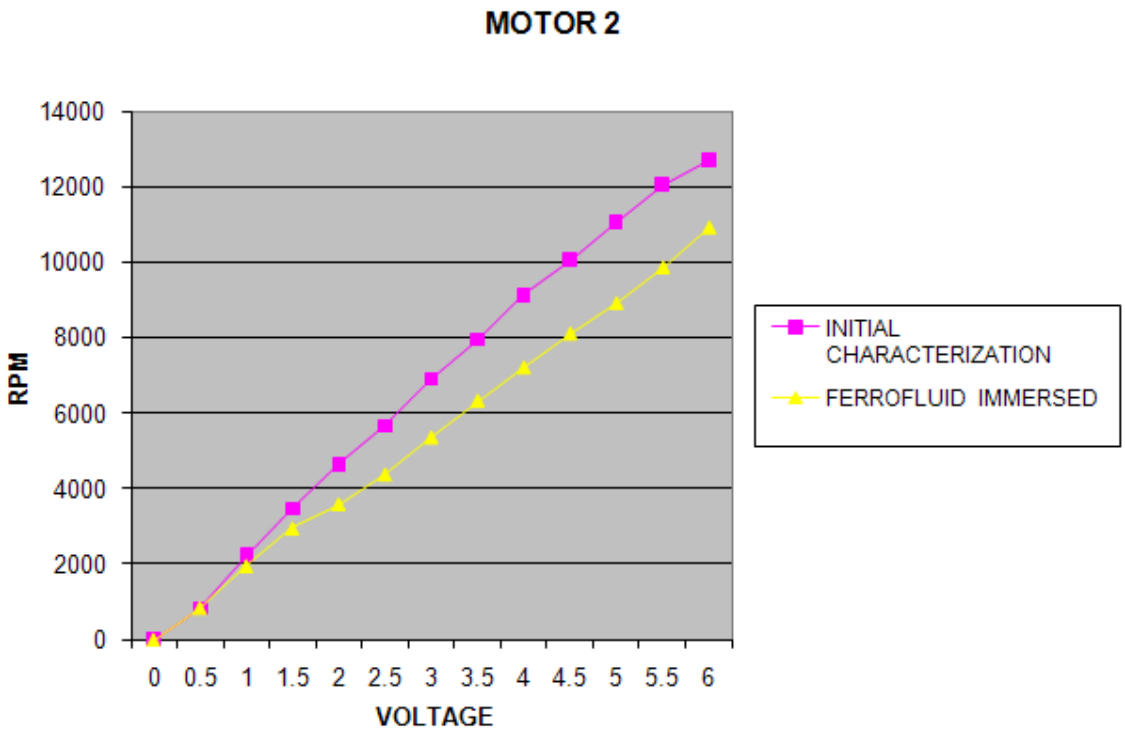


Figure 4.2-10 – RPM vs. Voltage, Ferrofluid Immersed Motor. This figure shows a plot of the measured speed vs. voltage for experiment 1 for the baseline air gap and for the ferrofluid immersed system. Note that the ferrofluid immersed motor shows a decline in system performance compared to the baseline air gap, but improved performance compared to the oil immersed system.

Studying the test results, as predicted, the gain from the improved permeability of the ferrofluid did not make up for the increased shear losses of the fluid immersion. However, as shown in Figure 4.2-11, the losses were much greater in a standard fluid than a ferrofluid, showing some benefit from the approach, even more than predicted. In terms of Voltage Constant, the SAE oil immersed motor was measured to be 916 RPM / Volt, a 57% decreased from the baseline Voltage Constant of 2125 RPM / Volt. The ferrofluid immersed system was measured at 1817 RPM / Volt, a decrease of only 15% from the baseline air gap system. For applications where the system must be fluid

immersed for heat transfer purposes and Voltage / RPM is a critical factor, ferrofluid immersion can offer significant gains.

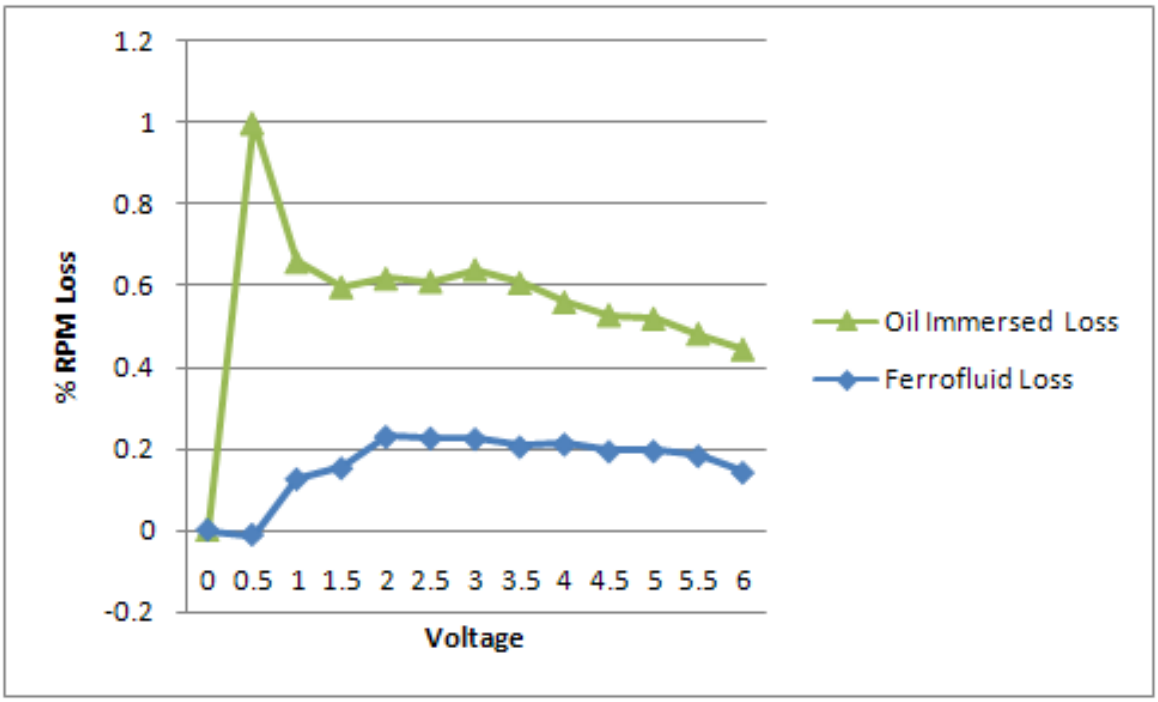


Figure 4.2-11 - Performance Comparison, Ferrofluid vs. SAE Oil. This figure shows a plot of % RPM Loss vs. voltage for experiment 1 for the oil immersed system and for the ferrofluid immersed system. Summarizing, both the ferrofluid and oil immersed motors showed reduced performance compared to a standard air gap system. However, the percentage loss for the ferrofluid system was much lower than that of the standard oil system.

Also, we can see that there was less of a current draw in the ferrofluid motor. While torque data was not captured for this experiment, as the low torque output from the motor was below the range of sensitivity for the force gauge, this implies an efficiency gain for the ferrofluid system vs. the traditional fluid immersed PMM.

In both systems, the efficiency loss unexpectedly declined as the RPM went up. The anticipated effect was that shear losses would be proportional to speed, and would increase linearly with RPM. However, other effects, such as a possible lowering of viscosity due to temperature increases at higher power levels or, for the ferrofluid, a lowering of viscosity due to ferrohydrodynamic effects at high RPM, seem to have offset the shear loss.

An initial experimental test has shown that ferrofluid immersion of a permanent magnet machine can show increased performance compared to immersion in a fluid of similar viscosity, as the improved magnetic permeability of the ferrofluid offsets some of the shear loss gain from liquid as opposed to air operation.

# CHAPTER 5 – EXPERIMENT 2 – PROOF OF CONCEPT GENERATOR

This chapter presents the results of the second experiment. A "proof of concept" generator system was designed and constructed. This unit was baselined, then immersed in ferrofluid to measure the performance gain. As predicted by the mathematical models, gains were seen from ferrofluid immersion.

## 5.1 BACKGROUND

For the second phase of the experimental research, an axial flux ("pancake" style) motor / generator, was designed and built, with the concept of ferrofluid immersion as a design consideration, offering the thermal and magnetic benefits while minimizing shear losses. In the design, fluid can be added to a point just before the magnets, and all other rotating elements (shaft, back iron for magnets, et al.) are isolated from unnecessary viscous losses.

Rather than suffering the shear losses of the ferrofluids, ideally, the generator should be designed as such that the stator is completely immersed in fluid, while the rotor is completely isolated from the liquid. This provides the benefits of the magnetic circuit, such as improved permeability of the gap and reduction in cogging torque, while eliminating the offsetting increase in viscous losses that would occur if the rotor was fluid immersed.

A containment tank would need to be a feature of the system to prevent ferrofluid leakage. Containing the ferrofluid in a stationary tank prevents the need to dynamically

seal a rotating shaft immersed in liquid, which is often a practical design challenge in rotating machinery with a fluid coolant or lubricant. The containment tank should be non-magnetic, or have a very low permeability, to avoid increases in leakage flux. Also, the windings would be highly dense with a high stator pole count to prevent areas for ferrofluid to flow between stator poles, increasing leakage flux.

A provision must be provided to pass the electrical power from the stator to the end application. Connectors must be provided to pass the power through the containment tank wall. This connector must be hermetic to prevent fluid leakage.

Figure 5.1-1 shows a concept design for a ferrofluid-optimized axial flux system, which features a containment tank to separate the stationary components, including the ferrofluid, from the rotating components, including the shaft and bearing.

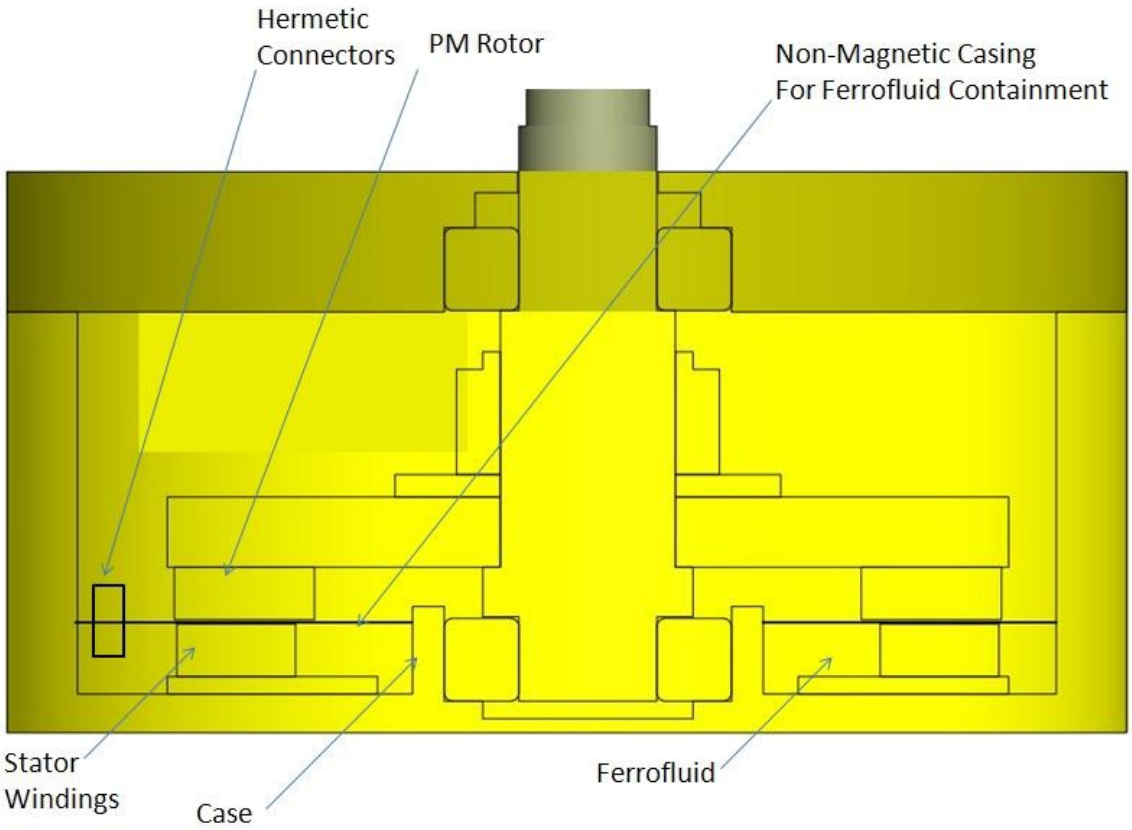


Figure 5.1-1 –Concept Design, Axial Flux System with Ferrofluid Consideration. This figure shows a concept for axial flux permanent magnet machine with ferrofluid immersion consideration. The rotating components are separated from the stationary stator in a containment tank, which reduces the shear losses associated with ferrofluid immersion.

Similarly, an ideally designed radial flux system would need to provide a containment tank for the ferrofluid, isolating the liquid from the rotating components. Figure 5.1-2 shows a concept design for a radial flux system with ferrofluid consideration.

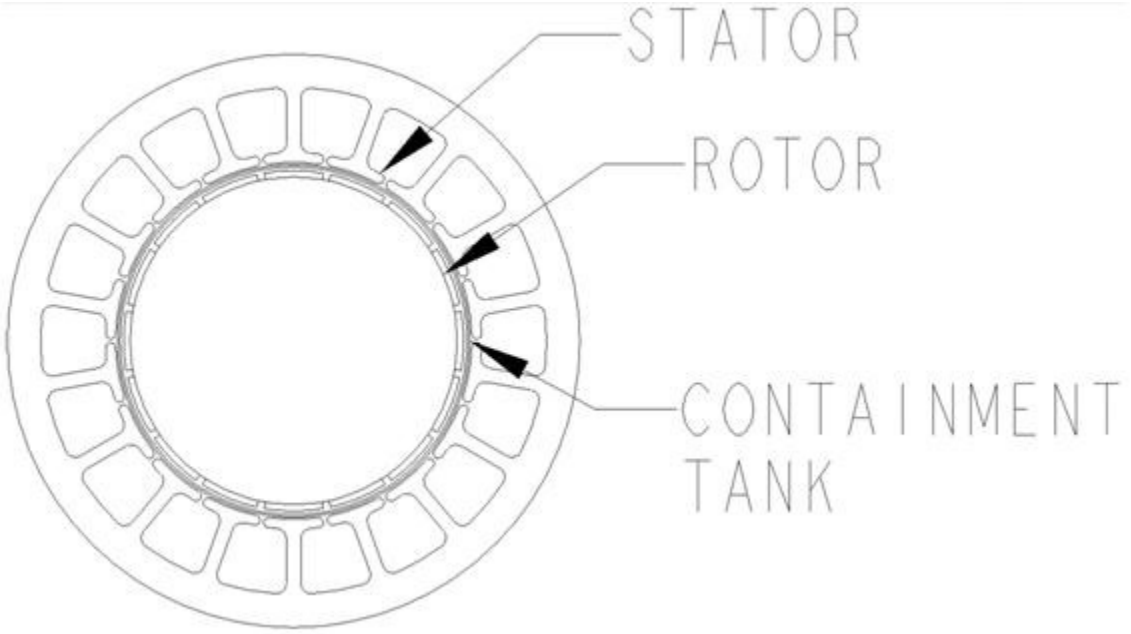


Figure 5.1-2 – Concept Design, Radial Flux System with Ferrofluid Consideration. This figure shows a concept radial flux permanent magnet machine with ferrofluid consideration. The rotating components are separated from the stationary stator in a containment tank, which reduces the shear losses associated with ferrofluid immersion.

Comparing the radial flux system vs. the axial flux system, we can see that the axial flux system has advantages in simplicity of design, with the containment tank separated by a simple plane, as opposed to the concentric cylinders required for a radial flux system. The radial flux concentric cylinders would present difficulties in tolerance stack-up and manufacture. Also, axial flux ferrofluid systems have not been identified in prior research, offering a new contribution to the field for this dissertation. For these reasons, axial flux systems were focused upon, with experiments 2, 3, and 4 featuring axial flux systems designed and built for this research effort.

## 5.2 EXPERIMENTAL RESULTS

The generator is an axial flux design, with a stator and rotor diameter of 8". An off the shelf ring of twelve axial flux wedge style magnets of Neodymium Iron Boron, N42 material [1.2 Tesla Br, 12,000 Oersted Hc] was used for the rotor. The stator is 1018 steel, with 0.5" in winding height, with a 0.25" baseplate, with 15 poles wound for three phase output power. Figure 5.2-1 shows the CAD model of the tested generator.

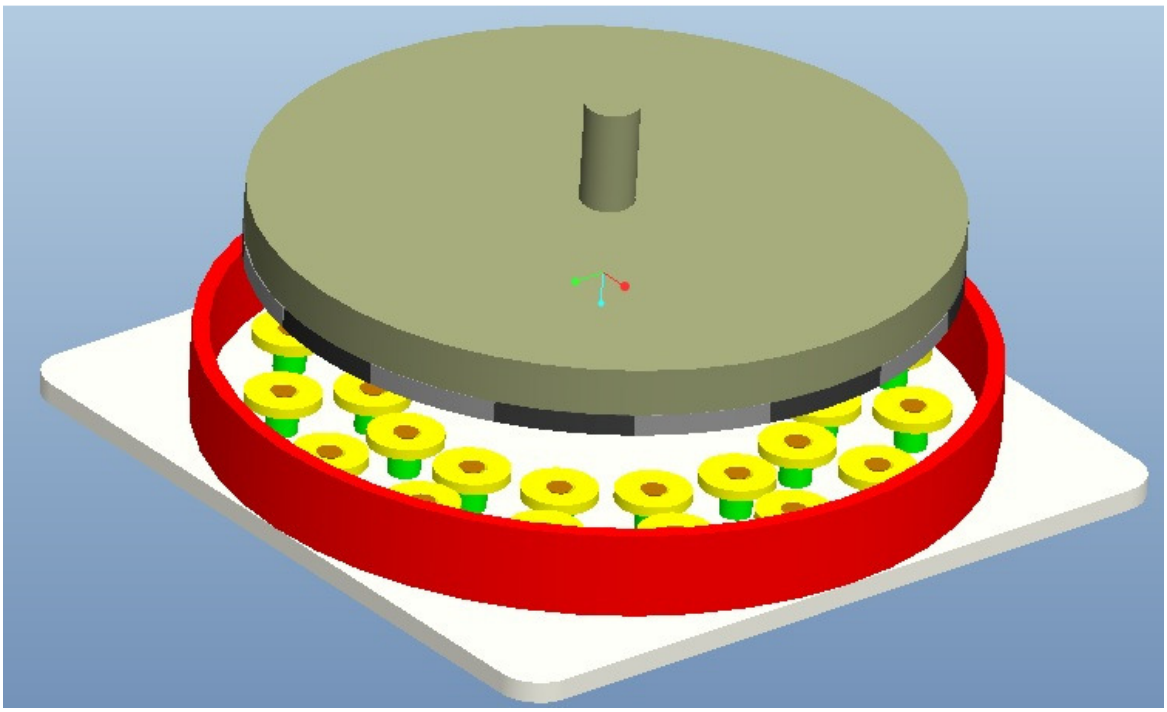

Figure 5.2-1- Proof of Concept Design Test Set-Up CAD Model. This figure shows the CAD model for experiment 2, an 8" diameter axial flux style generator.

Spray electrically insulating varnish was used for electrical isolation. The same type of ferrofluid used in experiment 1 was used in experiment 2, contained in an 8" PVC pipe coupling (8.625" ID). A drill press AC motor was used to drive the system as a generator, Raw AC power was run to a three phase bridge rectifier AC-DC converter, then sent to a

resistive load for power dissipation. Baseline measurements were taken, and additional measurements were taken with the tank filled with ferrofluid. Figure 5.2-2 shows a photograph of the tested generator.

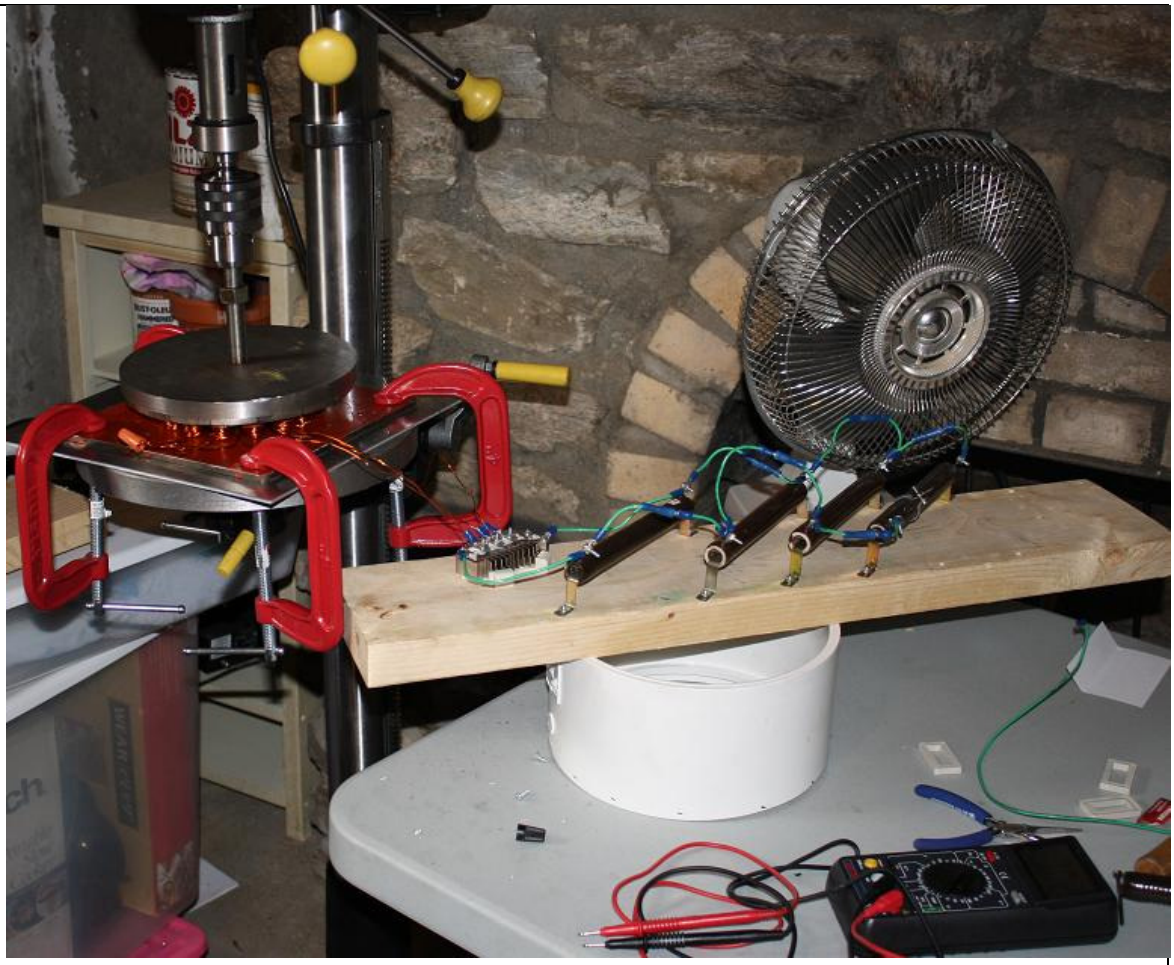

Figure 5.2-2- Proof of Concept Design Test Set-Up Photo. This figure shows a photo of the test set up for experiment 2, an 8" diameter axial flux style generator.

For the experimental design, a large airgap (.25") was used. Although this provided poor system efficiency, this decision was made based on several factors, including:

- The low efficiency baseline demonstrates large performance increases with ferrofluid immersion.
- Low voltage / low RPM operation provided a measure of safety for the experiment.
- In earlier prototypes, small airgap systems experienced magnetic forces that exceeded the limits of the drill press retaining forces (chuck, collet, et al.).

Baseline predicted performance, using the developed computational model, shows a linear relationship between voltage and RPM, shown in figure 5.2-3.

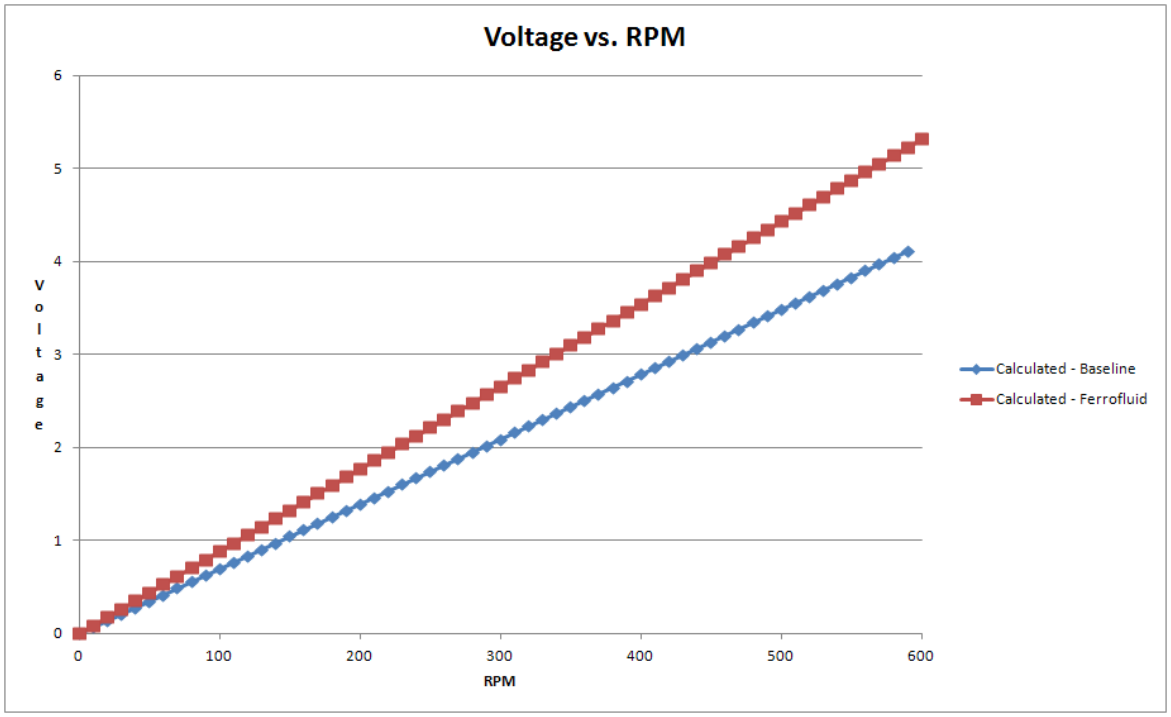


Figure 5.2-3 – Calculated Generator Performance. This figure shows the predicted performance in terms of voltage vs. speed within the tested range for the generator used in experiment 2.

FEA results for the model are shown in figure 5.2-4 and figure 5.2-5. Note that some saturation is seen in the back iron of the stator in the ferrofluid system, limiting potential magnetic gains. Flux leakage shows a slight increase in the ferrofluid system.

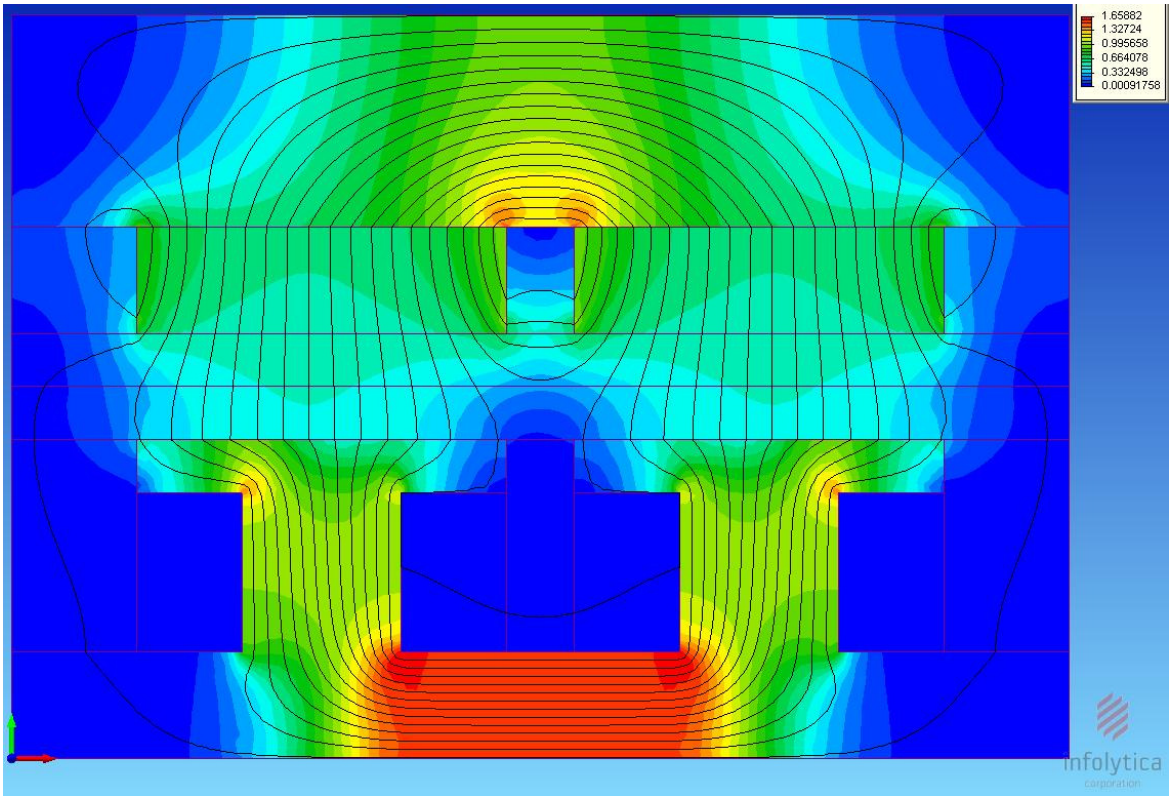


Figure 5.2-4 – FEA –Experiment 2, Traditional Air gap. This figure shows the baseline finite element analysis for the generator used in experiment 2. Note that there is some leakage flux in the design, and that the stator back iron is close to magnetic saturation.

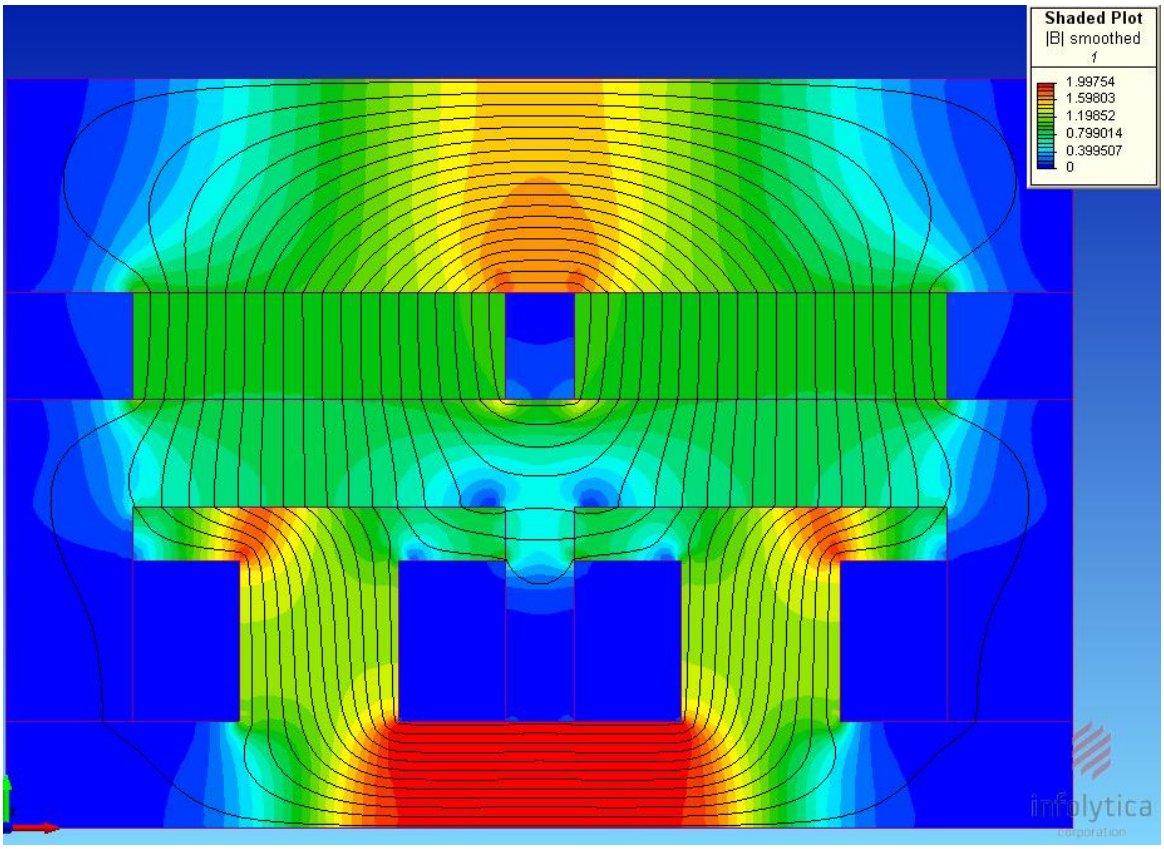


Figure 5.2-5 – FEA –Experiment 2, .25 Ferrofluid Immersed. This figure shows the finite element analysis for the generator used in experiment 2 with ferrofluid immersion up to the point of the rotor. Note the slight increase in leakage flux in the design, and that the system is magnetically saturated in the stator back iron.

The output speed was adjusted through changing positions on the three driving pulleys. A multimeter recorded the output voltage. RPM vs. Voltage provided a measure of system improvement. The baseline system's speed constant was measured to be 0.0063 Volts / RPM. For the ferrofluid immersed system, the speed constant was measured to be 0.0069 Volts / RPM, a 9% improvement from the baseline system. Figure 5.2-6 shows the raw data from the experiment.

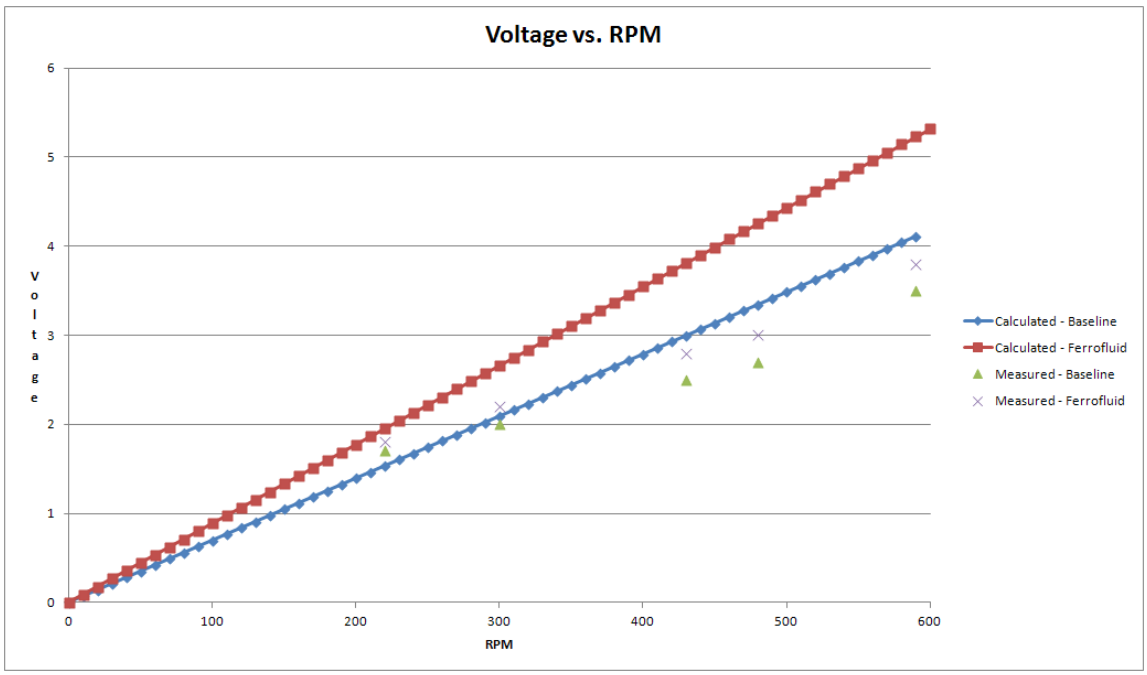


Figure 5.2-6 – Experiment 2 Results. This figure shows the graphs of the air gap and ferrofluid systems, with calculated and experimental values shown. Summarizing, the ferrofluid system shows increased performance across the RPM range, and the calculated values match the experimental data <30%.

Worth noting from the test was that the initial test plan featured filling the system to various fill levels, with multiple measurements taken. However, at the first fill level, it was observed that the ferrofluid was drawn to the rotor. In order to provide a stable system, the generator was completely immersed in ferrofluid for Experiment 2, and only the baseline and one set of ferrofluid immersed data was collected. Figure 5.2-7 shows the rotor post-test, with the ferrofluid magnetically attached to the rotor.

Figure 5.2-7 – Experiment 2, Rotor, Post-Test. This figure shows Experiment 2's rotor after the test. Note the ferrofluid magnetically attached to the permanent magnets, with the magnetic forces exceeding the gravitational forces. This highlights the need for a containment tank, a lesson learned that was incorporated into experiments 3 and 4.

While this experiment was unsuccessful in providing the range of testing desired to study ferrofluid effects, it did offer numerous lessons learned for future experimental designs. Numerous considerations in the design of the generators used in experiment 3 and experiment 4 were driven from this experiment, including:

- In order to avoid the ferrofluid / rotor attraction shown in figure 5.2-7, a containment tank was designed into the assembly.

- A larger system was originally thought to be desired in order to demonstrate a large system improvement. However, the large system inherently involves large magnetic forces, which made handling of the magnets difficult in manufacturing and fixturing. A smaller system was developed for future experiments.
- The open frame system was low cost and easy to assemble, but presented a safety hazard, especially in high RPM. Future systems featured a closed casing, allowing high RPM operation
- At low Voltage, additional electrical insulation beyond the enamel on the magnet wire, such as spray-on varnish, is not required for the application
- A positive retention system for the magnets beyond the magnetic attraction of the magnets to the rotor is required for high RPM operation.
- For the experimental set-up, direct AC voltage can be measured, eliminating the need for bridge rectifiers.

# CHAPTER 6 – EXPERIMENT 3 – LARGE GAP FERROFLUID EXPERIMENT

This chapter presents the results of the third experiment. A generator system was designed and constructed, with the goal of demonstrating magnetic improvement from ferrofluid immersion. This unit was baselined with a standard air gap, then immersed in ferrofluid to measure the performance gain.

## 6.1 BACKGROUND

For the third phase of the experimental research, an axial flux ("pancake" style) motor / generator was designed and built, utilizing lessons learned from the prior experiment. A low power, smaller system, designed with a containment tank and a magnet retention system was constructed, providing a reliable, repeatable experiment

## 6.2 EXPERIMENTAL RESULTS

The generator used for experiment 3 was designed utilizing lessons learned from the prior experiment where it was discovered that a ferrofluid containment tank was required. In the design, the stator is completely isolated and ferrofluid immersed, and all other rotating elements (shaft, back iron for magnets, et al.) are isolated from unnecessary viscous losses. It features a stator and rotor diameter of 2". Two 5/8" disc style magnets of Neodymium Iron Boron, N42 material [1.2 Tesla Br, 12,000 Oersted Hc] were used for the rotor. The stator is 1018 steel, with 0.125" in winding height, with a 0.25" baseplate, with three poles wound with 70 turns per pole for one phase output power. The

magnets feature a countersunk thru-hole, which allows a non-magnetic screw to fasten the magnets to the rotor. The rotor-stator gap consists of a 0.032” air gap between the magnets and the containment tank, the 0.032” stator cover, and a 0.282” stator to cover gap, as opposed to the 0.032” stator-cover gap of experiment 4. Figure 6.2-1 shows the CAD model of the tested generator.

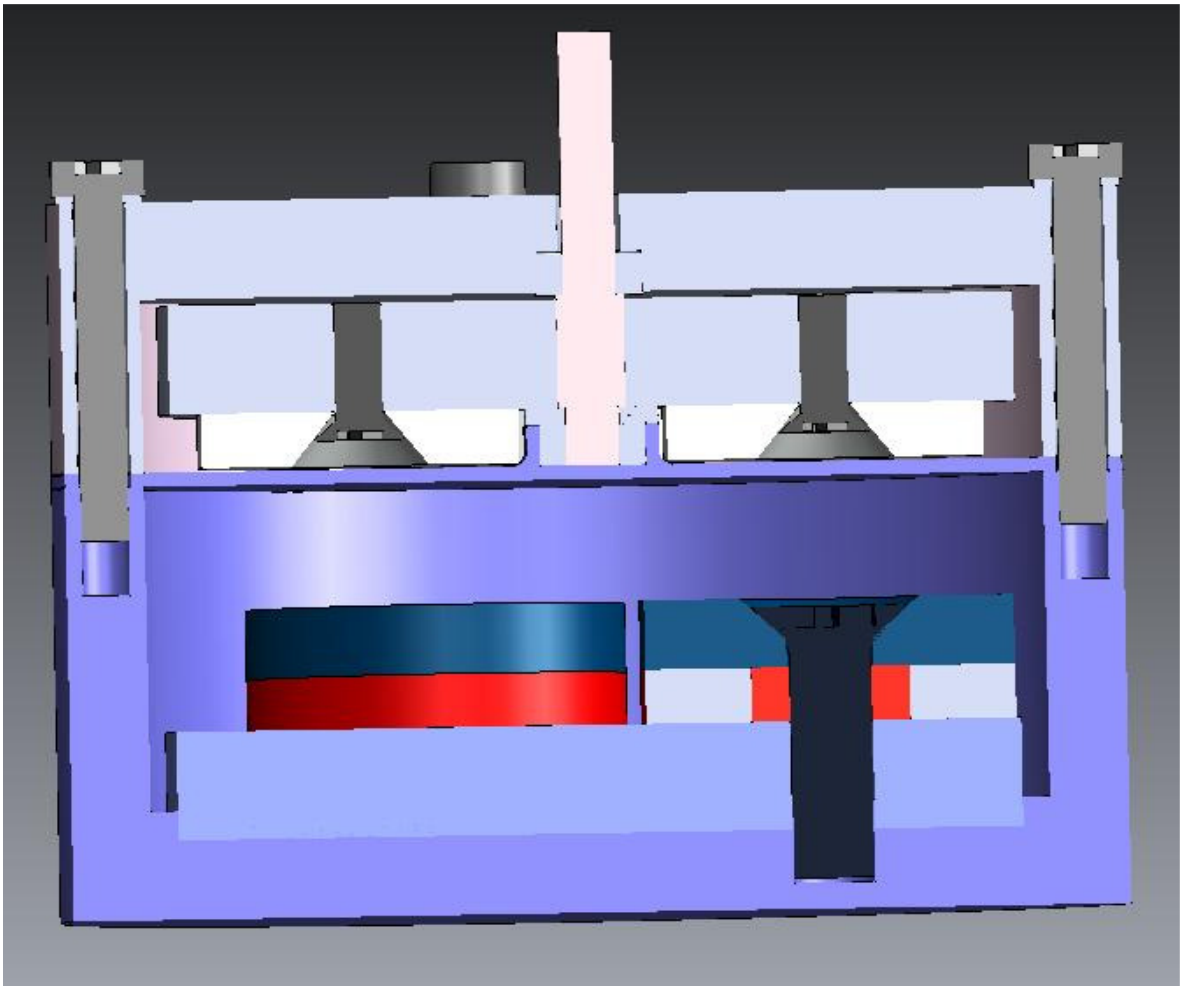

**Figure 6.2-1 - Experiment 3 CAD Model.** This figure shows a CAD model of the generator used for experiment 3, a 2” diameter axial flux generator featuring a 0.282” stator to stator cover gap.

Given the expected low voltage of the system, no electrical insulation was used other than the supplied wire enamel. The same type of ferrofluid used in experiment 1 and experiment 2 was used in experiment 3, fully contained in the casing. A drill press AC motor was used to drive the system as a generator. Raw AC power was run to a resistive load for power dissipation. Baseline measurements were taken, and additional measurements were taken with the tank filled with ferrofluid. Figure 6.2-2 shows a photograph of the tested generator.

Figure 6.2-2 – Experiment 3 Generator. This figure shows pictures of the generator used for experiment 3, a 2" diameter axial flux PMM.

Solving for the flux across the gap, and substituting into equation 3.2.1-1, we have for the baseline system:

$$Ke = 3.624\, N_1\, \Phi_f \quad (6.2\text{-}1)$$

$$\text{Ke=(3.624) (210) (4.185e-6)} \quad (6.2\text{-}2)$$

$$\text{Ke=0.003188 Volts / Rev / Second} \quad (6.2\text{-}3)$$

For the ferrofluid immersed system:

$$Ke = 3.624 * N_1 * \Phi_f \quad (6.2\text{-}4)$$

$$\text{Ke=(3.624) (210) (4.894e-6)} \quad (6.2\text{-}5)$$

$$\text{Ke=0.003728 Volts / Rev / Second} \quad (6.2\text{-}6)$$

Predicted performance, using the developed computational model for voltage / RPM is shown in figure 6.2-3.

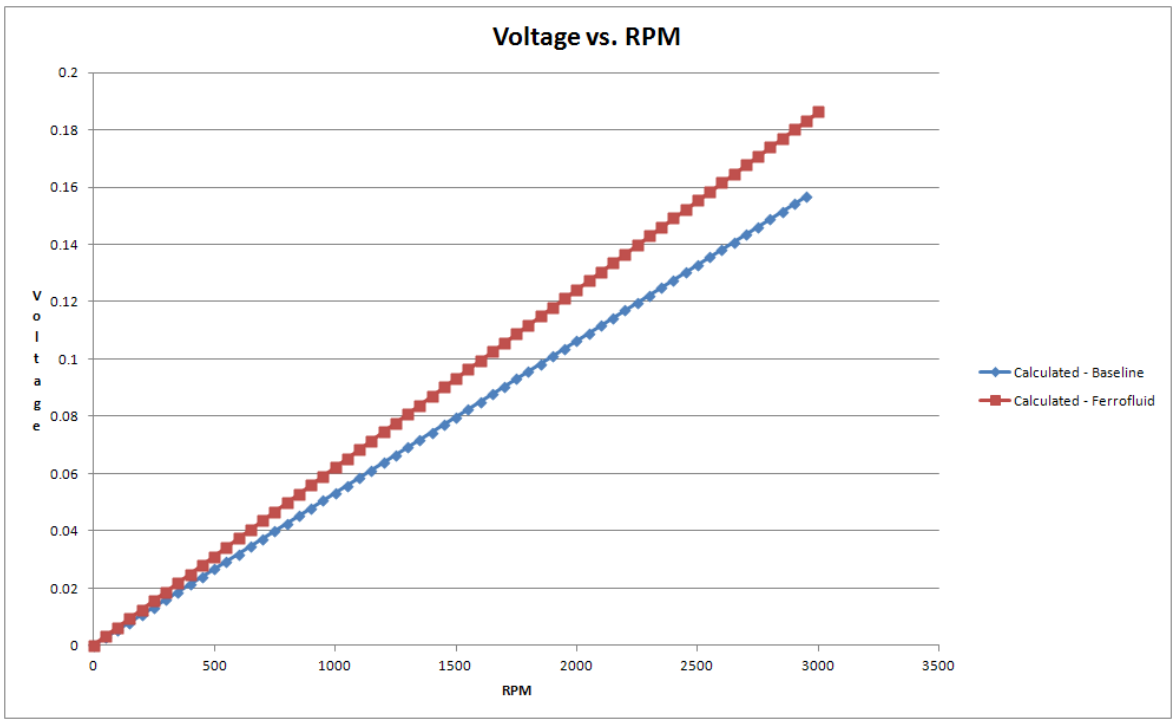


Figure 6.2-3 – Predicted Generator Performance, Voltage / RPM. This figure shows the predicted performance in terms of voltage vs. speed within the tested range for the generator used in experiment 3. Note the improved performance of the ferrofluid system.

Similarly, efficiency predictions, using equation 3.2.1-4, are shown in figure 6.2-4.

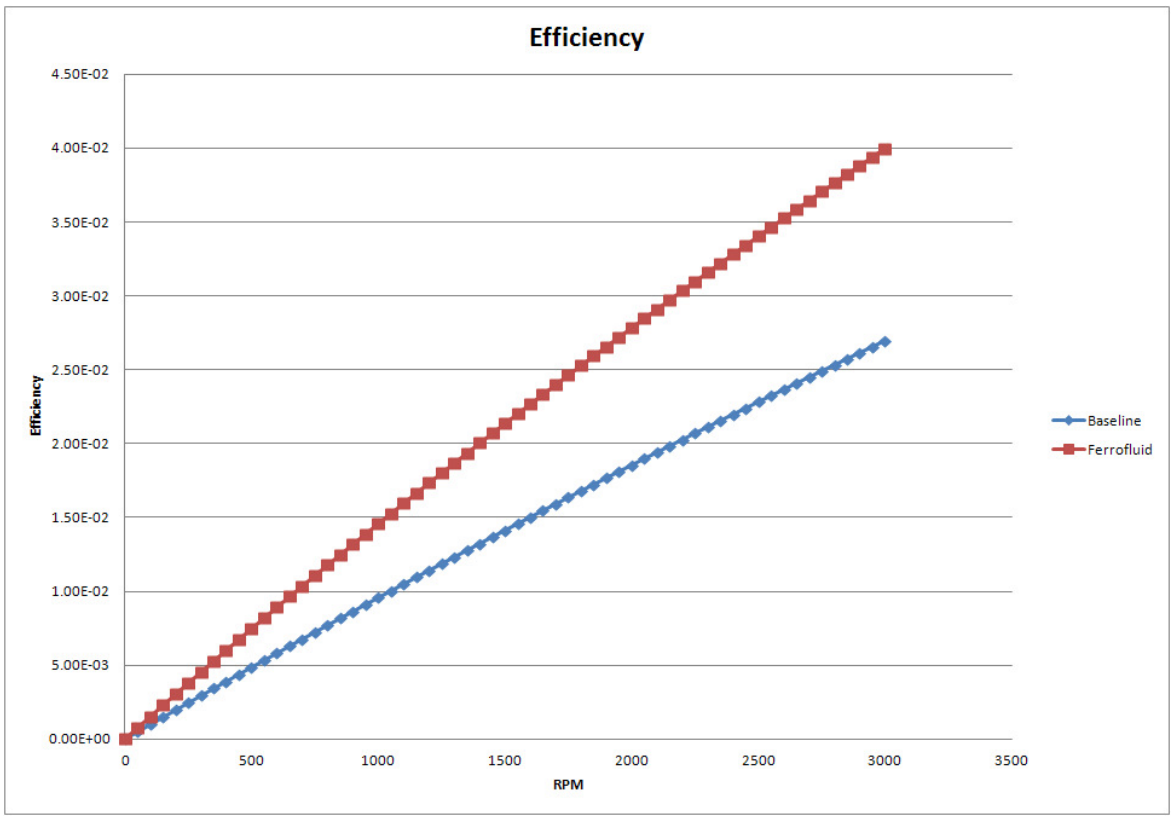


Figure 6.2-4 – Predicted Generator Performance, Efficiency. This figure shows the predicted performance in terms of efficiency within the tested range for the generator used in experiment 3. Note the improved performance of the ferrofluid system.

FEA results for the model are shown in figure 6.2-5 and figure 6.2-6. Note that the system is not saturated, as these effects were taken into account given the application, and could be expected, given the large gap. Flux leakage shows a slight increase in the ferrofluid system. A significant increase in flux across the gap is seen, predicting an increase in system performance, as shown in Figure 6.2-3 and Figure 6.2-4.

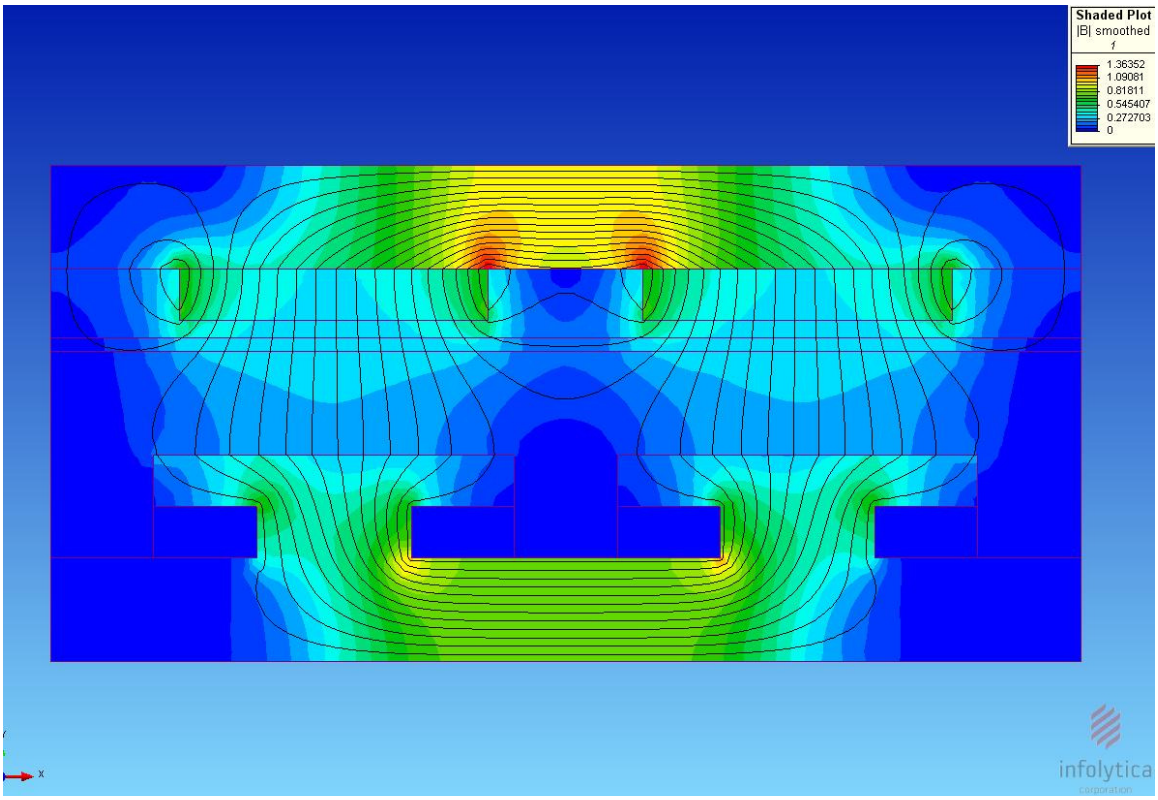


Figure 6.2-5 – FEA –Experiment 3, Traditional Air Gap. This figure shows the baseline finite element analysis for the generator used in experiment 3. Note that there is little leakage flux in the design, and that the system is not approaching magnetic saturation in any component in the magnetic circuit

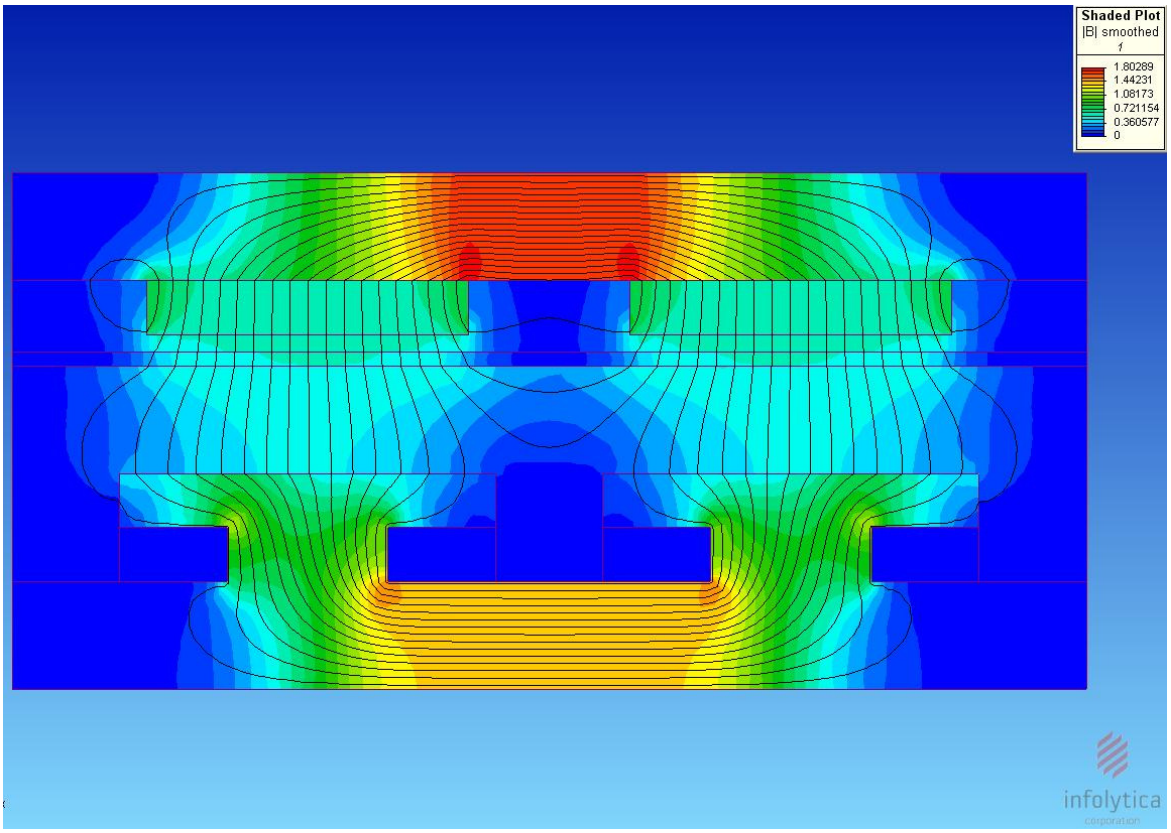


Figure 6.2-6 – FEA –Experiment 3, Ferrofluid Immersed. This figure shows the finite element analysis for the generator used in experiment 3 with ferrofluid immersion up to the point of the rotor. Note the slight increase in leakage flux in the design and that the system is not approaching magnetic saturation in any component in the magnetic circuit

The output speed was adjusted through changing positions on three driving pulleys of the motor system, which provided set RPM values, as detailed in Table 6.2-1. A multimeter recorded the output voltage. RPM vs. Voltage provided a measure of system improvement.

Table 6.2-1 shows the raw data from the experiment. Figure 6.2-7 shows the experiment's graphs.

| Experiment 3, 70 turns / stator pole, .28" Gap | | | | | | | |
|---|---|---|---|---|---|---|---|
| RPM | Air Gap, Volts, Measured | Air Gap Volts, Predicted | % Error, Air Gap | Ferrofluid, Volts, Measured | Ferrofluid, Volts, Predicted | % Error, Ferrofluid | % Performance Change |
| 0 | 0 | 0 | 0% | 0 | 0.00 | 0 | |
| 220 | 0.01 | 0.011 | 10% | 0.01 | 0.01 | 32% | 0% |
| 300 | 0.01 | 0.015 | 50% | 0.02 | 0.02 | -10% | 100% |
| 430 | 0.02 | 0.0215 | 8% | 0.03 | 0.03 | -14% | 50% |
| 480 | 0.02 | 0.024 | 20% | 0.03 | 0.03 | -4% | 50% |
| 590 | 0.03 | 0.0295 | -2% | 0.04 | 0.04 | -12% | 33% |
| 650 | 0.03 | 0.0325 | 8% | 0.04 | 0.04 | -3% | 33% |
| 720 | 0.04 | 0.036 | -10% | 0.04 | 0.04 | 8% | 0% |
| 850 | 0.04 | 0.0425 | 6% | 0.05 | 0.05 | 2% | 25% |
| 900 | 0.05 | 0.045 | -10% | 0.05 | 0.05 | 8% | 0% |
| 950 | 0.05 | 0.0475 | 6% | 0.06 | 0.06 | -5% | 33% |
| 1600 | 0.08 | 0.08 | 0% | 0.09 | 0.10 | 7% | 13% |
| 1900 | 0.09 | 0.095 | 6% | 0.12 | 0.11 | -5% | 33% |
| 2000 | 0.10 | 0.1 | 0% | 0.13 | 0.12 | -8% | 30% |
| 2500 | 0.12 | 0.125 | 4% | 0.15 | 0.15 | 0% | 25% |
| 2900 | 0.13 | 0.145 | 12% | 0.16 | 0.17 | 9% | 23% |

Table 6.2-1 – Experimental Data, Experiment 3. This table shows the data for experiment 3's generator performance in terms of voltage vs. speed for both the baseline air gap and the ferrofluid immersed systems. Summarizing, the ferrofluid system shows increased performance across the RPM range, and the calculated values match the experimental data <33%.

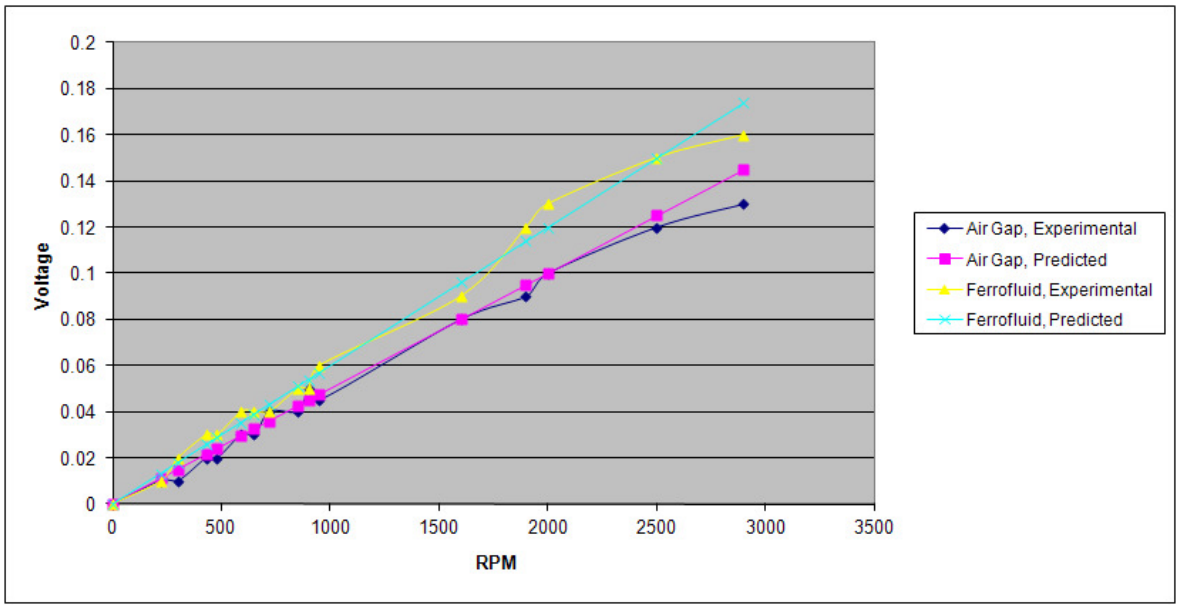


Figure 6.2-7 – Experiment 3 Results. This figure shows the graphs of the air gap and ferrofluid systems, with calculated and experimental values shown.

Studying the data, it is apparent that ferrofluid stator immersion was a net benefit on the system's electromagnetic performance. Using the speed constant as a measure of performance, the ferrofluid system showed an average increase of 30% across the tested range compared to the baseline air gap system.

# CHAPTER 7 – EXPERIMENT 4 – SMALL GAP FERROFLUID EXPERIMENT

This chapter presents the results of the fourth and final experiment. A generator system was designed and constructed, identical to experiment 3, but with a reduced air gap. This unit was baselined with a standard air gap, then immersed in ferrofluid to measure the performance effects.

## 7.1 BACKGROUND

For the fourth phase of the experimental research, an axial flux ("pancake" style) motor / generator, was designed and built, identical to experiment 3, but with a reduced air gap. This is predicted to have a negative performance effect on the system, demonstrating that the air gap must be a significant portion of the electromagnetic circuit to have a positive effect on the overall system.

## 7.2 EXPERIMENTAL RESULTS

The generator is an axial flux design, with a stator and rotor diameter of 2". Two disc style magnets of Neodymium Iron Boron, N42 material [1.2 Tesla Br, 12,000 Oersted Hc] were used for the rotor. The stator is 1018 steel, with 0.375" in winding height, with a 0.25" baseplate, with three poles wound with one hundred turns per pole for one phase output power. The magnets feature a countersunk thru-hole, which allows a non-magnetic screw to fasten the magnets to the rotor. The rotor-stator gap consists of a 0.032" air gap

between the magnets and the containment tank, the 0.032” stator cover, and a 0.032” stator to cover gap. Figure 7.2-1 shows the CAD model of the tested generator.

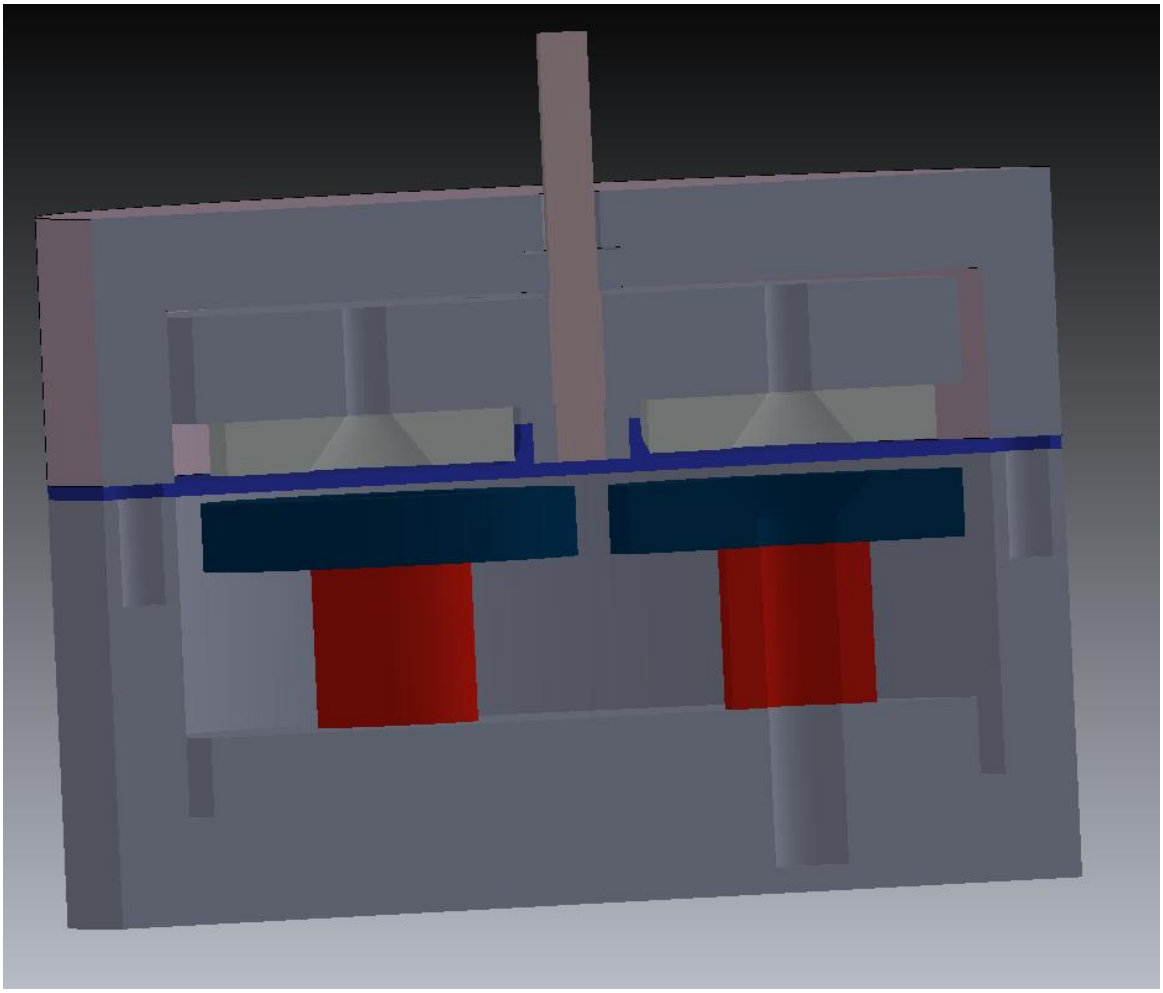

Figure 7.2-1 - Experiment 4 CAD Model. This figure shows a CAD model of the generator used for experiment 4, featuring a 2” diameter axial flux generator with a 0.282” stator to stator cover gap.

Given the expected low voltage of the system, no electrical insulation was used other than the supplied wire enamel. The same type of ferrofluid used in experiments 1, 2, and 3 was used in experiment 4, fully contained in the casing. A drill press AC motor was

used to drive the system as a generator. Raw AC power was run to a resistive load for power dissipation. Baseline measurements were taken, and additional measurements were taken with the tank filled with ferrofluid.

Figure 7.2-2 shows a photograph of the stator from experiment 3, while Figure 7.2-3 shows the stator for experiment 4. Note the decreased gap in experiment 4.

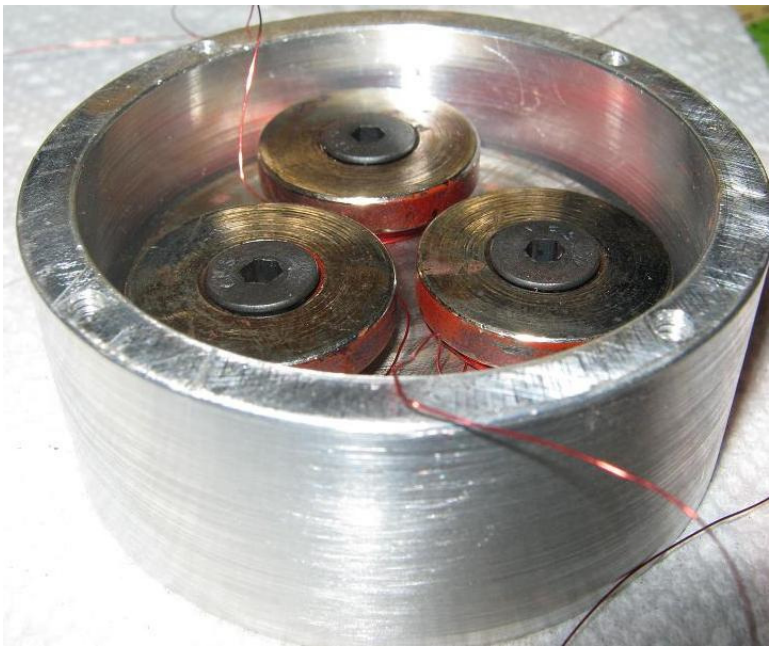

Figure 7.2-2 – Experiment 3 Stator. This figure shows a picture of the stator used for experiment 3. Note the small distance between the top of the stator poles to the top of the stator case.

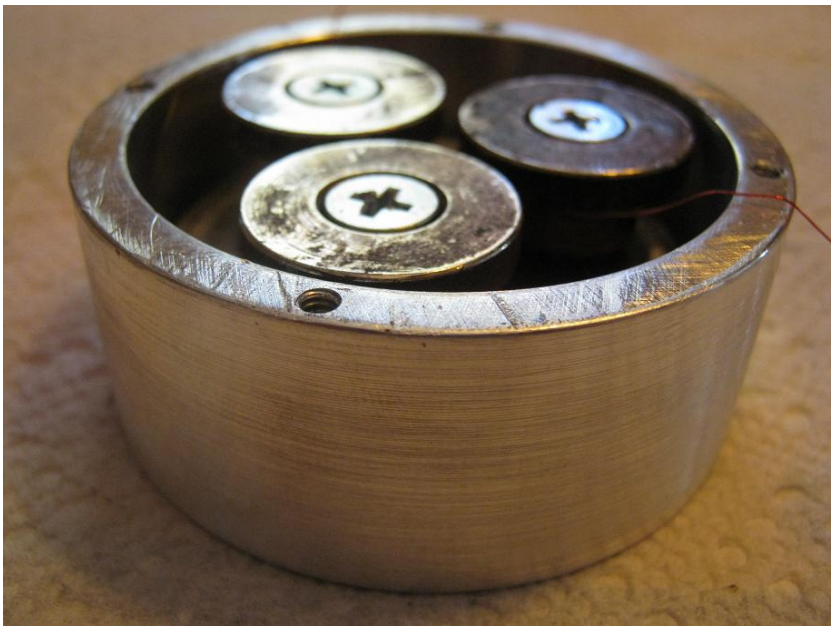

Figure 7.2-3 – Experiment 4 Stator. This figure shows a picture of the stator used for experiment 4. Note the large distance between the top of the stator poles to the top of the stator case.

Solving for the flux across the gap, and substituting into equation 3.2.1-1, we have for the baseline system:

$$Ke = 3.624 N_1 \Phi_f \quad 7.2\text{-}1$$

$$\text{Ke} = (3.624)\ (300)\ (1.029\text{e-}5) \quad 7.2\text{-}2$$

$$\text{Ke} = 0.01120 \text{ Volts / Rev / Second} \quad 7.2\text{-}3$$

For the ferrofluid immersed system:

$$Ke = 3.624\, N_1 \Phi_f \quad 7.2\text{-}4$$

$$\text{K e= } (3.624)\ (300)\ (1.016\text{e-}5) \quad 7.2\text{-}5$$

Ke = 0.01106 Volts / Rev / Second 7.2-6

Predicted performance, using the developed computational model for voltage / RPM is shown in figure 7.2-4.

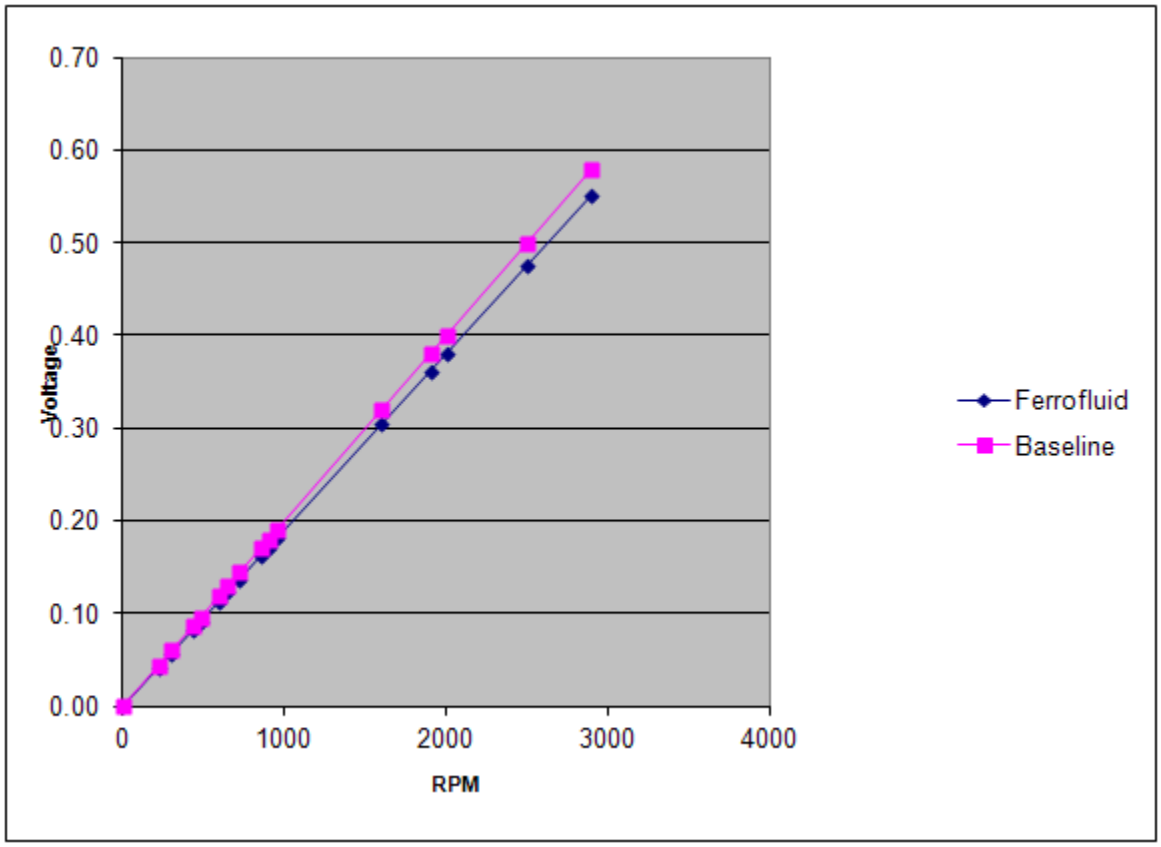


Figure 7.2-4 – Predicted Generator Performance, Voltage / RPM. This figure shows the predicted performance in terms of voltage vs. speed within the tested range for the generator used in experiment 4. Note the lower performance of the ferrofluid system.

Similarly, efficiency predictions, using equation 3.2.1-4, are shown in figure 7.2-5.

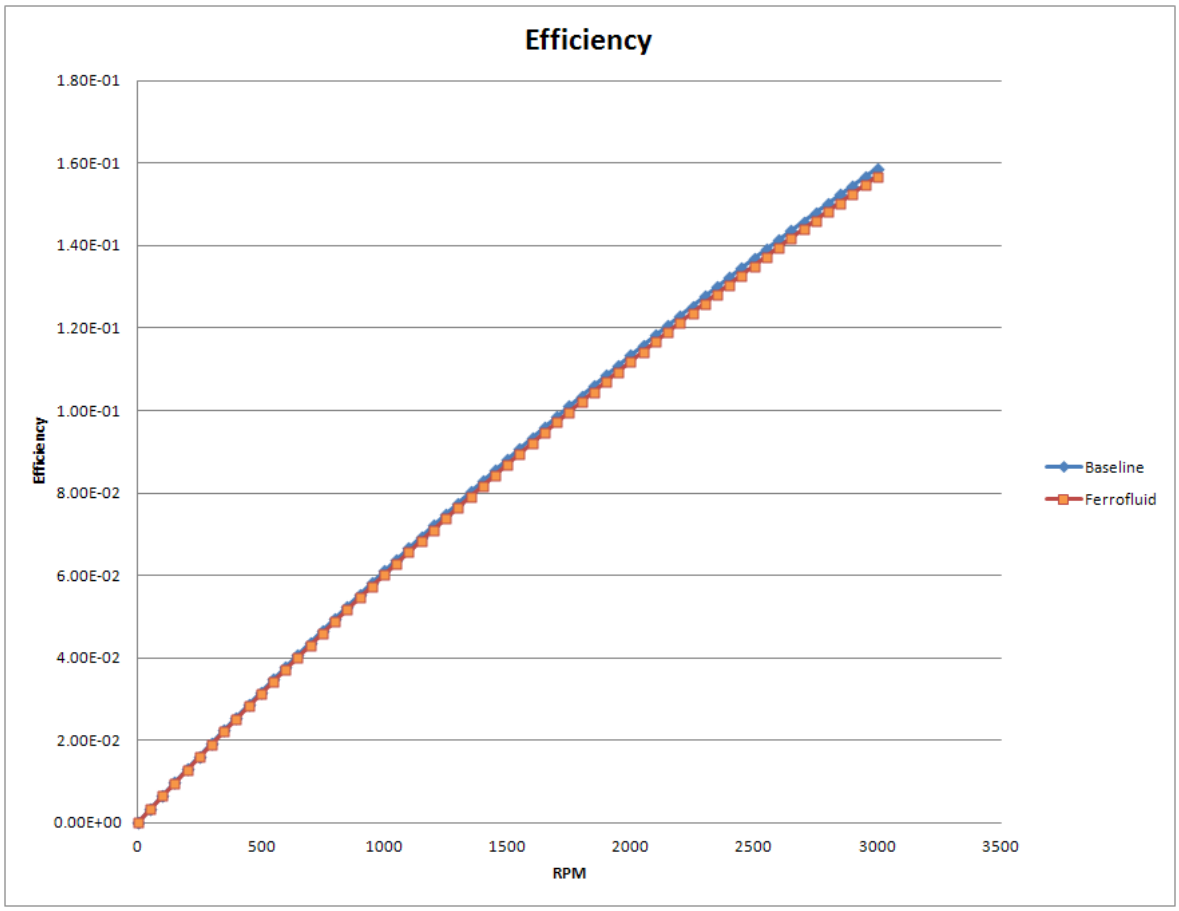


Figure 7.2-5 – Predicted Generator Performance, Efficiency. This figure shows the predicted performance in terms of efficiency within the tested range for the generator used in experiment 3. Note the lower performance of the ferrofluid system.

FEA results for the model are shown in figure 7.2-6 and figure 7.2-7. With flux density of the rotor back iron >2 Tesla, greater than the knee point of 1018 steel, as shown in figure 2.2-3 the system is magnetically saturated in the rotor back iron. Flux leakage shows a slight increase in the ferrofluid system without a significant increase in flux across the air gap. With an increase in leakage flux without a corresponding increase in air gap flux, a performance decrease could be expected, as shown in Figure 7.2-5.

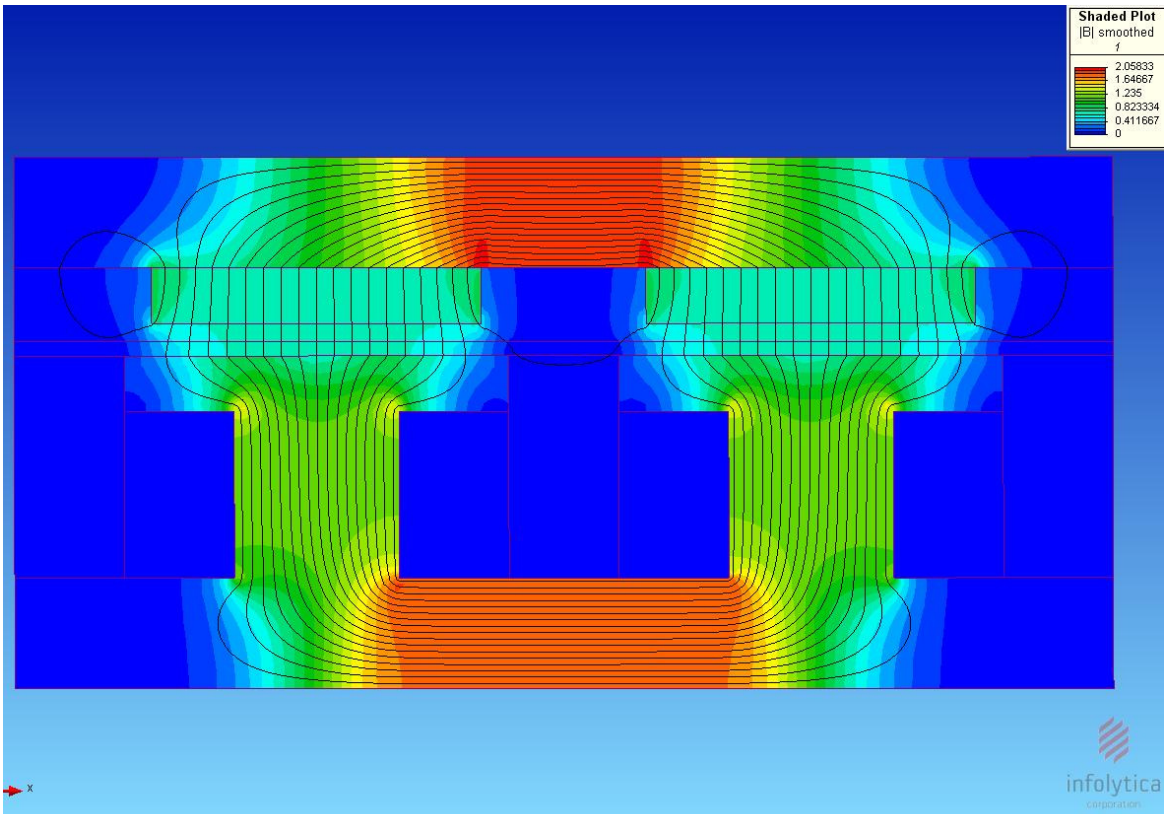


Figure 7.2-6 – FEA –Experiment 4, Traditional Air Gap. This figure shows the baseline finite element analysis for the generator used in experiment 4. Note that there is some leakage flux in the design, and that the system is magnetically saturated in the rotor back iron.

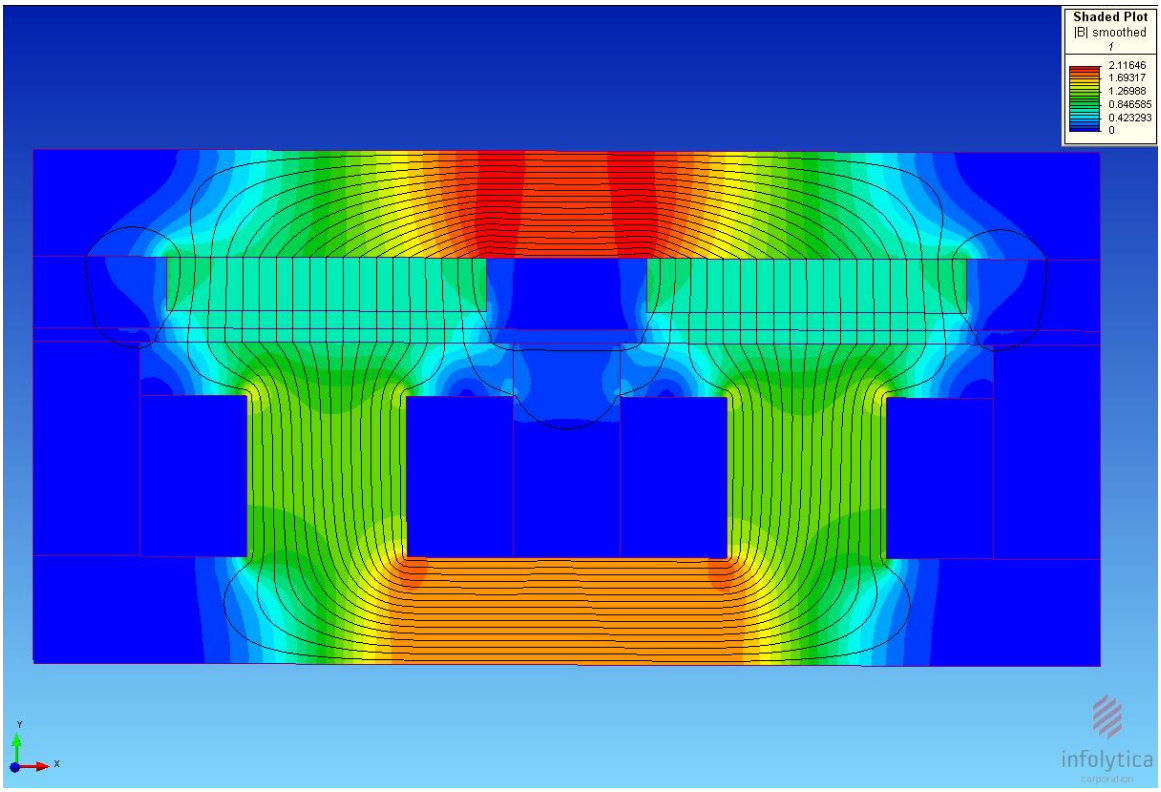


Figure 7.2-7 – FEA –Experiment 4, Ferrofluid Immersed. This figure shows the finite element analysis for the generator used in experiment 4 with ferrofluid immersion up to the point of the rotor. Note that there is leakage flux has increased in the design, and that the system is magnetically saturated in the rotor back iron.

The output speed was adjusted through changing positions on three driving pulleys of the motor system, which provided set RPM values, as detailed in Table 6.2-1. A multimeter recorded the output voltage. RPM vs. Voltage provided a measure of system improvement.

Table 7.2-1 and Figure 7.2-8 show the raw data from the experiment.

| Experiment 4, 100 turns / stator pole, .03" Gap | | | | | | | |
|---|---|---|---|---|---|---|---|
| RPM | Air Gap, Volts, Measured | Air Gap Volts, Predicted | % Error, Air Gap | Ferrofluid, Volts, Measured | Ferrofluid, Volts, Predicted | % Error, Ferrofluid | % Performance Change |
| 0 | 0 | 0 | 0% | 0 | 0.00 | 0 | |
| 220 | 0.04 | 0.044 | 10% | 0.04 | 0.04 | 5% | 0% |
| 300 | 0.06 | 0.06 | 0% | 0.07 | 0.06 | -19% | 17% |
| 430 | 0.08 | 0.086 | 8% | 0.08 | 0.08 | 2% | 0% |
| 480 | 0.10 | 0.096 | -4% | 0.09 | 0.09 | 1% | -10% |
| 590 | 0.13 | 0.118 | -9% | 0.12 | 0.11 | -7% | -8% |
| 650 | 0.14 | 0.13 | -7% | 0.13 | 0.12 | -5% | -7% |
| 720 | 0.14 | 0.144 | 3% | 0.13 | 0.14 | 5% | -7% |
| 850 | 0.18 | 0.17 | -6% | 0.16 | 0.16 | 1% | -11% |
| 900 | 0.18 | 0.18 | 0% | 0.16 | 0.17 | 7% | -11% |
| 950 | 0.20 | 0.19 | -5% | 0.18 | 0.18 | 0% | -10% |
| 1600 | 0.32 | 0.32 | 0% | 0.3 | 0.30 | 1% | -6% |
| 1900 | 0.37 | 0.38 | 3% | 0.35 | 0.36 | 3% | -5% |
| 2000 | 0.40 | 0.4 | 0% | 0.38 | 0.38 | 0% | -5% |
| 2500 | 0.46 | 0.5 | 9% | 0.44 | 0.48 | 8% | -4% |
| 2900 | 0.51 | 0.58 | 14% | 0.48 | 0.55 | 15% | -6% |

Table 7.2-1 – Experimental Data, Experiment 4. This table shows the data for experiment 4's generator performance in terms of voltage vs. speed for both the baseline air gap and the ferrofluid immersed systems. Summarizing, the ferrofluid system shows decreased performance across the RPM range, and the calculated values match the experimental data <20%.

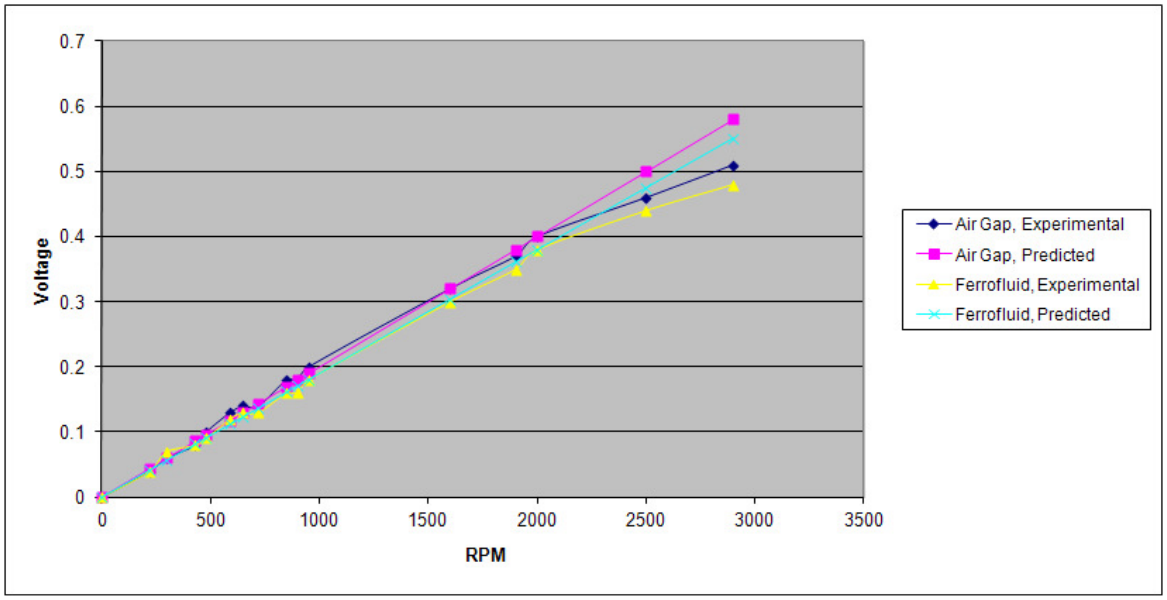


Figure 7.2-8 – Experiment 4 Results. This figure shows the graphs of the air gap and ferrofluid systems, with calculated and experimental values shown.

Studying the data, we can see that the overall effect of ferrofluid immersion was negative, even without an increase in viscous losses. Using the speed constant as a measure of

performance, the ferrofluid system showed an average decrease of 5% across the tested range. Without the air gap being a major part of the electromagnetic circuit, leakage flux dominated the change from a traditional air gap to a ferrofluid system. Any potential increase in flux across the gap was offset by magnetic saturation in the system. Comparing experiment 3 and experiment 4, the data shows that the effect of ferrofluid immersion is system and geometry dependent. For ferrofluid to have a positive magnetic effect, the gains from improved gap permeability must exceed any leakage flux losses, and the system must not be magnetically saturated.

# CHAPTER 8 – CONCLUSIONS

This chapter presents the conclusions of the thesis, as well as recommendations for future work.

## 8.1 REVIEW

Analytical and experimental methods have shown potential for increased system performance by replacing air gaps in permanent magnet machines with higher permeability materials, although with corresponding trade-offs and potential for negative overall system effects. These systems were developed in virtual prototypes, matching developed hardware, showing consistency in the approach and a validation of the analytical model across multiple design iterations of various sized generators.

However, the potential for improvements from ferrofluid immersion is not unlimited, as magnetic saturation may eliminate any magnetic gains if the system is not designed for it. Also, negative magnetic performance is possible, as at high relative permeability levels, leakage flux in the gap increases, which reduces the performance of the system. Leakage paths between stator poles can also provide a negative effect on overall system performance.

Experiment 1 demonstrated an off the shelf motor which showed improved performance with ferrofluids vs. fluids of equivalent viscosity, and even improved performance vs. an air gap at low RPM. Prior research [9] had demonstrated performance improvement for

ferrofluid immersed systems with a maximum speed of 500 RPM. This dissertation demonstrated similar gains at low RPM, with equivalent performance in the ferrofluid system compared to a traditional air gap system at speeds below 1000 RPM. Despite greater losses from the viscosity increase of the ferrofluid, the voltage constant and current draw were equivalent within the margin of error, demonstrating efficiency improvements in the magnetic circuit. This shows applications for the technique in areas where RPM would be limited, such as wind power in low wind areas, or where gear systems and / or high rotor speed are limiting factors for system reliability. Higher RPM tests, up to 12,000 RPM, showed a loss vs. a traditional air gap operation, as the corresponding viscosity related losses more than offset the magnetic gains. However, losses were less in the ferrofluid system, with a 15% decrease in Voltage Constant for a ferrofluid system compared to 57% for a system immersed in a non-magnetically permeable oil of equivalent viscosity.

In the generator applications, the effect of ferrofluid immersion was found to be system dependent. Experiment 2 demonstrated gains consistent with prior experiments for performance improvement in low RPM applications, showing an 8.9 % improvement in the speed constant for a fully ferrofluid immersed system compared to the baseline traditional air gap system up to 590 RPM, and provided a Proof of Concept for later experiments.

Experiment 3 demonstrated a net positive electromagnetic effect from ferrofluid stator immersion in a large rotor / stator gap system. In the tested system, a 30% improvement

was measured in the speed constant for the ferrofluid system compared to the traditional air gap baseline.

Experiment 4 demonstrated a net negative electromagnetic effect, with greater leakage flux loss than gap permeability gains in a small rotor / stator gap system, and saturation effects limiting additional magnetic improvement. In the tested system, a 5% reduction in performance was measured in the speed constant for the ferrofluid system compared to the traditional air gap baseline.

Summarizing the overall performance effects of air gap elimination in permanent magnet machines, increasing the gap permeability does not have a universally positive or negative effect. For ferrofluid immersion of a motor / generator, a system dependent change in performance is seen, related to the geometry and characteristics of the system such as speed and power. For Experiment 1, the high rotational losses, up to 12,000 RPM, increased the rotational losses from 0.64 Watts to 2.98 Watts at maximum speed. Despite the magnetic gains from the ferrofluid, the efficiency of the system was reduced from over 30% for the standard air gap system to less than 20% for the ferrofluid system. For Experiment 3, ferrofluid immersion of a large stator – cover gap led to an increase in the magnetic flux from 4.185e-6 Webers for the air gap system to 4.894e-6 Webers for the ferrofluid system, a 17% improvement. FEA showed no significant increase in leakage flux or saturation effects. With the design limiting increased fluid friction losses due to the isolated stator chamber, the magnetic gain led to a performance gain, doubling the efficiency at no load, and offering a 30% increase in the speed constant. For

Experiment 4, ferrofluid immersion of a small stator – cover gap led to a decrease in the magnetic flux from 1.029e-5 Webers for the air gap system to 1.016e-5 Webers for the ferrofluid system, a 1.3% decrease. This was driven by an increase in the leakage factor, determined through FEA to be 0.91 for the standard air gap, but 0.72 for the ferrofluid system, a 21% performance decrease, and the saturation factor, determined by FEA to be 0.95 for the standard air gap, but 0.90 for the ferrofluid system, a 5% performance decrease. Even without increased fluid friction losses, the magnetic effect of ferrofluid immersion was negative, with a small loss in efficiency at no load, and a 5% decrease in the speed constant.

## 8.2 CONCLUSION

This dissertation has added new knowledge to the study of permanent magnet machines, including:

- Experimental and analytical study of the effects of high rotational velocity on ferrofluid immersion of permanent magnet machines
- Consideration of ferrohydrodynamic effects in the analysis of ferrofluid-based PMM performance
- Application of the ferrofluid immersion approach to axial flux systems
- Design of the axial flux design to maximize magnetic gains from ferrofluid immersion while reducing the losses from increased shear forces

- Consideration of leakage flux effects as a negative factor of ferrofluid immersion of PMM's, demonstrated through analysis and experimentation.

Improved permanent magnet machine performance has been demonstrated by air gap elimination through means of improved permeability materials, subject to system design limitations. Increased voltage from low RPM (generator applications) and increased RPM from lower voltage (motor application) has been demonstrated in a repeatable fashion. Analytical predictions have been matched to <30% accuracy, providing a method for further iterations of motor / generator systems for future study and optimization.

Techniques using ferrofluid to improve PMM performance have been demonstrated, as have situations where ferrofluid usage detracts from overall system performance. In summary, design guidelines for ferrofluid immersion include:

- Leakage flux must be minimized. Ferrofluid should only exist in the gap between rotor and stator poles, and not between stator poles or between rotor poles.
- Immersion of rotating components should be minimized or eliminated. If possible, the ferrofluid should be contained in an isolation chamber with the stator, and all rotor components separated from liquid exposure. For fully immersed systems, at low speeds ferrofluid immersion can be a benefit, but high speed fluid frictional losses can overcome any electromagnetic gains from ferrofluid.
- Ferrofluid immersion is more beneficial for larger gap systems, as smaller gaps correlate to larger shear losses. Also, ferrofluid is only a significant benefit if the gap being replaced with ferrofluid is a significant part of the magnetic circuit.

- Ferrohydrodynamics must be taken into consideration. Viscosity in ferrofluids increases with stronger magnetic fields and slower velocity systems. Formulations with very small average nanoparticle size eliminate ferrohydrodynamic viscosity increases.
- The magnetic circuit must account for the ferrofluid. Any saturation effects in the rotor or stator iron would negate any gains from the ferrofluid permeability increase. Saturation effects in the ferrofluid itself may limit gains in high flux density systems.
- Control systems must account for ferrofluid effects. By changing the flux in the system, the torque constant and voltage constant are affected. Control systems designed and calibrated for a given system must be recalibrated for the modified rotating machine.

This research has shown a focus on improved permanent magnet machine performance, with a specialization in improved permeability in the material between the rotor and the stator. Finite element analysis, macro scale calculations, and experimental methods were used. This research could provide the baseline for additional study in academia, or improved performance of numerous products.

Results from this dissertation have numerous applications in research and industry. Any area where permanent magnet machines are employed can use the technology. Some applications include vehicle motors and alternators, wind power, generators, pumps, fans, compressors, et al. From early work, it appears that the best applications may be areas of

low speed / high torque (which shear forces / friction losses will be minimal), where thermal management is most critical (possibly deep drilling or hot metals processing), and where air cooling is not available for the stator (such as space applications or tidal power generators).

## 8.3 RECOMMENDATIONS FOR FUTURE WORK

This research has focused on one component of a permanent magnet machine system, the rotating machine. Other areas of the system include motor controls or generator regulators. The effects of the modifications proposed in this paper could be studied including these higher level system components. Also, due to time constraints on the research, long term effects, such as corrosion, MTBF, et al., were not evaluated, but are open to future study.

Controls are a vital part of the overall motor / generator system. A focus on the development of control systems for varying gap permeabilities could be part of a multi-disciplinary study for a well rounded individual, or, more likely, a diverse research team.

A major area open to future work would be magnetic gears. Although initial plans for this dissertation included additional research on the topic of magnetic gears, time and financial constraints moved the work towards a greater focus on motor / generator applications. Some of the early research on magnetic gears has been provided in Appendix A, which could be expanded upon for a separate dissertation topic such as

"Magnetic Gear Performance Improvements from Ferrous Coatings of Intermediate Poles".

Due to a limited budget available for this research topic, experimentation methods were likewise limited in sophistication. Additional funding would provide a more thorough investigation of the system effects, and could include other areas, such as torque and efficiency. Also, higher power and higher efficiency systems could be constructed and tested.

Finally, the main focus on this paper has been on the magnetic system, not in the ferrofluid itself. A greater focus on ferrofluid material formulation, optimized for the application, would be a key area for future research.

## REFERENCES

[1] Lonngren, K.E., Savov, S.V., and Jost, R.J. (2007) “Fundamentals of Electromagnetics with MATLAB ®”, Scitech Publishing.

[2] Hendershot, J.R. and Miller, T.J.E. (2010) “Design of Brushless Permanent-Magnet Motors”, Magna Physics Publishing and Clarendon Press.

[3] Gieras, J., Wang, R., and Kamper, M. (2008) “Axial Flux Permanent Magnet Brushless Machines”, Springer.

[4] Lovatt, H.C., Ramsden, V.S., and Mecrow, B.C. (1997) “Design of an In-Wheel Motor for a Solar-Powered Electric Vehicle”. Eighth International Conference on Electrical Machines and Drives, Cambridge, UK, 1-3 Sept. Conf. Publ. No. 444, pp234 - 238.

[5] Hsu, J. S., Ayers, C. W., and Coomer C. L. (2004) Report on Toyota Prius Motor Design and Manufacturing Assessment, Oak Ridge National Laboratory, ORNL/TM-2004/137.

[6] Hanselman, D. C. (2003) “Brushless Permanent Magnet Motor Design”, The Writers' Collective.

[7] Gieras, J. (2010) “Permanent Magnet Motor Technology: Design and Applications”, 3rd Edition, CRC Press.

[8] Bonnett, A.H., and Yung, C. (2008) “Increased Efficiency Versus Increased Reliability”, IEEE Industry Applications, Volume 14, Issue 1, pp. 29-36.

[9] Nethe, A, Scholz, T., and Stahlmann, H. (2006) “Improving the Efficiency of Electric Machines Using Ferrofluids”, Journal of Physics: Condensed Matter, Volume 18, Number 38, pp. S2973-S2998.

[10] Fuchsloch, J.F., Finley, W.R., and Walter, R.W. (2008) “The Next Generation Motor”, IEEE Industry Applications Magazine, Vol 14, No.1, pp. 37-43.

[11] Rosenweig, R.E. (1997) “Ferrohydrodynamics”, Dover Publications.

[12] Mefford, O. (2007) Physical Properties of Macromolecule-Metal Oxide Nanoparticle Complexes: Magnetophoretic Mobility, Sizes, Interparticle Potentials”, Virginia Polytechnic Institute and State University.

[13] Lopez-Lopez, M.T., Kuzhir, P., Lacis, S., Bossis, G., Gonzalez-Caballero, F., and Duran, J.D.G. (2006) “Magnetoheology for Suspensions of Solid Particles Dispersed in Ferrofluids”. Journal of Physics: Condensed Matter, Volume 18, Number 38, pp. S2803-S2813.

[14] Hendershot, J.R. and Miller, T.J.E. (2008) SPEED Software Training Manuals, Glasgow University.

[15] He, X., Elborai, S., Kyung Kim, D., Lee, S., and Zahn, M. (2005) “Effective Magnetoviscosity of Planar-Couette Magnetic Fluid Flow”, Journal of Applied Physics, Volume 97, Issue, pp. 10Q302-1-10Q302-3.

[16] Odenbach, S. (2002) “Magnetoviscous Effects in Ferrofluids”, Springer.

[17] Vrancik, J. (1968) “Prediction of Windage Power Loss in Alternators”, NASA TN D-4849.

[18] Hsu, J. (2004) “Flux Guides for Permanent-Magnet Machines”, Oak Ridge National Laboratory, ORNL/TM-102603.

[19] Zhiyi, Y., Han, Z. and Hong, Y. (2002) “Torque Calculation and Analysis of Permanent-Magnetic Gears”, Physic Status Solidi (a) Volume 189, Issue 3, pp. 1057-1061.

[20] Lipo, T.A., and Aydin, M. (2004) “Field Weakening of Permanent Magnet Machines – Design Approaches”, Research Report 2004-13, University of Wisconsin-Madison Electrical and Computer Engineering Department.

[21] Siemens, Inc. (2010) “AC Motors”, Training Manual from Course “Basics of AC Motors”.

[22] Richardson, E. and Dent, P. (2007) “The Implications of DFARS and Sourcing Magnets from China”, Magnetics Conference, Denver, CO.

[23] Kozawa, S. (2011) “Trends and Problems in Research of Permanent Magnets for Motors: Addressing Scarcity Problem of Rare Earth Elements”, Science and Technology Trends Quarterly Review, #38.

[24] Halbach, K. (1980) “Design of Permanent Multipole Magnets with Oriented Rare Earth Cobalt Material”, Nuclear Instruments and Methods, 169, pp. 1-10.

[25] ThinGap, Inc. (2011) ”ThinGap’s New Brushless PM Ring Motor” Product Design and Development, January Edition.

[26] Covey, G. (2011) “Brushless Basics”, Amp’d Magazine, Issue 21.

[27] Nethe, A, Scholz, T and Stahlmann, H., (2005) “Concept of a New Type of Electric Machine Using Ferrofluids”, Journal of Magnetism and Magnetic Materials, Volume 293, Issue 1, May 2005, Pages 685-689.

[28] Nethe, A, Scholz, T and Stahlmann, H., (2004) “Simulation of a Ferrofluid Supported Linear Electric Machine”, Applied. Organometallic Chemistry, Volume 19, 2004; Pages 529–531.

[29] Hsu, J. S., Nelson, S. C., Jallouk, P. A., Ayers, C. W., Wiles, R. H., Campbell, S. L. , Coomer, C.L. , Lowe, K. T., and Burress, T. A. (2005) “Report on Toyota Prius Motor Thermal Management”, Oak Ridge National Laboratory, ORNL/TM-2005/33.

[30] Redman , C. US Patent #4,064,409, “Ferrofluidic Electrical Generator”.

[31] Chass, J. US Patents # 6,489,694, “Ferrofluidic, Electrical Power Generator”.

[32] Burke, S. K. and Ibrahim, M. E. (2007), “Electrical and Magnetic Properties of D6ac Steel”, Australian Government Department of Defence, Maritime Platforms Division Defence Science and Technology Organisation, DSTO-TN-0757

[33] Price, T., McDonald, W, and Hatch, G.. (2007) “The MagneGear™ — Efficient Rotary and Linear Magnetic Gearing Devices for Downhole Applications”, Dexter Magnetics.

[34] Atallah, K., Calverlay, S. D., and Howe, D. (2004), “High-performance Magnetic Gears” Science Direct – Journal of Magnetism and Magnetic Materials, 272-276, Supplement 1, E1727-E1729.

[35] Atallah, K., Wang, J., Mezani, S., and Howe, D. (2001) “A Novel High-Performance Magnetic Gear”, IEEE Transactions on Magnetics, 37(46), 2844-2846

[36] Rasmussen, P. O., Andersen, T. O., Joergensen, F. T., and Nielsen, O., (2005) “Development of a High Performance Magnetic Gear”. IEEE Trans. on Industry Applications. 41(3), 764 – 770.

[37] Hatch, G.. (2010) “Recent Developments In Permanent Magnet Gear Systems & Machines”, Presented at the Magnetics 2010 Conference

[38] French, A. (2007) “Torque Test Report, MGT Magnetic Couplings and Transmissions”, Magnetic Gearing and Turbine Corporation.

[39] Constantinides, S. (2007) “Measurement and Evaluation of (Neodymium Iron Boron) Magnets”, Magnetics 2007, Lincolnshire, IL.

# APPENDIX A – MAGNETIC GEARS AND COUPLINGS

The basic physics of magnetic gear and coupling PMM's consists of alternating poles of permanent magnets rotating past a ferromagnetic material or other permanent magnets [33, 34, 35, 36]. For magnetic gears, power (in the form of torque and RPM) is transmitted through magnetic flux supplied by the input shaft, which travels through the ferromagnetic material, periodically altering its magnetic field, which in turn moves a second shaft with a second set of magnets of a different size and pitch. This provides a conversion either from high torque / low RPM to low torque / high RPM or vice versa. Magnetic couplings can also link directly pole to pole, offering simple, contact-free power transmission in a 1:1 torque and speed ratio.

Depending on system requirements for torque density and available space, several configurations of magnetic gears are available. Coaxial gears and couplings are available in axial and radial flux configurations. For high torque density applications, radial flux designs are common. In this case, a high torque rotor spins around a coaxial intermediate ferrous pole set, driving a high RPM shaft. Figure A1-1 shows an example radial flux magnetic gear system [33], designed for deep drilling applications, and claiming torque capabilities of 14,000 lb*ft, and a 6:1 gear conversion ratio.

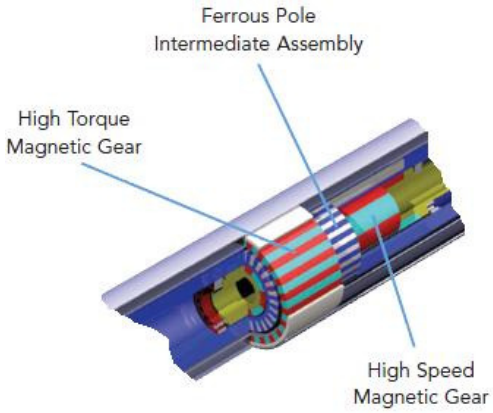


Figure A1-1 – Radial Flux Magnetic Gear [33]. This figure shows a CAD model of a radial flux magnetic gear.

If length constraints drive the design, but larger diameter form factors are available, axial flux magnetic gears and couplings can provide magnetic gears of a high efficiency. Figure A1-2 shows an example of an axial flux magnetic gear designed for 20 lb*ft and a 5:1 gear conversion ratio. Direct pole to pole magnetic couplings are common in this configuration.


Figure A1-2 – Axial Flux Magnetic Gear. This figure shows a CAD model of an axial flux magnetic gear.

In non-coaxial configurations, magnetic gears and couplings are available as drop-in replacements to existing gears or belt and pulley driven systems, and do not require ferrous pole intermediate assemblies. Right angle configurations and large gear ratios are possible with non-coaxial configurations. The design of this configuration is more straightforward and easier to engineer than co-axial systems. Figure A1-3 [38] shows several examples of non-axial magnetic gear power transmission systems from The Magnetic Gearing and Turbine Corporation.

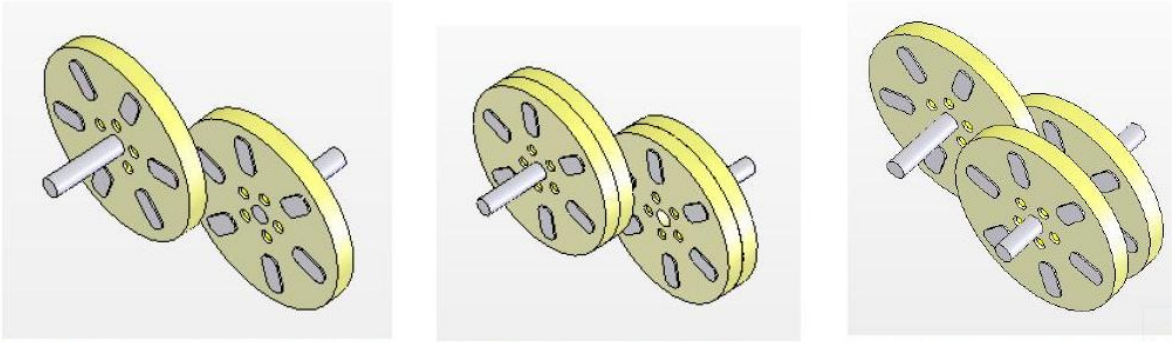


Figure A1-3 – Non-Coaxial Magnetic Gear [38]. This figure shows a photo of a non-coaxial flux magnetic gear.

Magnetic gears and couplings offer numerous advantages compared to traditional interlocking gear or belt driven systems [37], including:

- **Higher reliability.** PMM's do not have interlocking teeth, belts, or mechanical connections. These connections are a constant source of wear / fatigue failures in traditional gear or belt driven systems.
- **Maintenance free operation.** Changing belts, lubricating components, and other preventive maintenance tasks are eliminated with magnetic gearing.
- **High power density**. Permanent Magnets, especially high performance materials such as Neodymium/Iron/Boron, have exceptionally high magnetic flux densities, and can generate more power in low weight, small sized systems.

- **Higher efficiency**. Magnetic gears and couplings operate without contact, eliminating the friction losses of existing systems, providing greater fuel economy and overall improved system performance.
    - **Without belt / contact friction, less heat is generated, improving system thermal performance.**
- **Lower noise**. Grinding / clashing of gear teeth and squealing of belts are eliminated in magnetic systems, providing quiet applications.
- **Inherent over torque protection.** Magnetic gears can be designed to "slip" at high torque loads, re-engaging at designed values, protecting the system and extending life as opposed to the system failure of broken gears or belt failures in pulley systems.
    - Magnetic couplings can have additional features to either vary the air gap for engagement / disengagement, or provide electrical power through field windings to create and control the magnetic field for additional safety features and power engagement options.

As a tradeoff, there are numerous challenges inherent in the design of PMM's. Magnetic materials, shapes, temperature, and other factors all impact the overall system performance and are more difficult to design and fine tune than simple gear or pulley sizes. Magnetic gears consist of more parts than a gear or pulley system, driving costs factors, especially in low volume production. Ferrite-based magnetic gearing systems can be cost competitive with traditional gear / belt systems, but lack the power density of rare

earth magnet materials. However, for applications where the above factors are important, and given proper engineering time and support, the advantages of magnetic gears significantly outweigh the challenges.

One area for improvement on magnetic permeability is magnetic coatings. Iron based permanent magnets are very susceptible to oxidation / rust, and must be coated to eliminate long term corrosive effects. Platings such as aluminum (followed by chemical conversion coating to prevent aluminum oxidation) and nickel add significant cost to the material. Coating with epoxy is low in cost and performs well in corrosion testing, but adds to the magnetic material / stator pole gap, as much as 0.010" in low precision processes. Adding iron nanoparticles to the epoxy would provide improved magnetic performance without compromising corrosion protection.

As high torque density magnetic gears are a relatively newly actively researched area, no "textbook" style reference exists on the subject, and all are brief papers that do not delve into the critical areas of magnetic gear performance, such as air gap material. Applying the ferrofluid approach documented in this dissertation, or improving the magnetic permeability of the coatings of the intermediate magnetic poles, is an area of future study to make magnetic gears technically feasible for more applications.

# APPENDIX B – EXPERIMENTAL PART DRAWINGS

Figures B-1 – Figure B-9 show the drawings for the constructed axial flux generator used in experiment 3 and experiment 4.

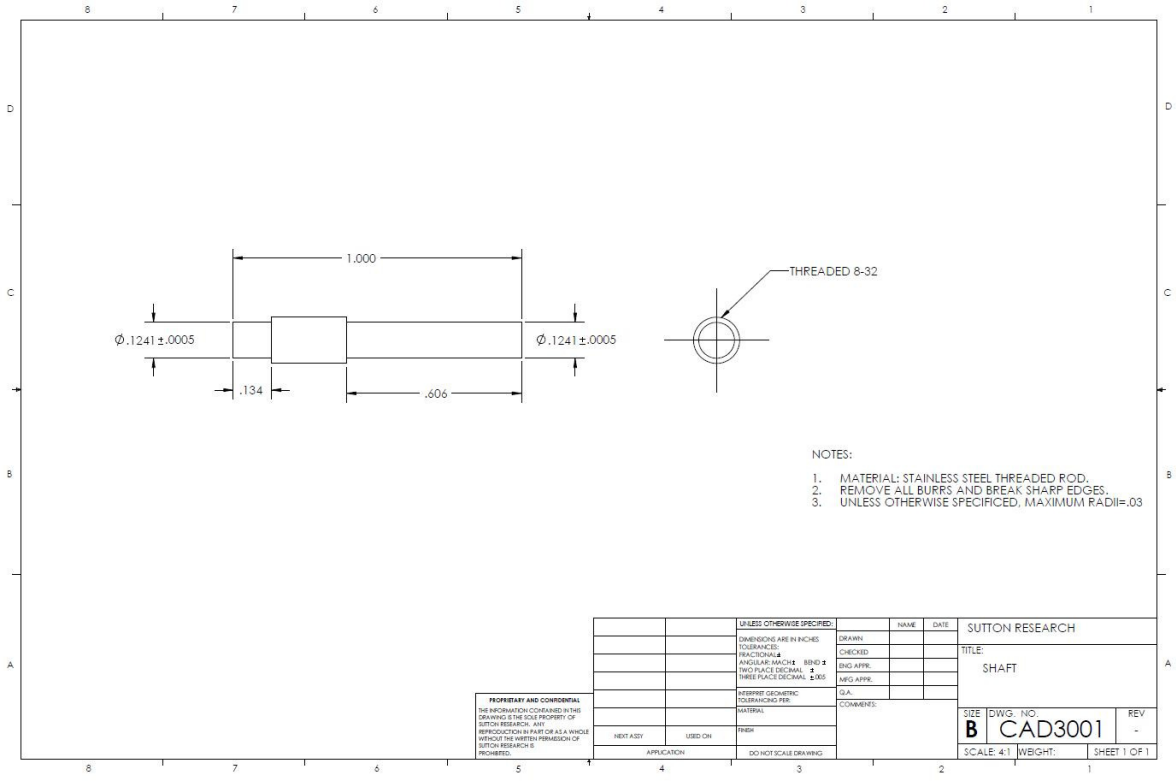


Figure B-1 - Shaft Drawing. This figure details the shaft for the permanent magnet machine built and tested for experiments 3 and 4.

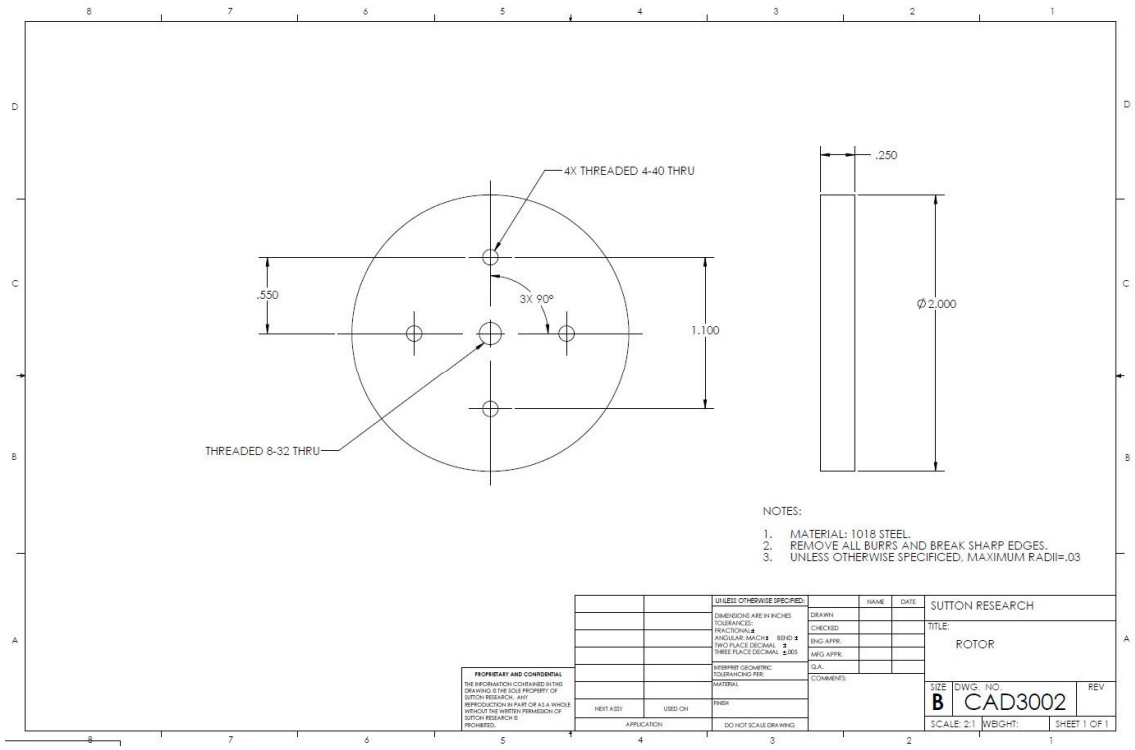


Figure B-2 - Rotor Drawing. This figure details the rotor for the permanent magnet machine built and tested for experiments 3 and 4.

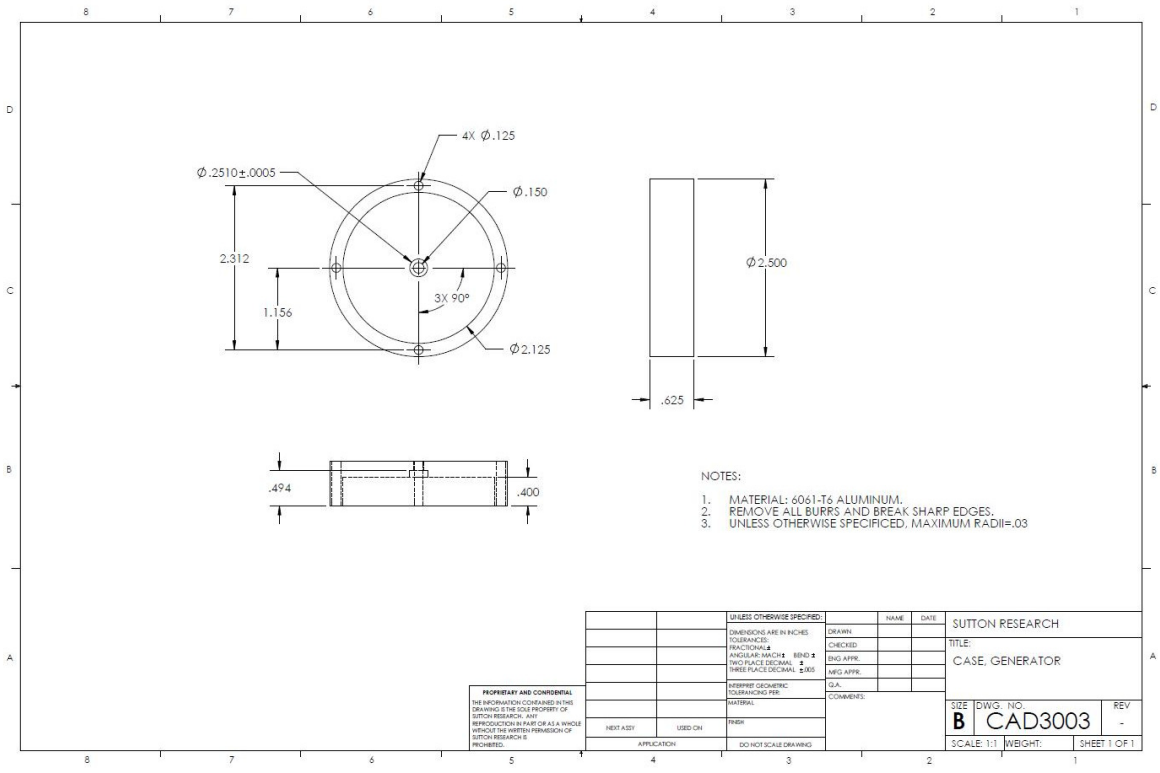


Figure B-3 - Case, Generator Drawing. This figure details the generator case for the permanent magnet machine built and tested for experiments 3 and 4.

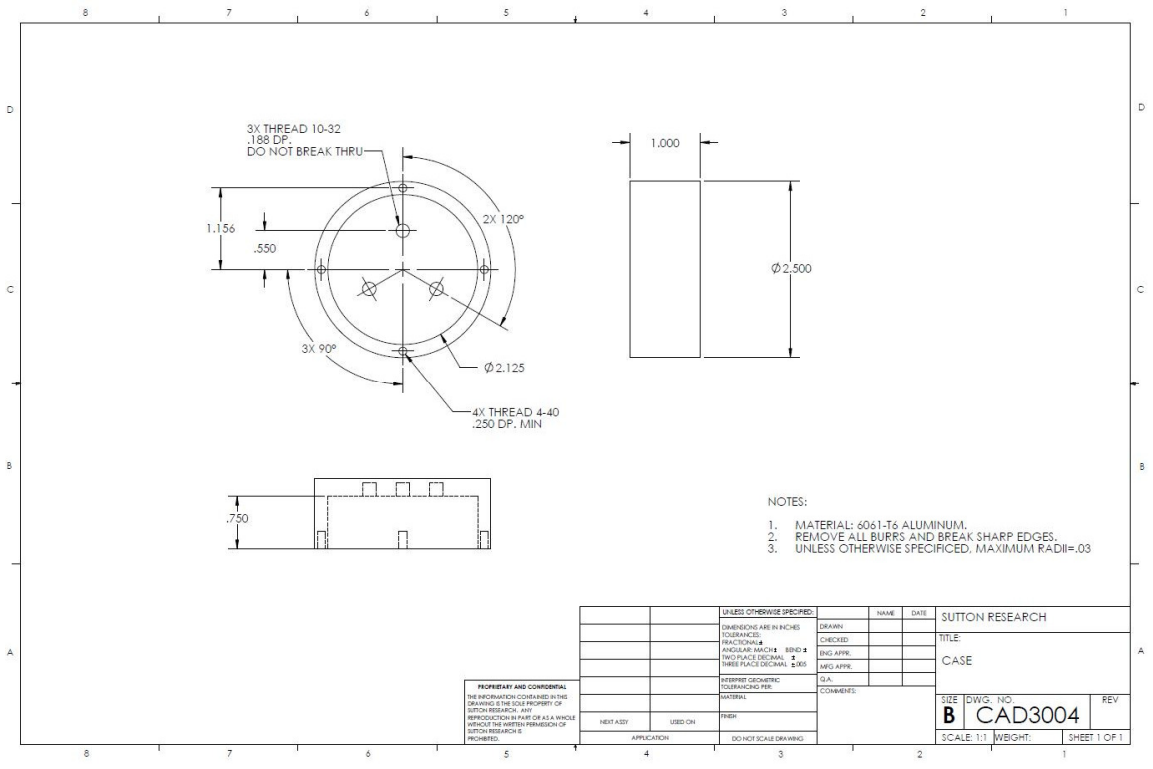


Figure B-4 - Case Drawing. This figure details the top level case for the permanent magnet machine built and tested for experiments 3 and 4.

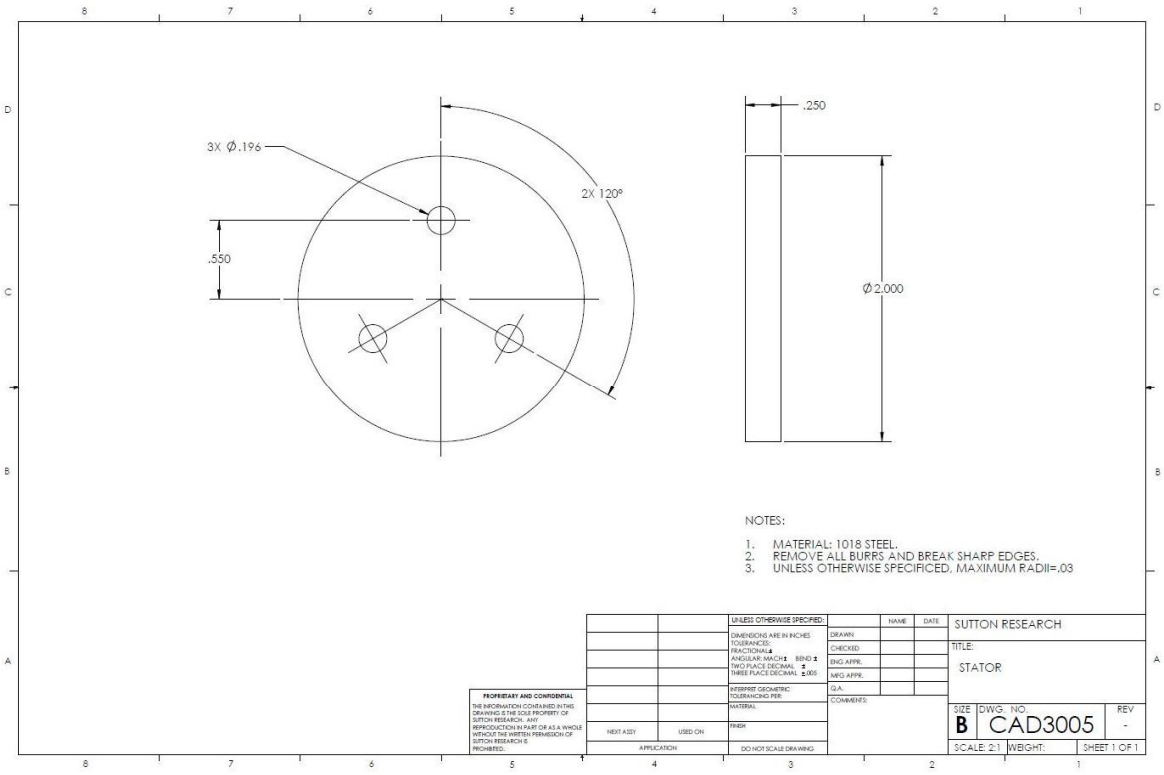


Figure B-5 - Stator Drawing. This figure details the stator for the permanent magnet machine built and tested for experiments 3 and 4.

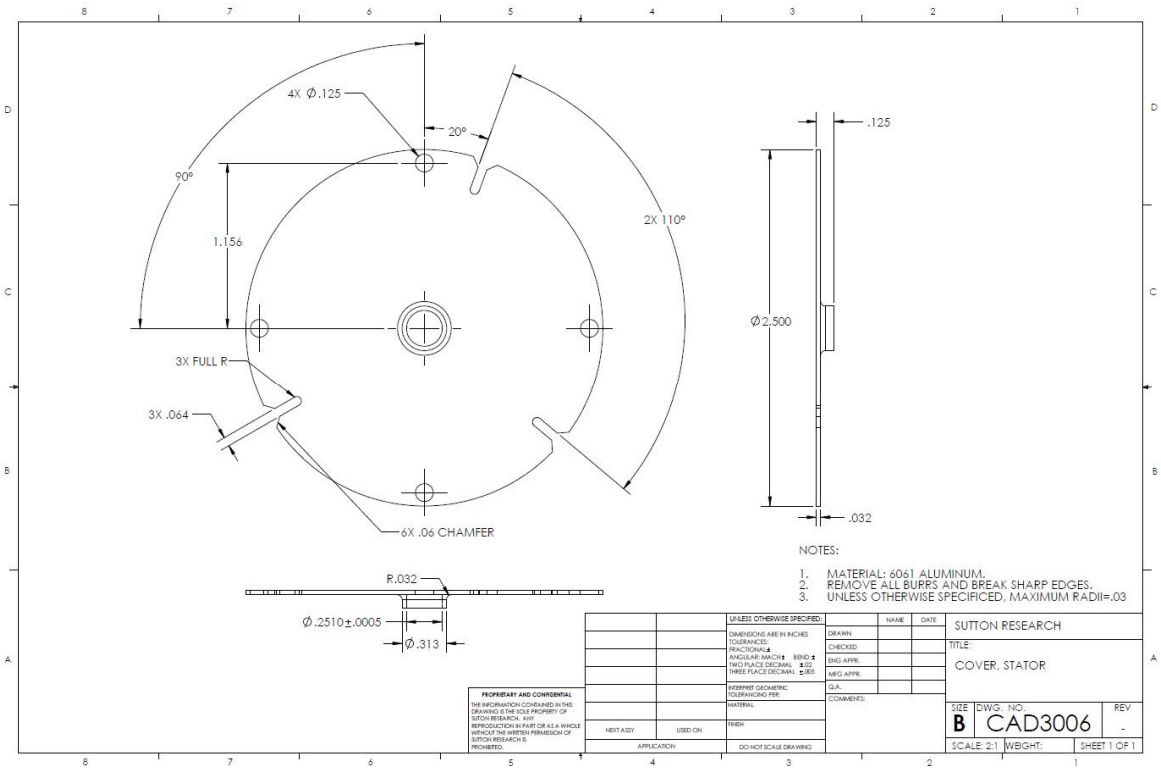


Figure B-6 - Cover, Stator Drawing. This figure details the stator cover for the permanent magnet machine built and tested for experiments 3 and 4.

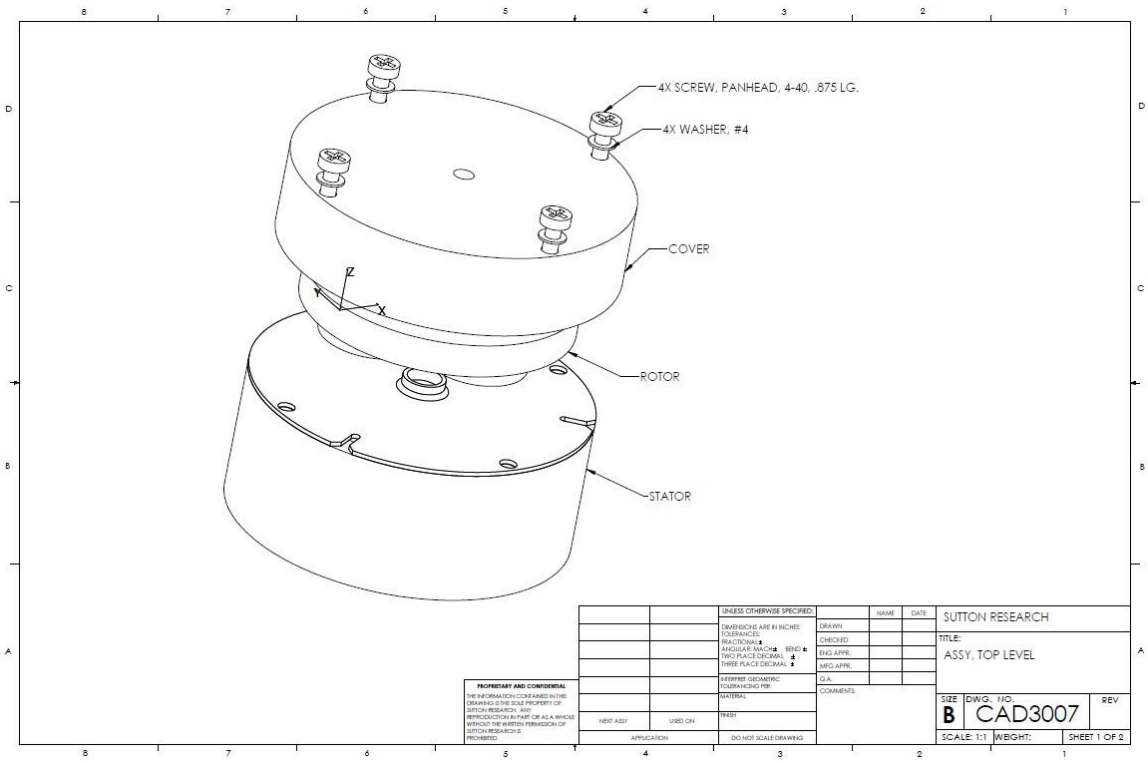


Figure B-7 - Assembly, Top Level, Drawing, Isometric View. This figure details the top level assembly for the permanent magnet machine built and tested for experiments 3 and 4.

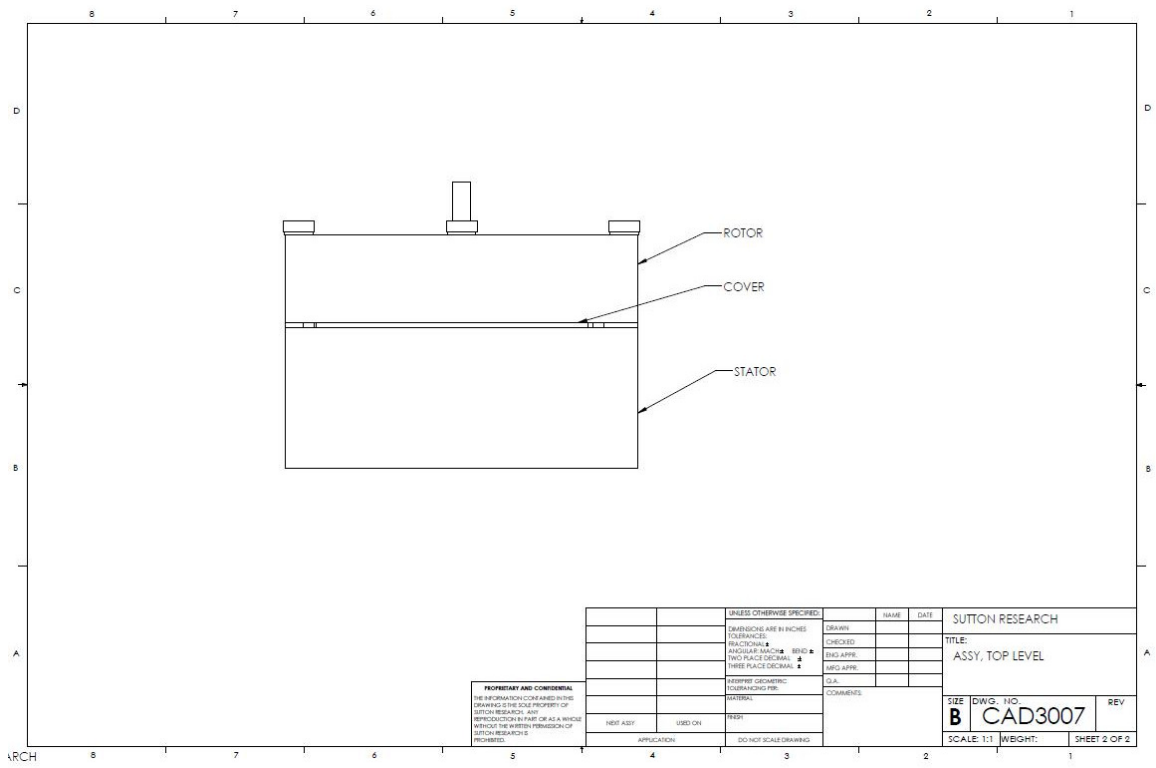


Figure B-8 - Assembly, Top Level, Drawing, Orthogonal View. This figure details the top level assembly for the permanent magnet machine built and tested for experiments 3 and 4.

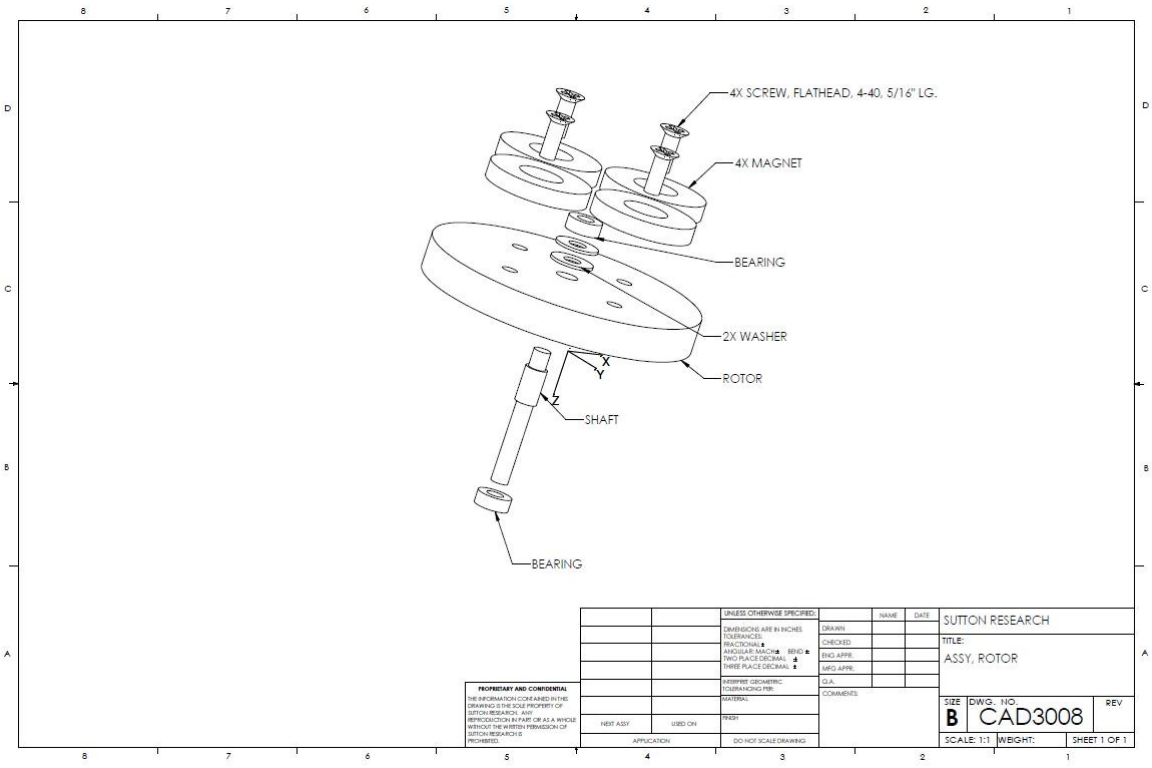


Figure B-9 - Subassembly, Rotor, Drawing. This figure details the rotor subassembly for the permanent magnet machine built and tested for experiments 3 and 4.

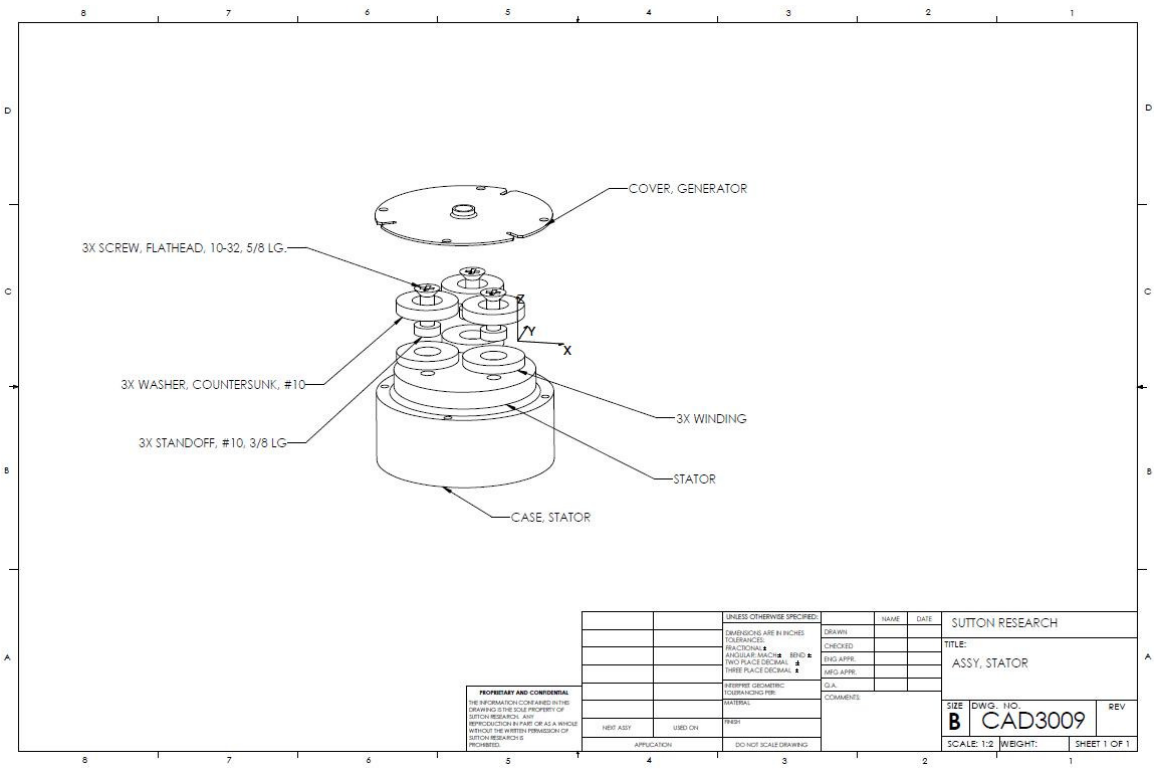


Figure B-10 - Subassembly, Stator, Drawing. This figure details the stator subassembly for the permanent magnet machine built and tested for experiments 3 and 4.